DRAFT

Appendix A

Details of numerical modelling of currents and
stratification conditions

Details of numerical modelling of currents and stratification conditions

## 1.	General

The annual current and stratification conditions are modelled by a 3D flow model. This model is able to simulate the stratified flow conditions found in Kattegat. The flow during the storm events is computed applying a depth-averaged 2D flow model. The two models are shortly described below. A more detailed description of these two models can be found at:

http://www.dhigroup.com/Software/Download/DocumentsAndTools/ShortDescriptions/Marine.aspx

## 2.	Model description

### 2.1	Modelling of annual flow and stratification conditions: 3D model

The 3D model MIKE 3 HD (hydrodynamics) is applied. The regional model, BANSAI, from which the local model developed in this study obtains input, is built in this system and so is the local model itself. Bansai is described in general terms in Chapter 5.3.1 in the main report.

 MIKE 3 HD is applicable to analysis of free-surface flow hydrodynamics in coastal areas and seas that are stratified. MIKE 3 HD is a part of an integrated model suite, MIKE 3, which includes also a:

- Transport module

- Ecology and water quality module

- Sand transport module

- Mud transport module

MIKE 3 is the result of more than 15 years of continuous development and is continuously developed through the experience gained from many applications worldwide.

MIKE 3 is applicable to the study of a wide range of phenomena, including:

- Tidal exchange and currents, including stratified flows

- Heat and salt recirculation

- Mass budgets of different categories of solutes and other components

MIKE 3 HD (hydrodynamics) is the basic module of the entire MIKE 3 system. It provides the hydrodynamic basis for computations by most other modules. MIKE 3 HD solves the time-dependent conservation equations of mass and momentum in three dimensions, the so-called Reynolds-averaged Navier-Stokes equations. The flow field and pressure variation are computed in response to a variety of forcing functions, when provided with the bathymetry, bed resistance, wind field, hydrographic boundary conditions, etc. The conservation equations for heat and salt are included as well. MIKE 3 HD uses the UNESCO equation of state of seawater (1980) as the relation between salinity, temperature and density.

The hydrodynamic phenomena included in the equations are:

- Tidal flows and currents

- Effects of buoyancy and stratification

- Turbulent (shear) diffusion, entrainment and dispersion

- Coriolis forces

- Barometric pressure gradients

- Wind stress

- Variable bathymetry and bed resistance

- Flooding and drying of inter-tidal areas

- The hydrodynamic effects of rivers and outfalls

- Sources and sinks (both mass and momentum)

- Heat exchange with the atmosphere including evaporation and

- precipitation

2.2 Modelling of storm events

The hydrodynamic modelling under storm conditions has been carried out using DHI's numerical hydrodynamic model, MIKE 21-FM HD. This model describes the depth-integrated current, driven by a combined forcing, which may comprise forces induced by wave breaking, Coriolis forcing and wind by solving the depth-averaged equations of continuity and momentum on a flexible mesh based on triangular or quadrangular elements.

Moreover, MIKE 21–FM HD is a part of DHI's 2D model system MIKE21, therefore output from other modules such as the Spectral Wave model can be supplied as forcing (i.e. radiation stress field) to the HD model provided they are in the same horizontal coordinates system.

This model may be applied wherever stratification can be neglected. In our case it is assumed that under storm weather conditions, the stirring effect from the waves and wind causes the water column to be well mixed.

3. Model setup

3.1 Model setup for 3D model

The local model is a sub-model of the larger Bansai model, which is described in general terms in Chapter 5.3.1 of the main report. The model area and the parameter settings in the local model are described in this section.

3.1.1 Model area and mesh

The Bansai model has a resolution of 3 nautical miles (nm) in Kattegat. The local model developed has this resolution in the outer mesh but by use of the nesting technique this is downscaled to a resolution of app. 1/3 nm (=617.33 m) in the finest area where the wind mills are located, see Figure 3.1. In the nesting procedure model parameters are transferred in the interfaces between areas with the coarser and the finer mesh. An overview of the bathymetry used is given in Figure 3.1. The distance between the wind mills is 600 m – 700 m which means that there will be approximately one mill in each cell in the wind mill area.
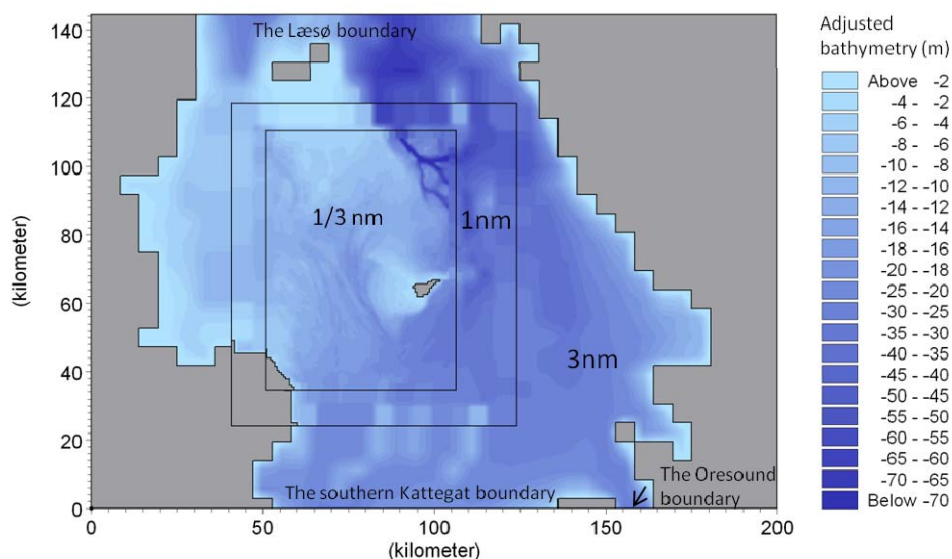
Figure 3.1   Model area of the local model for simulations of annual flow and stratification conditions. Mesh sizes are given in areas of decreasing grid size. The finest resolution is 617.33 m.

3.1.2   **Model settings and boundaries**

The local model is a submodel of the Bansai model. The local model applies the same settings for physical and numerical parameter settings as the larger Bansai model but on a much finer mesh as described above. The parameters are listed in Table 3.1.

The system has three boundaries. The Oresound, the southern Kattegat, and north of Læsø. All boundaries are forced with data extracted from the Bansai model. The northern boundary and the southern Kattegat boundary are forced with salinity, temperature and fluxes. The Oresound boundary is forced with surface elevation.

Initial fields of elevations, salinity and temperature came from the Bansai model.

The metheorological forcings came from Vejr2 in the form of numerically simulated winds, temperatures, insolations and precipitations. These are denoted the Hirlam fields.

The runoff data describing the fresh water input from rivers and fjords are applied to the model as statistical yearly values. For further information on the model forcings please see /1/.

The boundary conditions and forcings are illustrated in Figure 3.2-Figure 3.6.

The boundary conditions are illustrated by time series covering the entire model period showing the values of the respective parameters in the central location at the surface., see Figure 3.2. The water levels for each of the boundaries are illustrated along with the residuals. The residuals are the water levels from which the instantaneous tidal levels have been subtracted. This information describes hence the variation in the water level due to (mainly) storm surges.

In Figure 3.3 and Figure 3.4 time series of the water temperature and salinities applied at the local model boundaries are illustrated. In Figure 3.5 and Figure 3.6 the air temperature and wind speeds are shown for a central location in Kattegat. These are extracted from the 2D- fields from Vejr2.

Table 3.1 All settings for the baseline simulations

| Parameter	Value
Simulation mode	Non hydrostatic
Number of nestings	3
Number of layers	35
Vertical grid spacing	2m
Grid spacing area 1	5556m
Grid spacing area 2	1852m
Grid spacing area 3	617.33m
Simulation period	01/01/2005 -01/01/2006
Timestep	60 sec
Turbulence model vertical	k-ε
Turbulence model horisontal	Smagorinski
Initial surface elevations	2D fields from Bansai model
Initial salinity	3D fields from Bansai model
Boundary southern Kattegat	Transfer files from Bansai model (Flux based)
Boundary northern Kattegat	Transfer files from Bansai model (Flux based)
Boundary Oresund	Transfer files from Bansai model (Elevation based)
Bed friction area 1	0.005m
Bed friction area 2	0.005m
Bed friction area 3	0.005m
Smagorinsky coefficient area 1	0.4
Smagorinsky coefficient area 2	0.4
Smagorinsky coefficient area 3	0.4
Vertical dispersion factors salinity	$0.2 m^2/s$
Vertical dispersion factors temperature	$0.2\ m^2/s$
Heat exchange included	yes
Precipitation	2D map (Vejr2)
Air temperature	2D map (Vejr2)
Wind	2D map (Vejr2)
Wind friction	Linear (0-24m/s) 0.0016 – 0.0026
Clearness	2D map, time varying
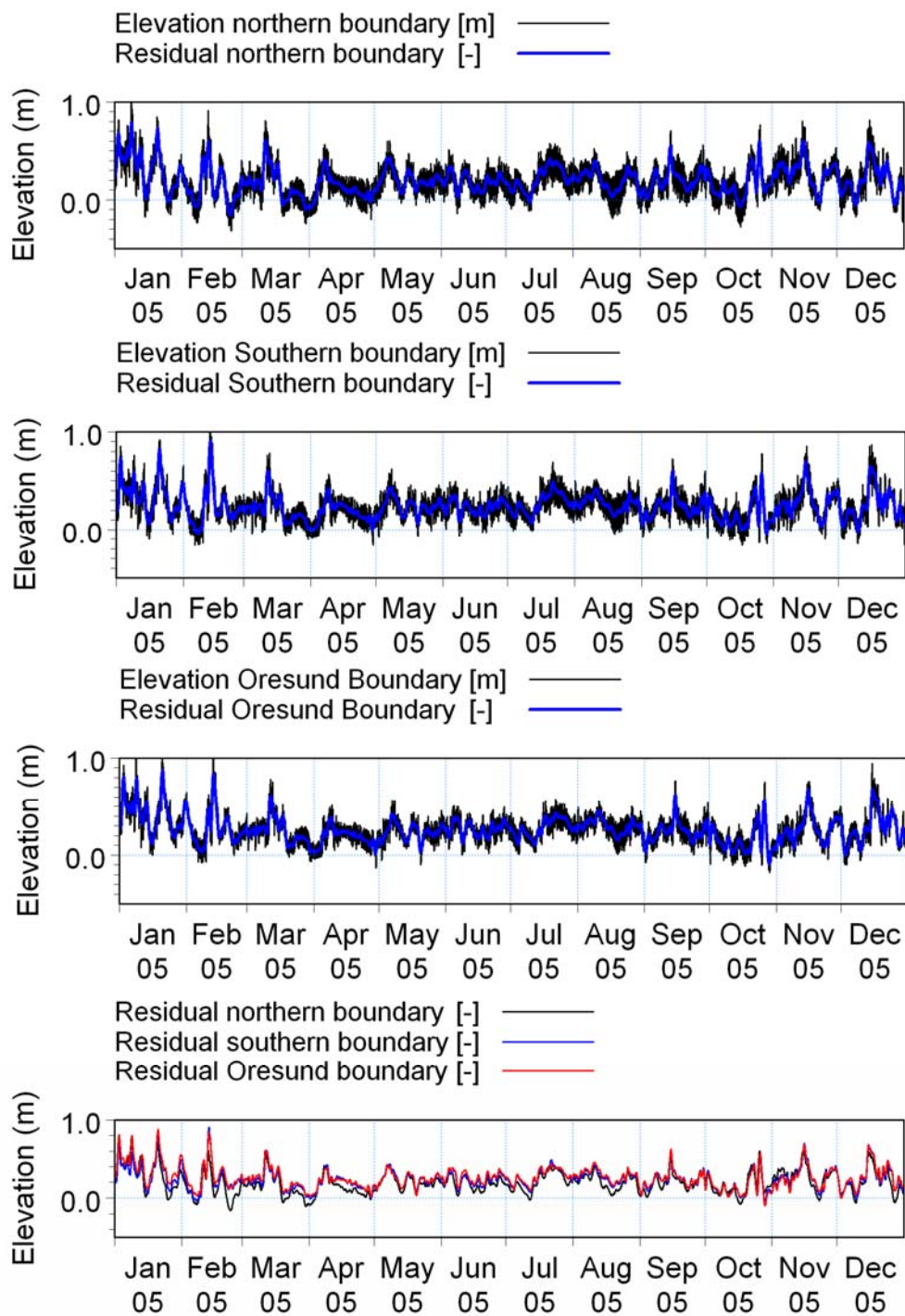
Figure 3.2   Time series of water levels and residuals for the central location of each bound-
ary in the local model. The water levels are extracted from the larger regional
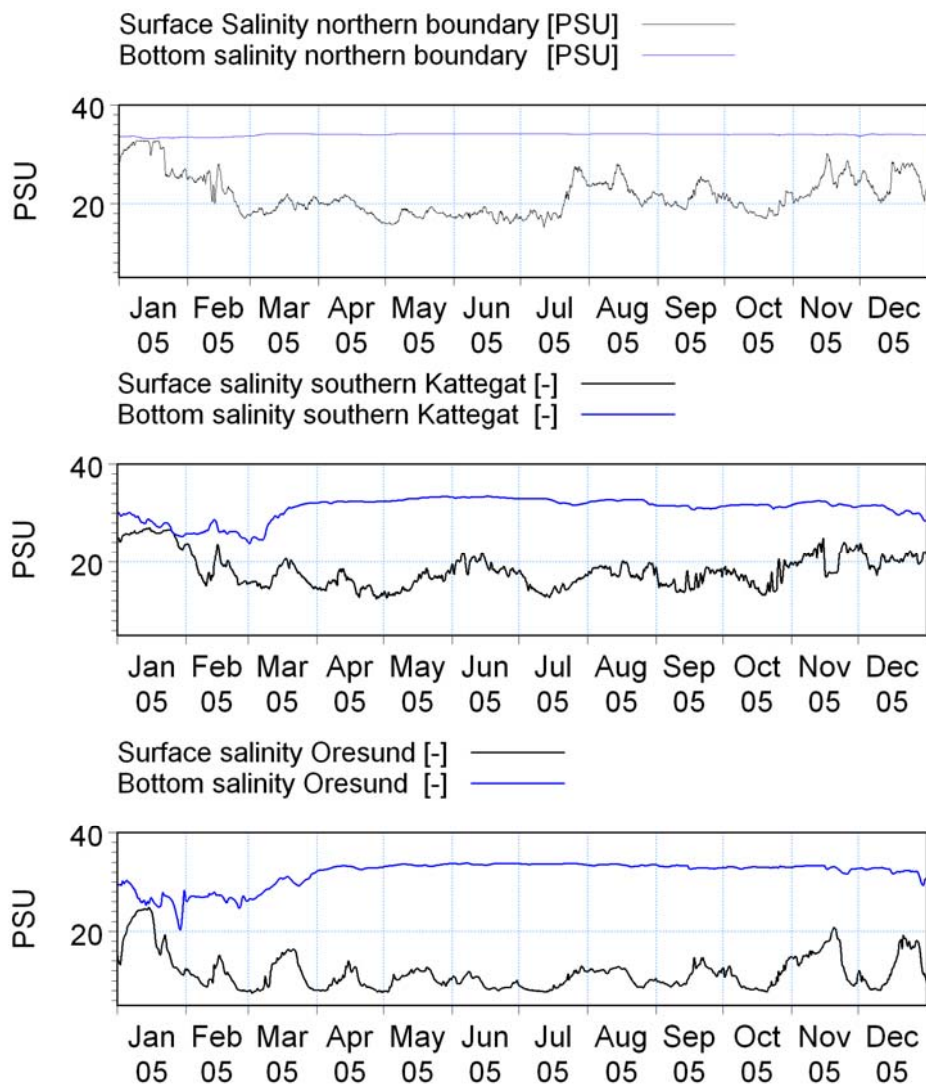model, Bansai.

Figure 3.3   Time series of salinities at the surface and at the lower layer for the central
                  location of each boundary in the local model. The salinities are extracted from
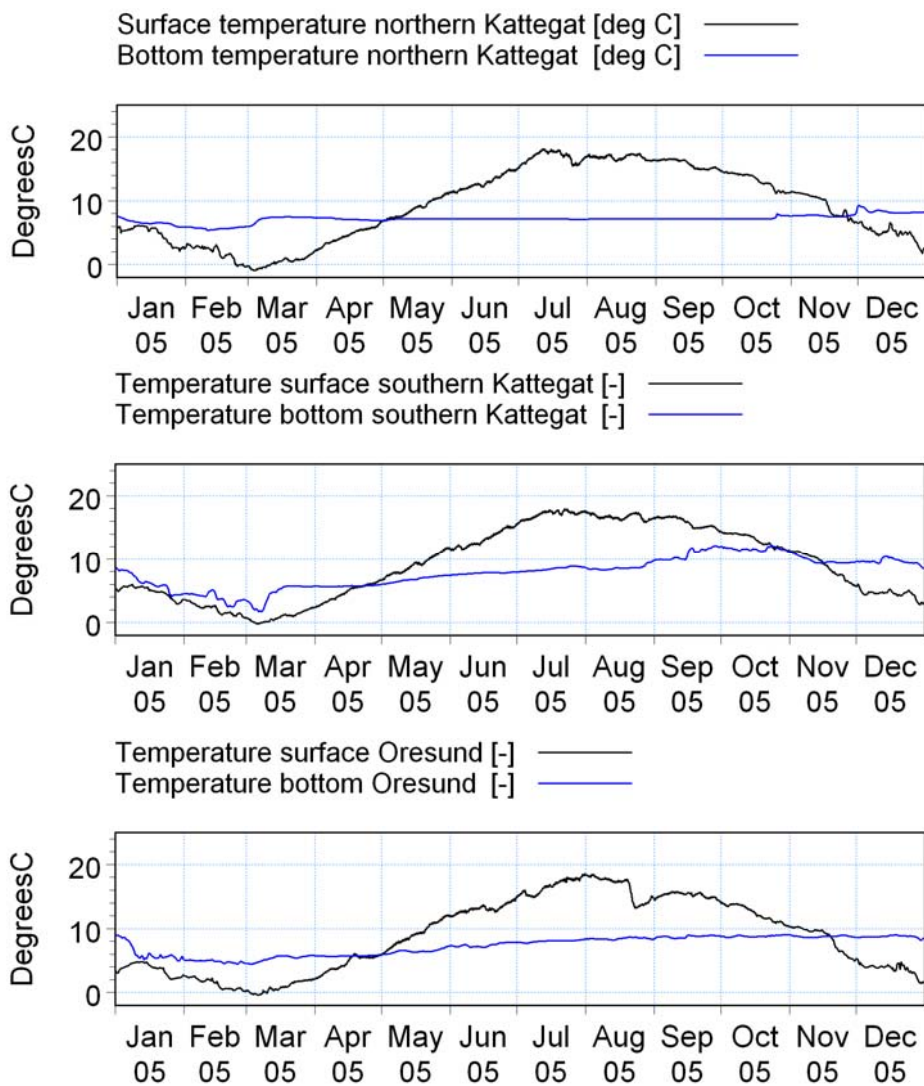   the larger regional model, Bansai.

Figure 3.4   Time series of temperatures at the surface and at the lower layer for the central location of each boundary in the local model. The temperatures are extracted from the larger regional model, Bansai.
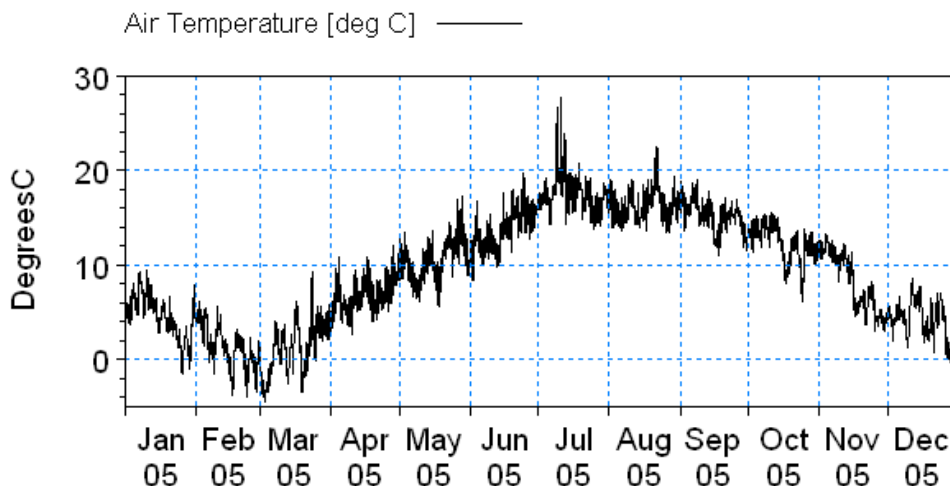
.

Figure 3.5   Time series of air temperature in the central part of Kattegat. The air tempera-
              ture shown is extracted from the 2D model data from Vejr2 applied as one of
              the forcing parameters for the local model.
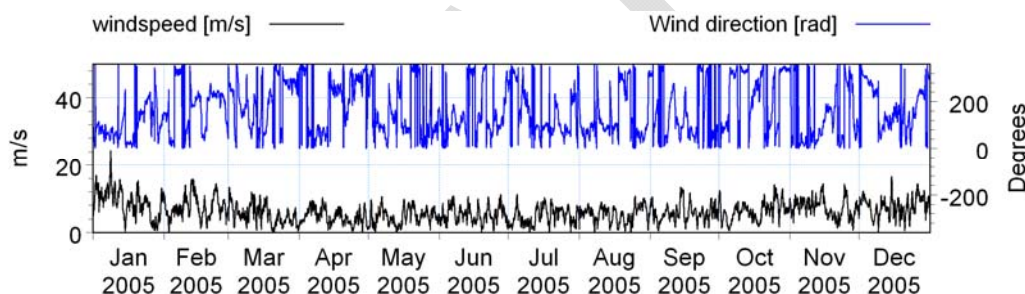

Figure 3.6   Time series of wind speed in the central part of Kattegat. The wind speed
              shown is extracted from the 2D model data from Vejr2 applied as one of the
              forcing parameters for the local model.

3.2   Model setup for 2D model

A description of the modelled area and the setup of the 2D hydrodynamic model
used for the prediction of the flow under storm weather conditions are presented in
the following section.

3.2.1   Model area and mesh

The modelled area and open boundaries used for the modelling of the storm condi-
tions are shown on Figure 3.7. The domain extends towards the north to south of
Læsø (Boundary 2) and towards the south to the boundary defined by the spit of
Odden and the southern tip of Djursland (Boundary 3). The northern entry to Øre-
sund (Boundary 4) is an open boundary as well.

A flexible mesh (Figure 3.7 and Figure 3.8) composed of approximately 101,000 tri-angular elements, whose resolution increases gradually from 1,800 m at the bounda-ries to 50 m in the project area, has been created. The resolution in the approach of Djursland and Anholt has been set to 800 m in order to describe carefully the impact of the wind mills on wave and current conditions near the shorelines at Djursland and Anholt.

The mesh is not resolving the very local effect on the currents. The minimum ele-ment size is about 50 m and the cone of the wind mill foundations for the 2.3 MW wind mills is varying between 5-14 m across the water depth. The local effects take place within a few diameters of the wind mill foundation and are described further in Section 6.2. Outside this local zone near each wind mill foundation, the variations in the flow (wave fields) are smaller and the mesh is fine enough to describe the varia-tions in the flow (and wave) field in the gaps between the wind mills and in the area surrounding the wind farm.

The available bathymetrical data were obtained from the Royal Danish Administra-tion of Navigation and Hydrography (Farvandsvæsenet) and from electronic sea maps in DHI's MIKE C-MAP. The model bathymetry shown in Figure 3.9 has then been generated by interpolation of these bathymetrical data to the flexible mesh.

Furthermore, the 2D hydrodynamic model requires input from the 3D regional model 'Vandudsigten' described in Section 5.3.1 set up in the horizontal coordinates system UTM-32(WGS84). For practical reasons, the 2D hydrodynamic model under storm conditions has been defined in the same coordinates system.
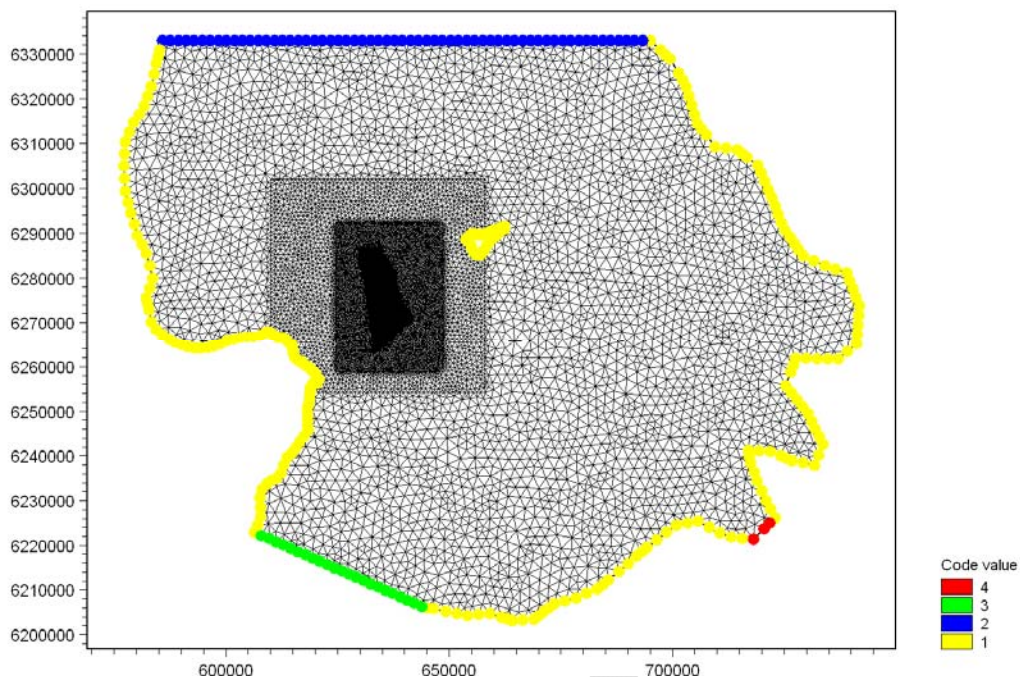
Figure 3.7   Extent of the modelled area, location of the open boundaries and definition of the flexible mesh used for the modelling of storm conditions. The horizontal co-ordinates system is UTM-32 (WGS84).
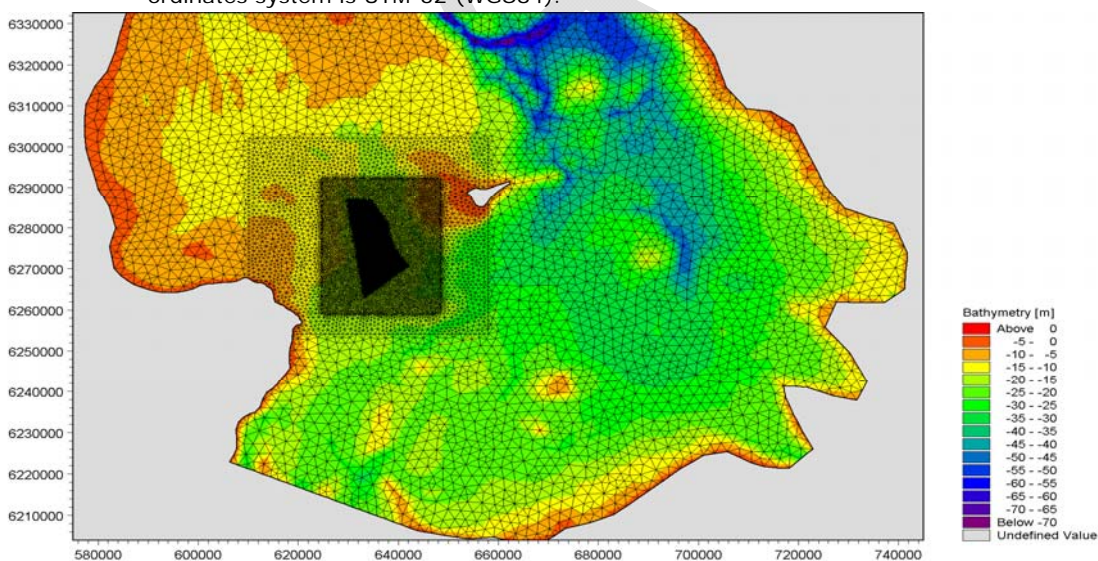

Figure 3.8   Bathymetry and mesh of the entire domain created for the modelling of storm conditions. The horizontal coordinates system is UTM-32 (WGS84).
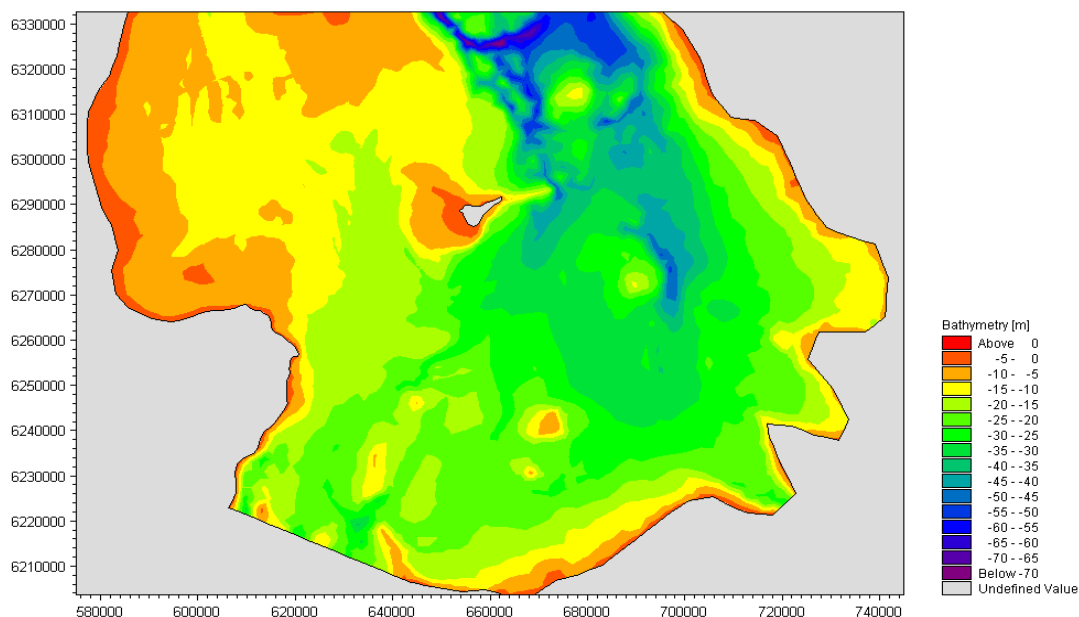
Figure 3.9   Bathymetry of the entire domain created for the modelling of storm conditions. The horizontal coordinates system is UTM-32 (WGS84).

3.2.2   Model setup

The 2D flow model has been set up using input extracted from DHI's 3D validated model 'Vandudsigten'.

The main calibration factors for a hydrodynamic modelling study are listed in Table 3.2 and described below.

The driving forces applied in the model consist of time and spatially varying wind forces and Coriolis force and flux applied at the boundary of the domain.

The flow is controlled by fluxes applied along the North and South boundaries. This has been created by extracting the depth-averaged time varying current speed along the boundaries from the 3D regional model and converting to fluxes. The boundary condition at the Øresund's entrance has been defined in the form of a time varying water level in order to maintain the right surface elevation in the domain.

The wind has been included through the definition of its x- and z- components and the pressure acting on the sea. These parameters are varying with time and space. The stress driven by the wind on the sea surface is expressed by the following equation:

$$\tau_s = \rho_a \cdot c_d \cdot |W_s| W_s$$

Where the drag coefficient c_d varies from 0.0013-0.0024 for a wind varying from 7 to 25 m/s, ρ_a is the density of air, W_s is the wind speed 10 m above the sea surface.

It has been observed that during the period of calibration, the 3D regional model predicts a depth-averaged current in the vicinity of Anholt which accelerates significantly towards the channel located between Anholt and Djursland (see upper plot of Figure 4.7). In order to reproduce this pattern a spatial varying bed roughness has been defined to force the flow through deep areas such as the channel mentioned above. As a result the bed roughness has been defined by Manning number varying gradually from $35 m^{1/3}/s$ in the shallow areas to $60 m^{1/3}/s$ in the deeper areas.

The Smagorinsky formulation is used for the eddy viscosity. The Smagorinsky coefficient is set to 0.28.

Table 3.2 Parameters used in the setup of the 2D hydrodynamic model used for the simulation of storm events.

Parameter	Value
Mesh size – coarsest mesh	1800m
Mesh size – finest mesh	50m
Simulation periods	25/11/1999-04/12/1999 (Storm 1) 13/01/2000-20/01/2000 (Storm 2) 18/12/1999-28/12/1999 (Storm 3) 26/10/2000-04/11/2000 (Storm 4)
Maximum time step	60s
Boundaries	3 boundaries: Boundary nb 2: South of Læsø Boundary nb 3: between the spit of Odden and the southern tip of Djursland Boundary nb 4: Øresund
Boundary conditions	Boundary nb 2: time serie of flux based on the depth integration of the current speed extracted from the model 'Vandudsigten' Boundary nb 3: time serie of flux based on the depth integration of the current speed extracted from the model 'Vandudsigten' Boundary nb 4: time varying water level
Flood and Dry	Included
Density	Barotropic
Horizontal eddy viscosity formulation	Smagorinsky - Smagorinsky coefficient of 0.28
Bed resistance	Manning number varying between $35 m^{1/3}/s$ (at the shallow areas) to $60 m^{1/3}/s$ (deeper areas)
Coriolis forcing	Varying in the domain, it is obtained from the geographical latitude of the model
Wind forcing	Spatial and time varying wind extracted from the model 'Vandudsigten'. The wind forcing is calculated with a wind friction factor varying between 0.0013 and 0.0024 for wind in the range of 7 -25m/s
Wave radiation stresses	not included
Initial conditions	surface elevation extraction form the model 'Vandudsigten'

4. Calibration and validation

4.1 Calibration and validation of 3D model

The Bansai model has been calibrated and validated continuously since 2000 and model results can hence be considered as high quality reliable input to the local model developed in the present study. Further details of the validation of BANSAI are included in the main report and in /1/.

The validation of the local model is carried out against data from the BANSAI model. It is not expected that the two models will give exactly the same results since the bathymetry is different due to the finer grids in the present study.

Model data for two locations respectively north and south of the Anholt Offshore Wind Farm area are compared in Figure 4.1 (salinities and temperatures in the northern location) and Figure 4.2 (salinities and temperatures in the southern location). Comparisons are provided for the surface layer and the bottom layer of the models. The two locations are shown in Figure 4.3.

The comparisons show that the local model reproduces the results from the original model to a satisfying level and thus the model is considered adequate for the present purpose.
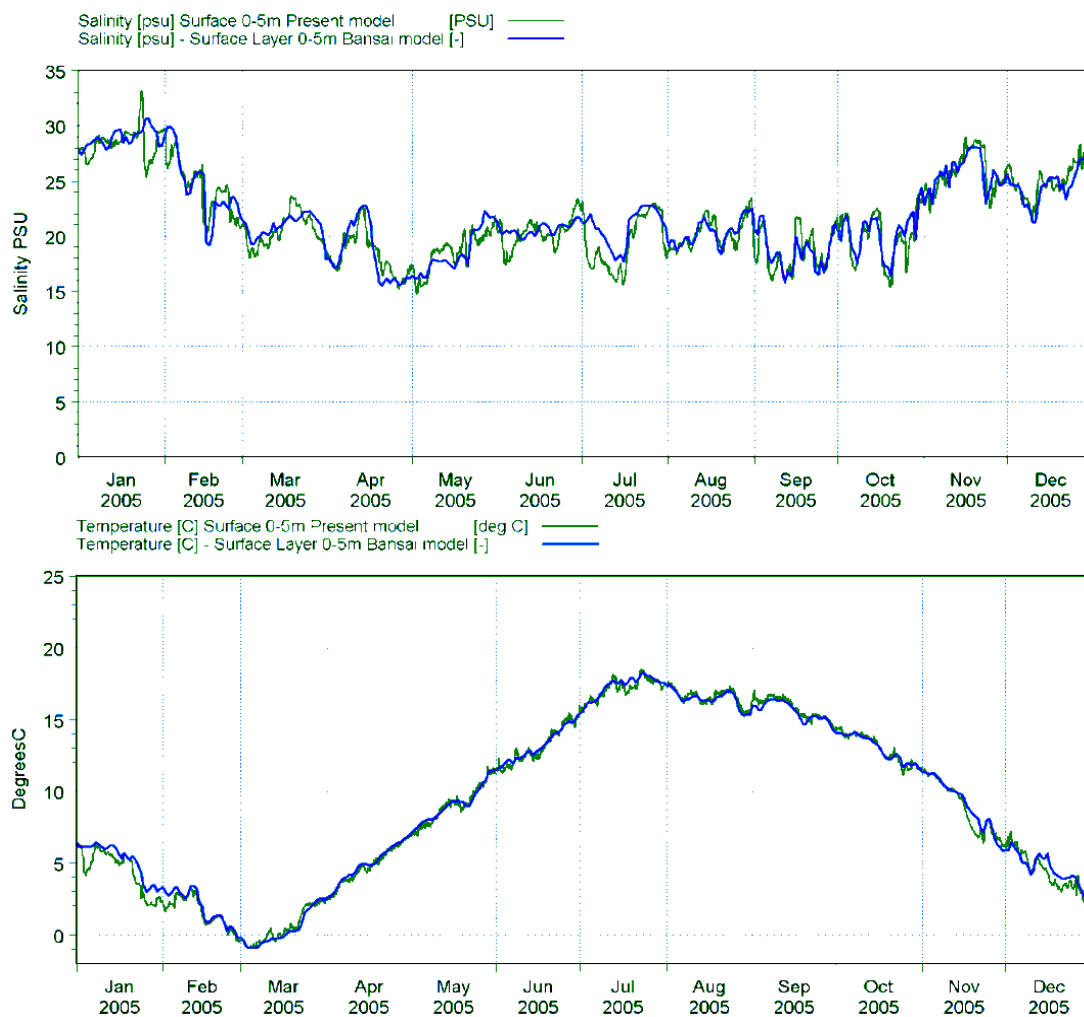
Figure 4.1   Validation of local 3D model salinities and temperatures with salinities and temperatures from the regional model (Bansai) at location 1 in the northern end of the study area.
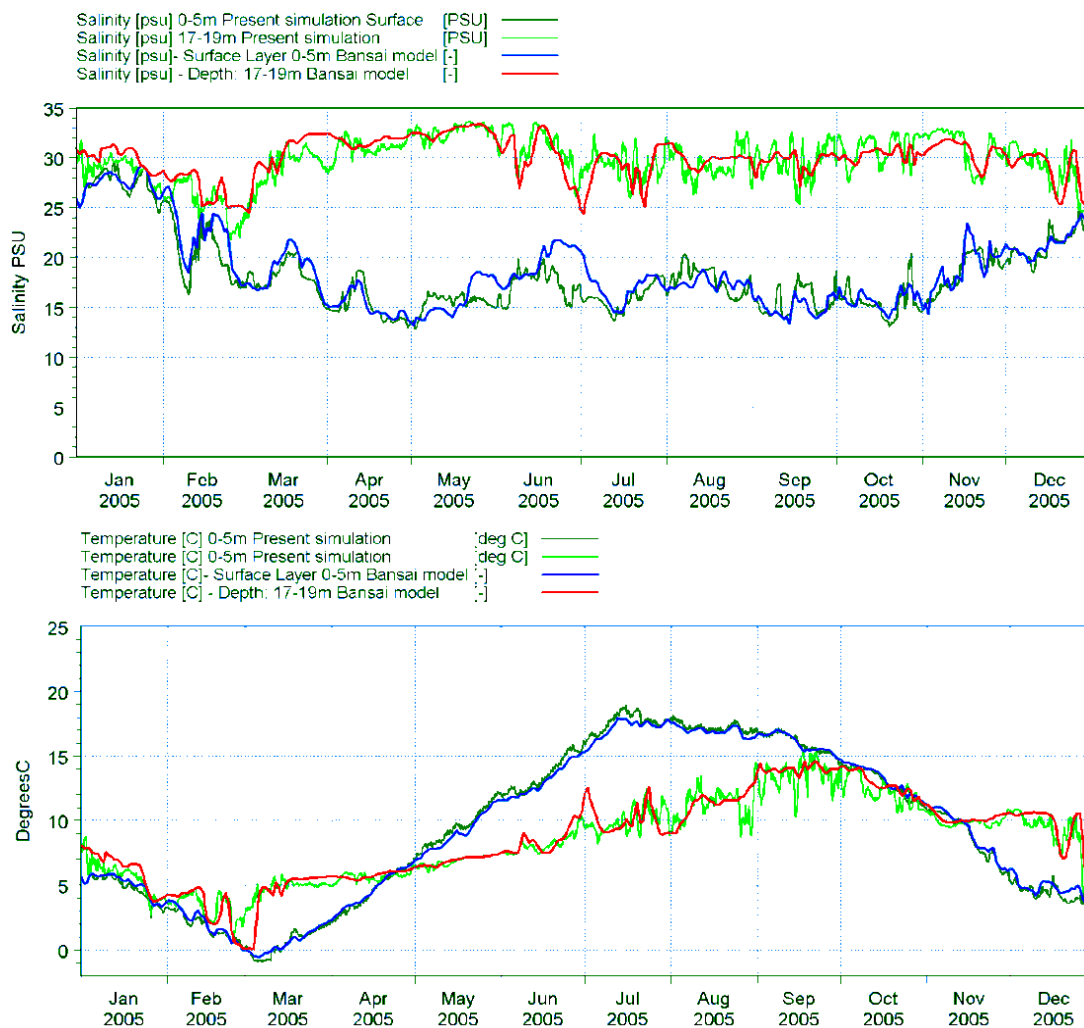
Figure 4.2   Validation of local 3D model salinities and temperatures with salinities and temperatures from the regional model (Bansai) at location 2 in the southern end of the study area.
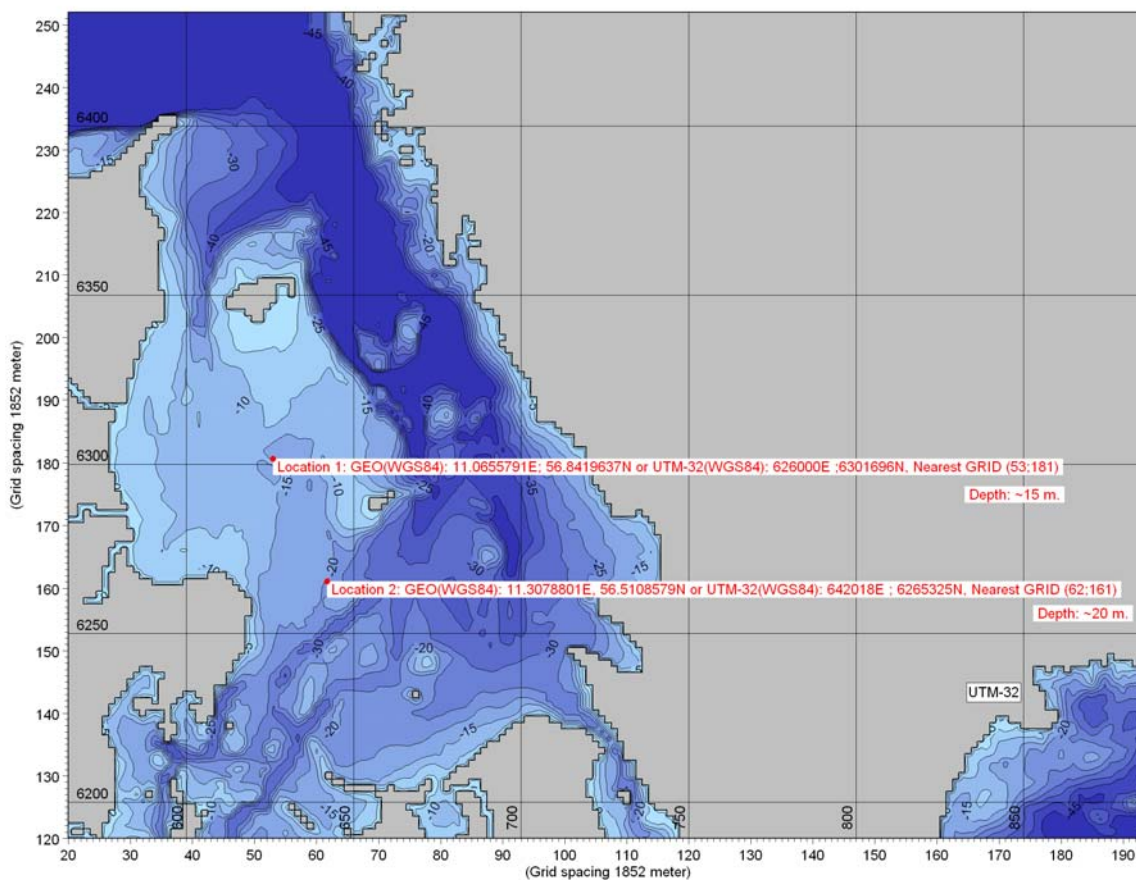
Figure 4.3   The two locations investigated.

4.2   Calibration and validation of 2D model

The 2D resulting computed current has then been compared and validated against depth-averaged current from the 3D model in terms of patterns and magnitude. It can be observed that the bathymetry north of Anholt is subjected to extremely strong variation changing from -60 m to -7 m in about 15 km. Thus the correct flow pattern nearby Anholt wind farm seems most critical to be reproduced for a situation with south directed current. The calibration of the 2D model has therefore been carried out with Storm 2 which is characterized by a strong south directed current in the approach of the area of interest.

Figure 4.5 and Figure 4.6 represent the depth-averaged current speed and direction extracted from the 2D and 3D model at 2 points located at the northern and southern limit of the future wind farm area; they are indicated on Figure 4.4. Instantaneous 2D flow fields are shown on Figure 4.7 for the 3D (upper figure) and 2D (lower figure) model, respectively. The chosen time step corresponds to the time step during Storm 2 where the current has the highest intensity.

From Figure 4.5 and Figure 4.6, it can be seen that the 2D hydrodynamic model predicts satisfying results which fit closely the 3D model in terms of current speed and direction within the wind farm during Storm 2. The difference in the model resolution in the area of interest set to 1850 m in the 3D regional model and to 50 m in the 2D model may explain small differences.

At the northern point, the current speed predicted by the 2D model shows a tendency to be slightly lower than the depth-integrated current from the 3D model whereas the current direction matches perfectly. At the southern point, the current magnitude from the two models is nearly the same but the current direction from the 2D model is slightly deflected clockwise of approximately 10° compared to the 3D model.

The 2D patterns of the instantaneous flow presented in Figure 4.7 are similar for the 2D and 3D models. The general anticlockwise circulation of the flow around Anholt is well reproduced. On both models, the south-going flow concentrates north of Anholt and converges in the deep area between Anholt and Djursland with a magnitude of 0.6 m. The only main difference between the hydrodynamic results from the 2D and 3D models is that acceleration of the flow on the shallow areas such as north of Odden's spit tends to be slightly higher with the 2D model.

The impact of the waves on the hydrodynamic of the system during storm events has been tested. Gradients in the wave radiation stress field impose additional forcing on the water. Therefore in addition to the forcing induced by the water level gradients and the wind, wave radiation stress field calculated in Section 5.5.3 of the main report has been applied to the 2D model to test the sensitivity.

Resulting flow velocities extracted at the 2 points shown in Figure 4.8 and Figure 4.9 are presented for the 2D model with (in green) and without (in black) the effect of the waves. Instantaneous 2D flow fields are shown on Figure 4.10 for the 2D model with (lower figure) and without (upper figure) the impact on waves. The chosen time step corresponds to the time step during Storm 2 where the current has the highest intensity.

Within the area of interest, wave breaking does not take place due to the water depth varying between 15 and 18 m. This results in the absence of significant radiation stress gradients and the waves have only a weak impact on the currents (see Figure 4.8, Figure 4.9). Only some minor local effects of the wave forcing on the current can be seen mainly in wave breaking areas such as the NW coast of Anholt and N-NE coast of Djursland (see Figure 4.10).

To conclude, 2D flow results from the 2D and 3D models fit well in terms of intensity and direction over the entire modelled area. Wave-induced currents are insignificant and the 2D modelling of the storms has been continued without including wave forcing in the 2D hydrodynamic model.
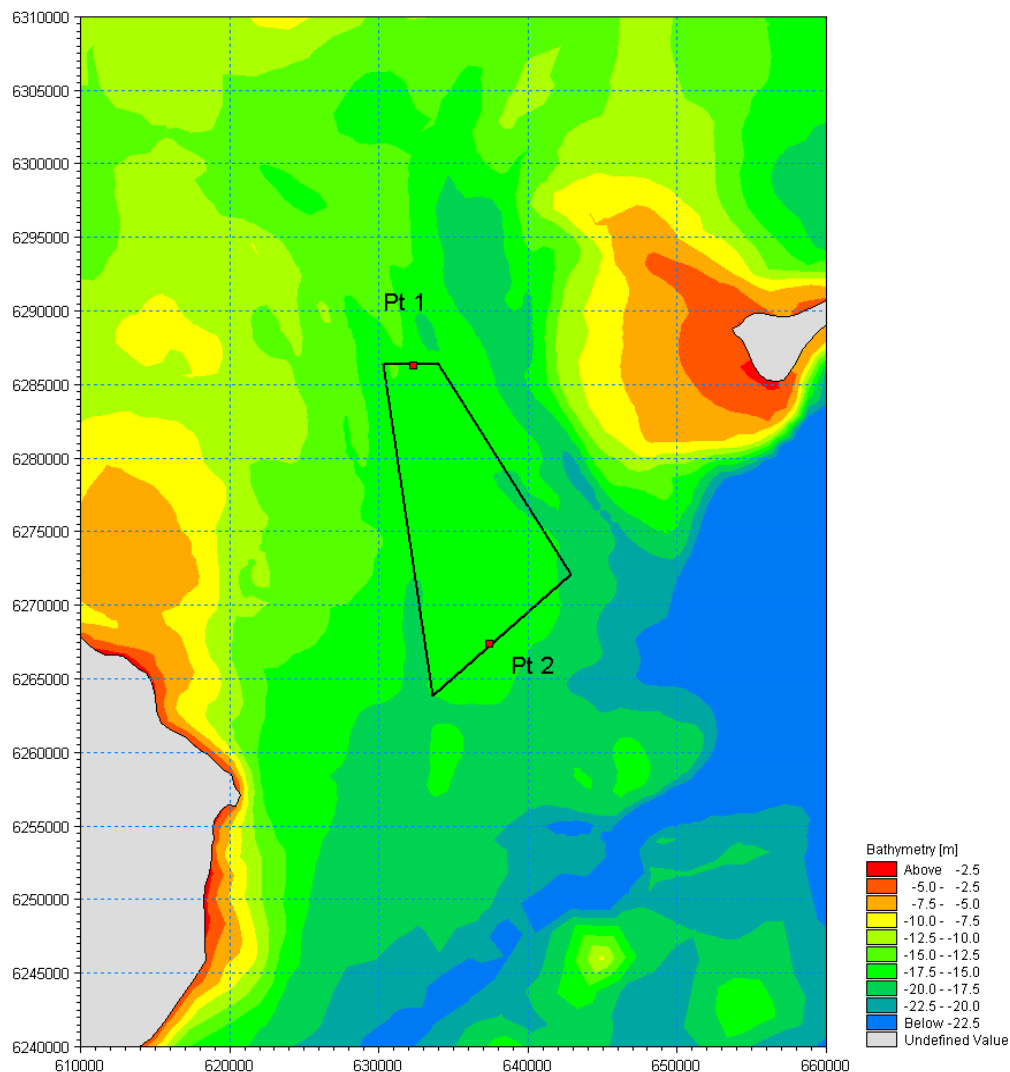
Figure 4.4   Location of the 2 extraction points used to validate the 2D hydrodynamic model against the 3D regional model 'Vandudsigten' in term of current speed and direction.
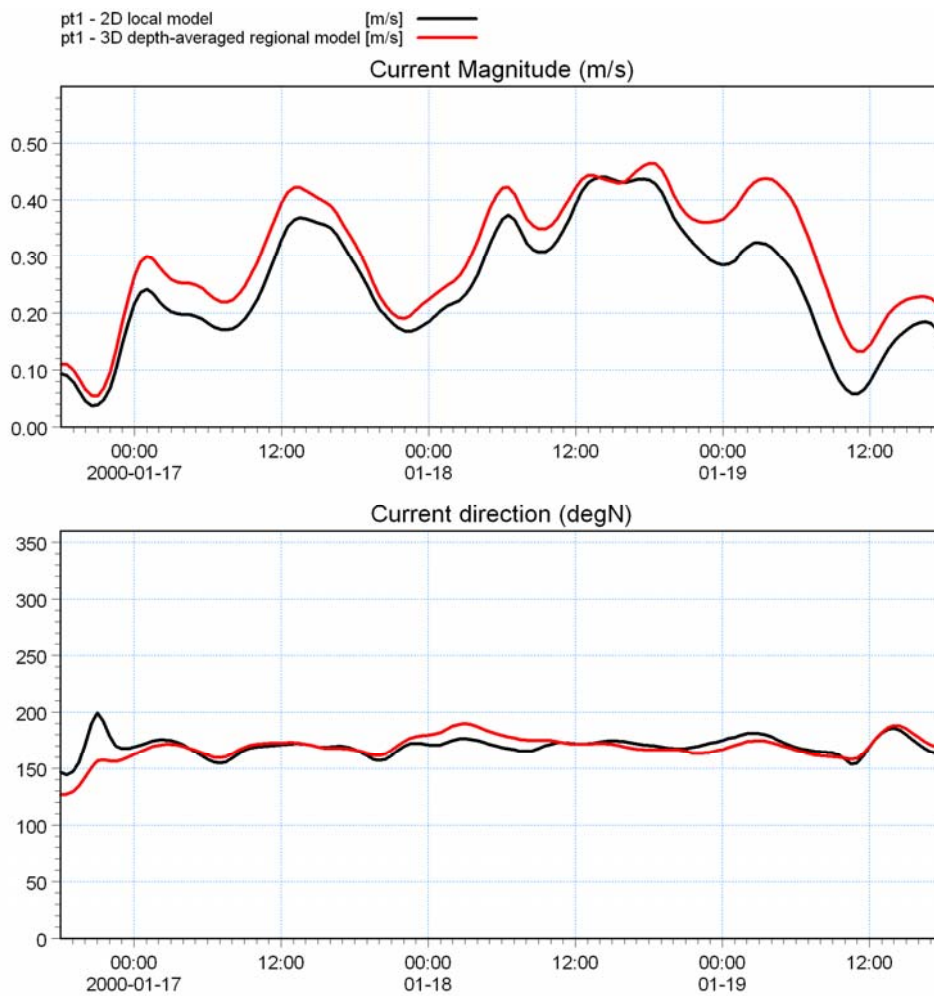
Figure 4.5   Depth-averaged current speed and direction extracted at the northern point indicated on Figure 4.4 from the 2D (in black) and the 3D model (in red) for Storm 2.
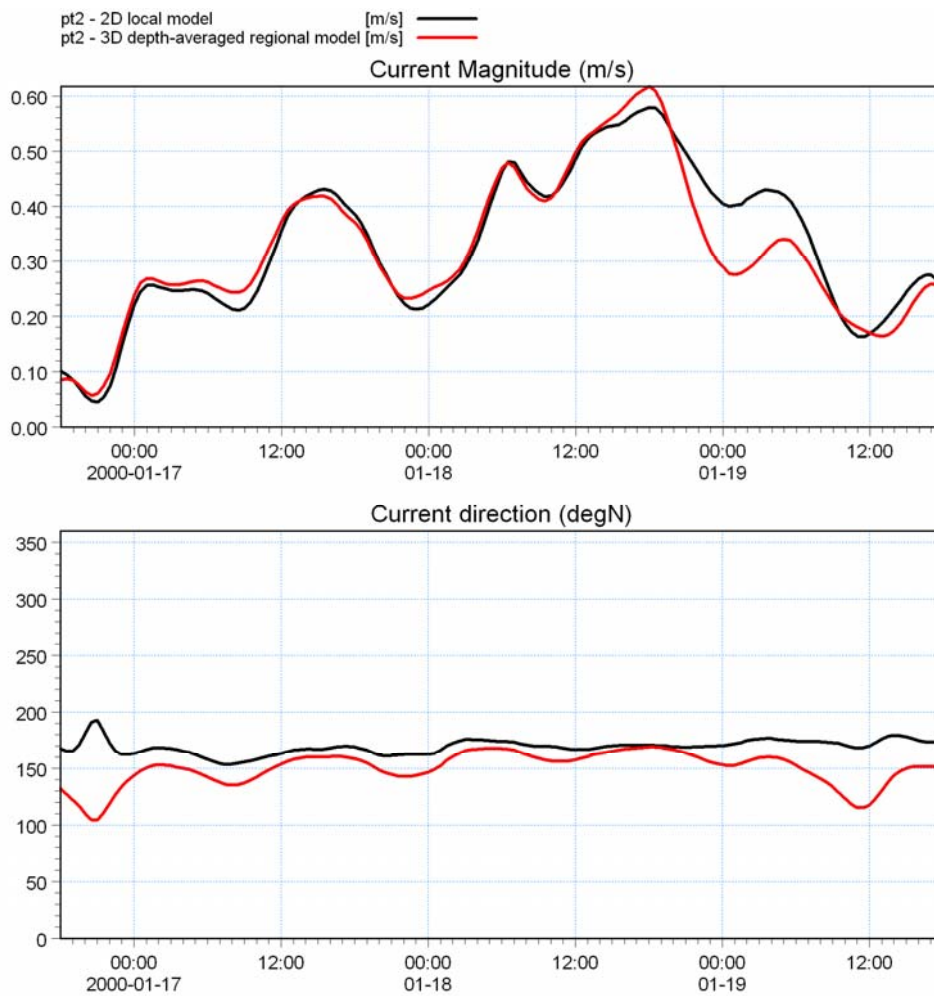
Figure 4.6   Depth-averaged current speed and direction extracted at the southern point indicated on Figure 4.4 from the 2D (in black) and the 3D model (in red) for Storm 2.
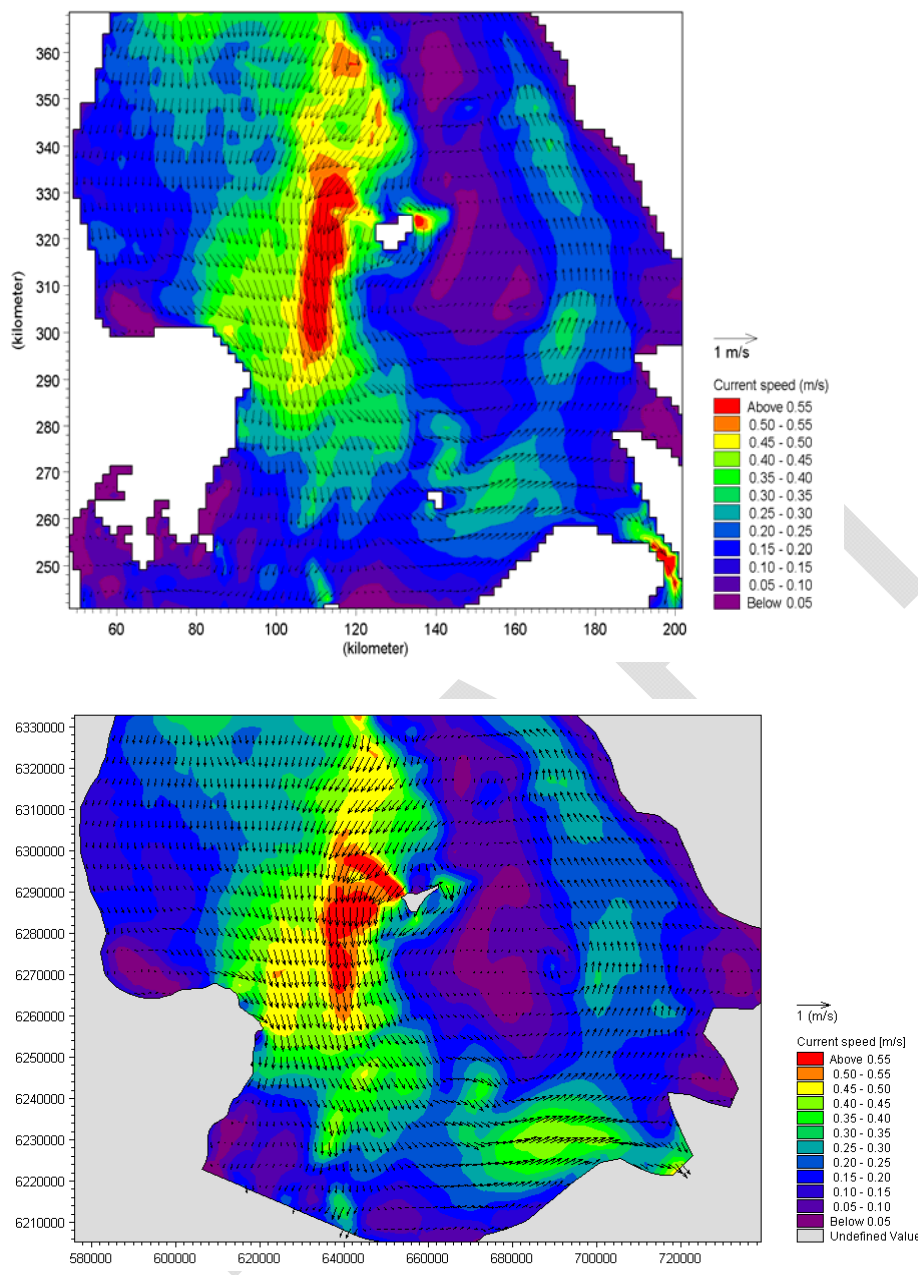
Figure 4.7   Instantaneous depth-averaged current field extracted from the 3D model (up) and from the 2D model (down) at 18-01-2000 at 15:30. The chosen time step corresponds to the time step during Storm 2 where the current has the highest intensity.
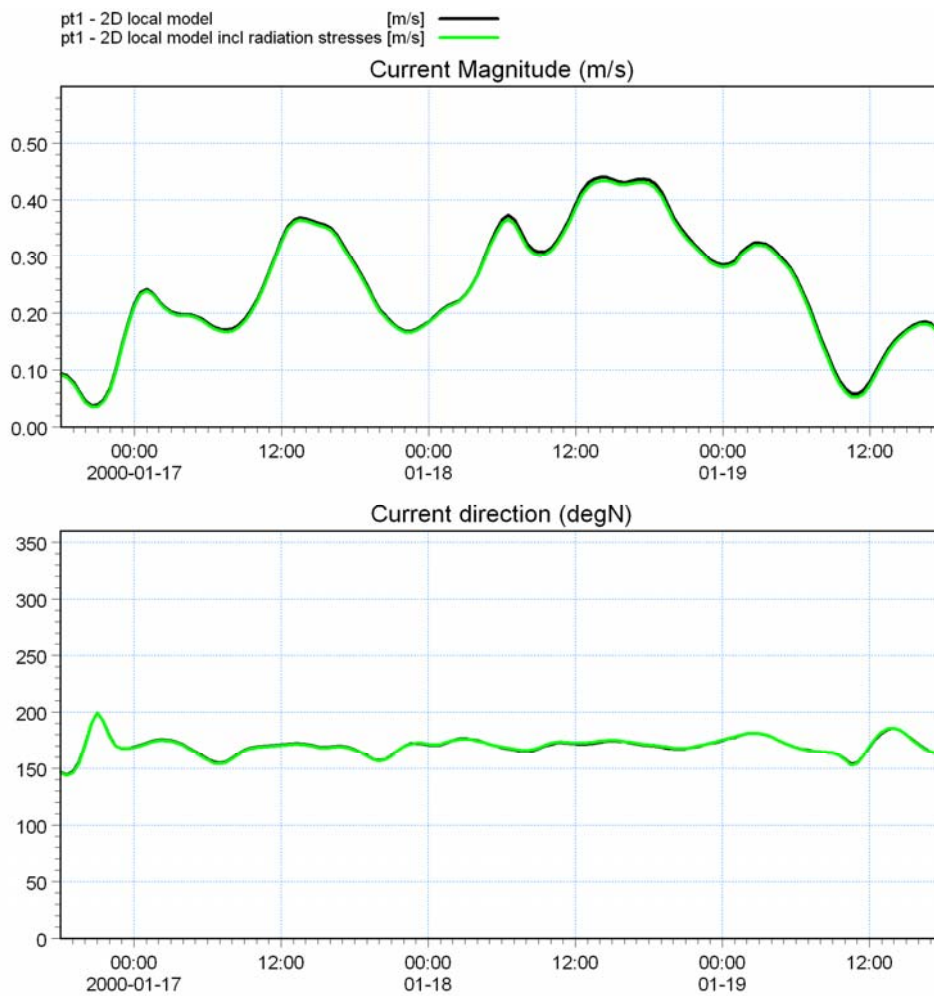
Figure 4.8   Depth-averaged current speed and direction extracted at the northern point indicated on Figure 4.4 from the 2D model for Storm 2 with (in green) and without wave effect (in black).
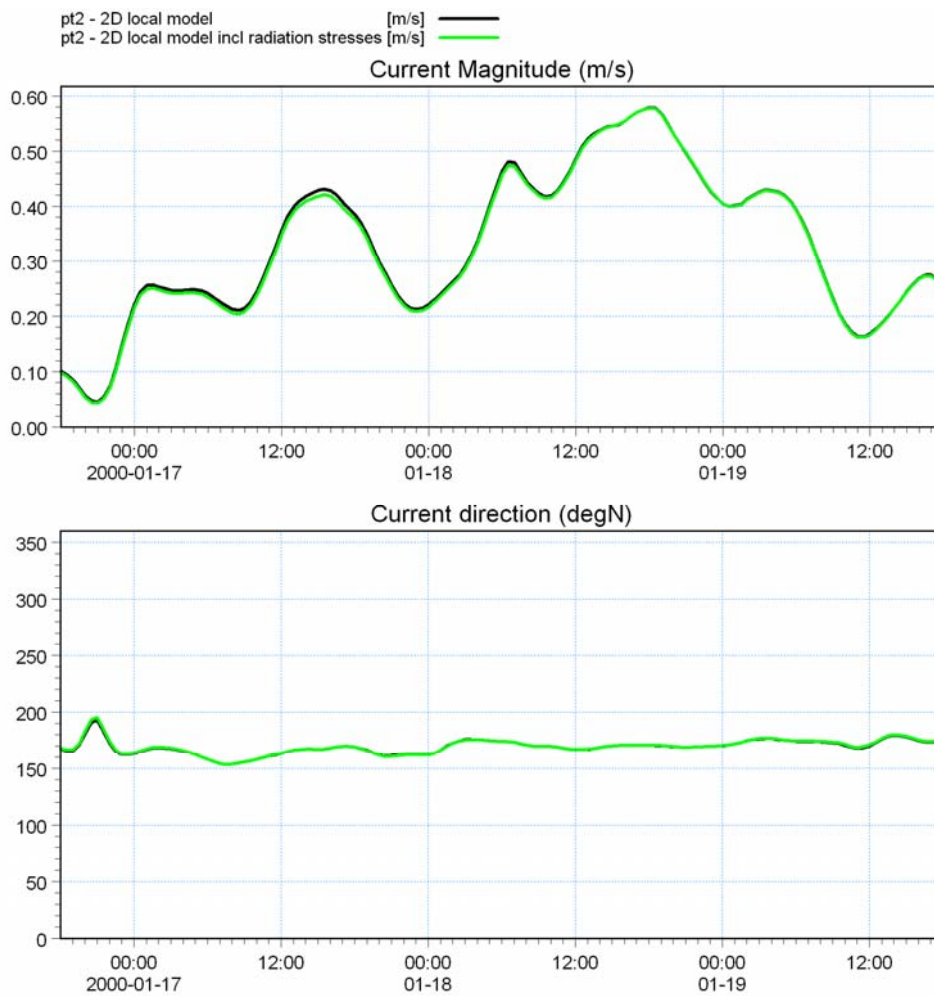
Figure 4.9   Depth-averaged current speed and direction extracted at the southern point
              indicated on Figure 4.4 from the 2D model for Storm 2 with (in green) and
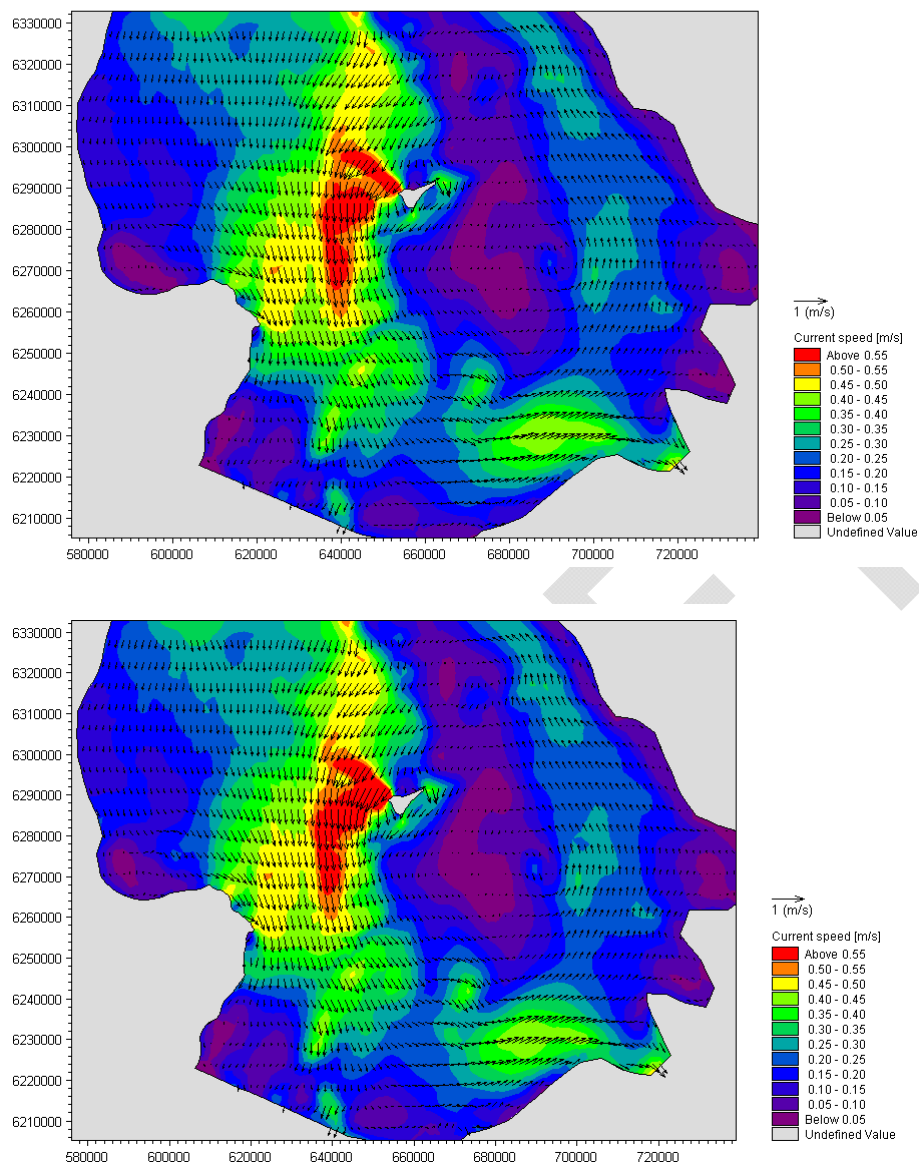   without wave effect (in black).

Figure 4.10   Instantaneous depth-averaged current field extracted at 18-01-2000 at 15:30
from the 2D model not including (upper figure) and including (lower figure) the
effect of waves on the hydrodynamic. The chosen time step corresponds to the
time step during Storm 2 where the current has the highest intensity.

4.3 Selection of model year for the annual flow and stratification conditions

A representative year is to be selected for numerical modelling of the annual current, salinity, temperature and water quality conditions. Representative in this context is defined as a year that statistically is close to the long term average of the hydrographic conditions and water quality parameters. The criteria for selecting a representative year is hence that the selected year, statistically deviates the least from the long time average.

The methodology in selecting a representative year is carrying out a statistical analysis of available data over a period of time. The measurements applied are measurements of salinity, temperature, precipitation, insolation and wind speeds gathered through the Novana project (/2/) at station "Læsø Rende Vest" located in Læsø Rende between Læsø and Jutland.

 As earlier described the method is to calculate monthly averages for each component and calculate the deviation from the monthly averages found for the full length of the measurement period (2004-2008). By averaging the monthly averages over the year a mean deviation for the individual years has been determined. Based on this the individual years could be ranked with the smallest deviations ranking highest (1) and the years with the largest deviation from the long time average as the lowest ranking (5).

The results of this analysis are given in Table 4.1 and Table 4.2. Note that insolation, salinity and temperature deviations are calculated as yearly average deviations as well as the deviations during summertime. The latter is because this is the more important time from an ecological point of view.

Year 2005 is selected as the year which in general ranks the best and hence represents the long time average the best.

Data are also available from DHI's operational numerical model system covering the inner Danish waters, the Baltic Sea and the North Sea. The currents, salinity and water temperature have been modelled over a period of ten years from 1998 to 2008. The model has been progressively improved and the present analysis of the available model data will be based on data extracted from this operational model for the years 2004 – 2008. The analysis was carried for two locations; a northern location (location 1) and a southern location (location 2) both near the wind mill area. The locations are shown in Figure 4.3. These locations are expected to cover spatial variations in the hydrographic conditions within the wind farm area. At both locations the following parameters: current speed, current direction (analyses as time of the year where the current direction is N-going), water temperature, salinity are considered. The five years are for each parameter ranked according to the same methodology as applied for the measured data.

Results are shown in

Table 4.3 (current speed and direction) and

Table 4.4 (salinity and temperature). Taking all parameters into account year 2005 also ranks the best model data, and 2005 is hence chosen as the representative year in modelling the current field.

Table 4.1 Ranking of years based on calculations of annual deviations of measured precipita-
tion, wind speed, insolation and dissolved oxygen at Læsø Rende from the averaged
values for the entire period 2004 to 2008. Lowest rank is given to the year, where
the annual average is nearer the average for the entire period. Selected year (2005)
is marked with yellow.

Rank	Læsø precipitation	Læsø wind	Læsø insolation, year	Læsø insolation, summer	Læsø dissolved oxygen
1	2004	2005	2005	2005	2005
2	2005	2004	2004	2004	2006
3	2008	2007	2008	2006	2004
4	2007	2006	2007	2008	2008
5	2006	2008	2006	2007	2007

Table 4.2 Ranking of years based on calculations of annual deviations of measured salinity
(surface and bottom) and temperature (surface and bottom) at Læsø Rende from the
averaged values for the entire period 2004 to 2008. Lowest rank is given to the year,
where the annual average is nearer the average for the entire period. Selected year
(2005) is marked with yellow.

| Rank	Læsø salinity, surface, year	Læsø salinity surface, summer	Læsø salinity bottom, year	Læsø salinity bottom, summer	Læsø temp. surface, year	Læsø temp. surface, summer	Læsø temp. bottom, year	Læsø temp. bottom, summer
1	2006	2005	2008	2005	2004	2006	2006	2005
2	2004	2006	2006	2008	2006	2005	2008	2006
3	2005	2008	2005	2006	2005	2004	2005	2008
4	2007	2007	2004	2004	2007	2007	2004	2007
5	2008	2004	2007	2007	2008	2008	2007	2004
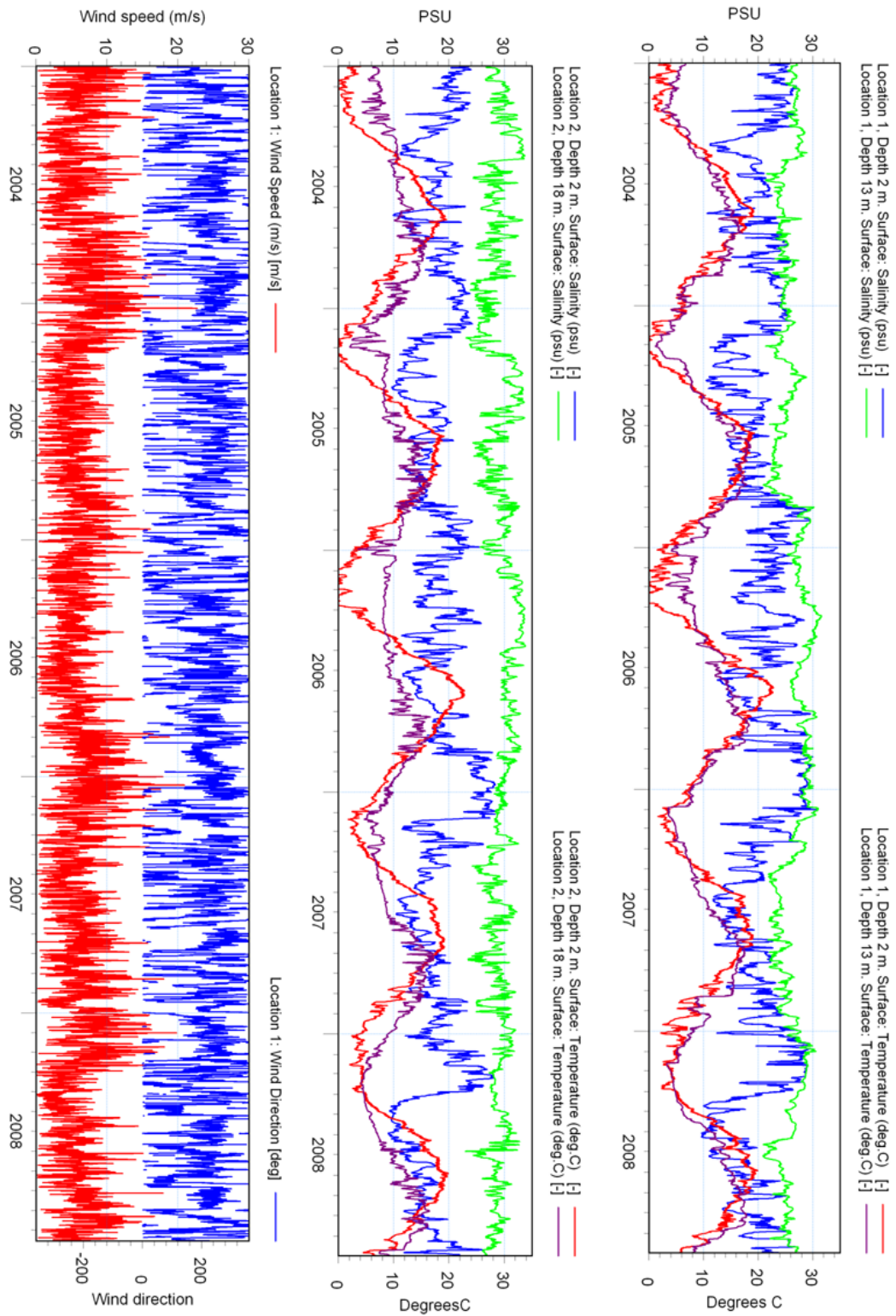
Figure 4.11   Salinities, temperatures, and wind speeds.

Table 4.3 Ranking of years based on calculations of annual mean deviations of current speeds and timely share of north-/south-going current direction from the averaged values for the entire period 2004 to 2008. Calculations based on model data at locations 1 and 2 (see Figure 4.3) at the top and bottom. Lowest rank is given to the year, where the annual average is nearer the average for the entire period. Selected year (2005) is marked with yellow.

Rank	Location 1, top, average current speed	Location 2, top, average current speed	Location 1, bottom, average current speed	Location 2, bottom, average current speed	Location 1, top, time of year where curr. direction is towards N	Location 2, top, time of year where curr. direction is towards N	Location 1, bottom, time of year where curr. direction is towards N	Location 2, bottom, time of year where curr. direction is towards N
1	2004	2006	2004	2005	2004	2005	2006	2005
2	2006	2005	2008	2008	2005	2004	2008	2008
3	2005	2004	2005	2007	2007	2008	2004	2007
4	2008	2007	2007	2004	2006	2006	2007	2004
5	2007	2008	2008	2006	2008	2007	2005	2006

Table 4.4 Ranking of years based on calculations of annual mean deviations of salinity and temperature from the averaged values for the entire period 2004 to 2008. Calculations based on model data at locations 1 and 2 (see Figure 4.3) at the top and bottom. Lowest rank is given to the year, where the annual average is nearer the average for the entire period. Selected year (2005) is marked with yellow.

Rank	Location 1, top, average salinity	Location 2, top, average salinity	Location 1, bottom, average salinity	Location 2, bottom, average salinity	Location 1, top, temperature	Location 2, top, temperature	Location 1, bottom, temperature	Location 2, bottom, temperature
1	2007	2007	2008	2004	2007	2007	2008	2005
2	2004	2005	2004	2005	2006	2006	2005	2007
3	2008	2004	2007	2008	2005	2005	2007	2006
4	2005	2008	2005	2007	2008	2008	2006	2004
5	2006	2006	2006	2006	2004	2004	2004	2008

5. References

/1/ http://www.waterforecast.com/Bansai/
/2/ http://www.blst.dk/Overvaagning/NOVANA/

Appendix B

Details of wave modelling

Details of wave modelling

1.   General

The annual wave climate is modelled with MIKE 21 SW during a representative year for the baseline study. Details of the model description, set up and choice of the modelling period are given below.

As a part of the environmental impact, the effects of the wind mills on the incoming waves have been included in the wave prediction. The calculation of the wave reflection around each wind mill foundation is carried out using DHI's tool WAMIT. The scientific background of this model is shortly described below.

2.   Model description

The wave climate was modelled based on DHI's numerical wave model, MIKE 21 SW, which has been used in numerous studies on waves. MIKE 21 Spectral Wave Model is a third generation spectral wind-wave model. The model simulates the growth, decay and transformation of wind generated waves and swells in offshore and coastal areas.

Mike 21 SW included two different formulations:

- Fully spectral formulation
- Directional decoupled parametric formulation

The fully spectral formulation is based on the wave action conservation equation, as described in e.g. Komen et al (1994) and Young (1999), where the directional-frequency wave action spectrum is the dependent variable.

The directional decoupled parametric formulation is based on a parameterization of wave conditions conservation equation. The parameterization is made in the frequency domain by introducing the zeroth and first moment of the wave action spectrum as dependent variables following Holthuijsen (1989).

MIKE 21 SW solves the spectral wave action balance equation. At each mesh point, the wave field is represented by a discrete two-dimensional wave action density spectrum. The model includes the following physical phenomena:

- Wave growth by action of wind
- Non-linear wave-wave interaction
- Dissipation by white capping
- Dissipation by depth induced wave breaking
- Dissipation due to bottom friction
- Refraction due to variations in the water depth
- Wave-current interaction

The discretization of the governing equation in geographical and spectral space is performed using cell-centered finite volume method. The time integration is performed using a fractional step approach where a multi-sequence explicit method is applied for the propagation of the wave action.

MIKE 21 SW is based on flexible meshes which allow high resolution of the area of interest and coarser spatial resolution elsewhere.

A short description of MIKE21 SW can be found under:
http://www.dhigroup.com/Software/Download/DocumentsAndTools/ShortDescriptions/Marine.aspx

3. Local model setup

The purpose of this wave study is to present the dampening effect of the wind mill farm on the annual wave field. A full year is modelled to visualize the individual impact of each wind mill.

A fine mesh is required (5.10^{-3}km^2) in the area of the future wind mill farm.

Despite the flexible mesh used by Mike 21 SW, the simulation time does not allow for computing a full year with a large model over the entire North Sea with such a fine local resolution. Consequently for time calculation reasons it has been decided to create a local model.

The local model covers an area of 41.5 km by 54 km which contains Anholt Island and extends to the west to Djursland as seen in Figure 3.1.
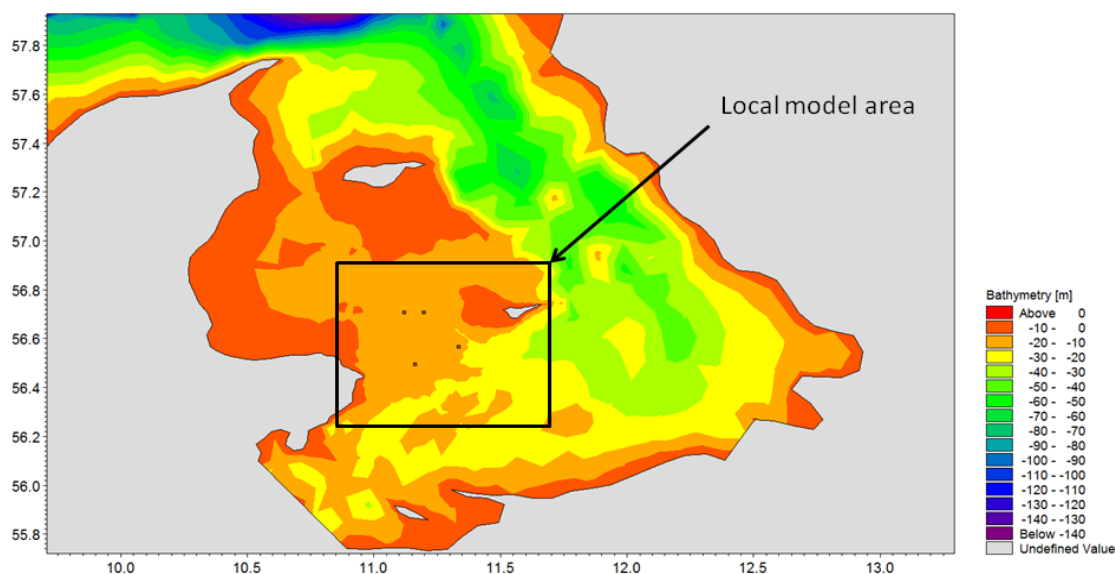
Figure 3.1   Extent of the local wave model domain. The four points indicate the wind farm
             area delimitation. The model is defined in geographical horizontal coordinates.

Due to its relatively small scale and for calculation time reasons the local model is applying the decoupled parametric formulation and a quasi stationary solution technique. This method, which can be used over relatively small domains, is a very fast computationally numerical method and allows the required high spatial resolution.

The bathymetry and the flexible mesh are depicted in Figure 3.2 and Figure 3.3. The main part of the domain is covered by a grid size about 1 km^2; the areas of interest are described by a very fine grid about 5.10^{-3} km^2 equivalent to 100 m length. A transition from the coarser mesh to the very fine mesh is carried out in a couple of cells surrounding those areas. The resolution at the west coast of Anholt and at Djursland has been increased at the early stage of the study in case a detailed study of the impact of the wind farm on the sediment transport at these two coasts had to be carried out.
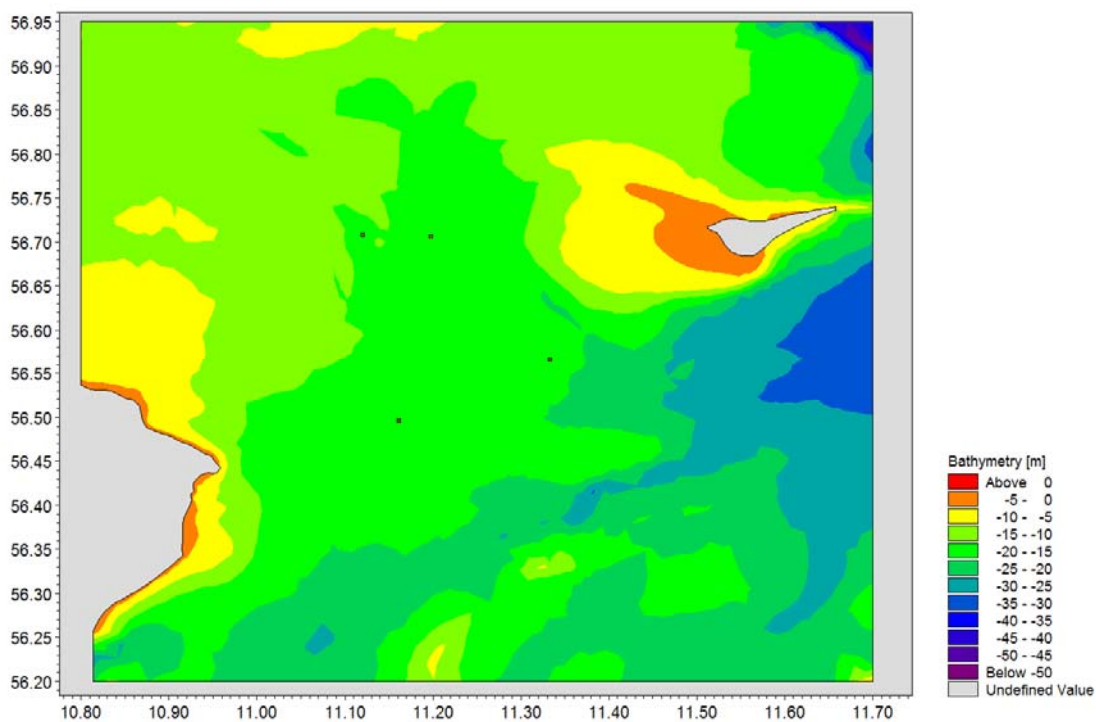
Figure 3.2   Extent of the local wave model and bathymetry. The four points indicate the
              wind farm area delimitation. The model is defined in geographical horizontal co-
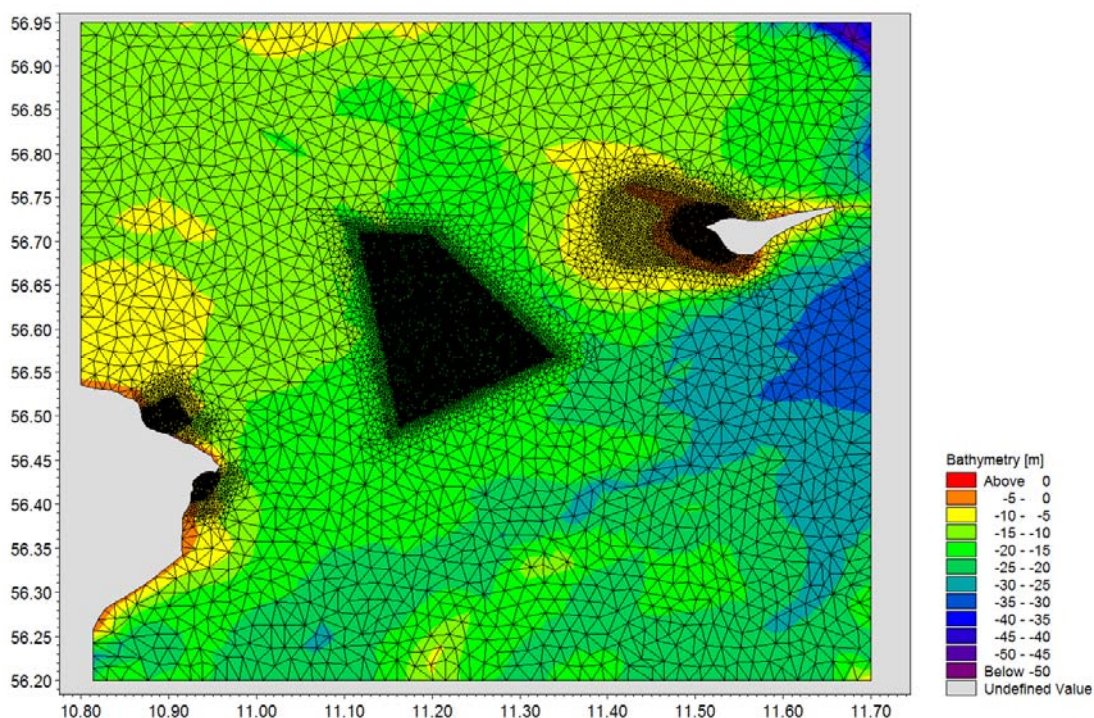   ordinates.

Figure 3.3   Extent of the local wave model, mesh and bathymetry. The grid size is about 1 km^2 and decreases to 5.10^{-3} km^2 in the area of interest. The model is defined in geographical horizontal coordinates.

Wind forcing and hydrodynamics conditions (water level, current data) are extracted from the existing regional model described in Section 5.3.2 in the main report. The model has been defined by 5 open boundaries indicated in Figure 3.4 (code 2 to code 6). The boundary conditions applied in the local wave modelling are supplied by the regional model and vary in time and along the boundaries. The parameters used to define the boundary conditions are the significant wave height (average of the largest 1/3 of the waves), the wave period at spectral peak, the mean wave direction and the directional standard deviation.
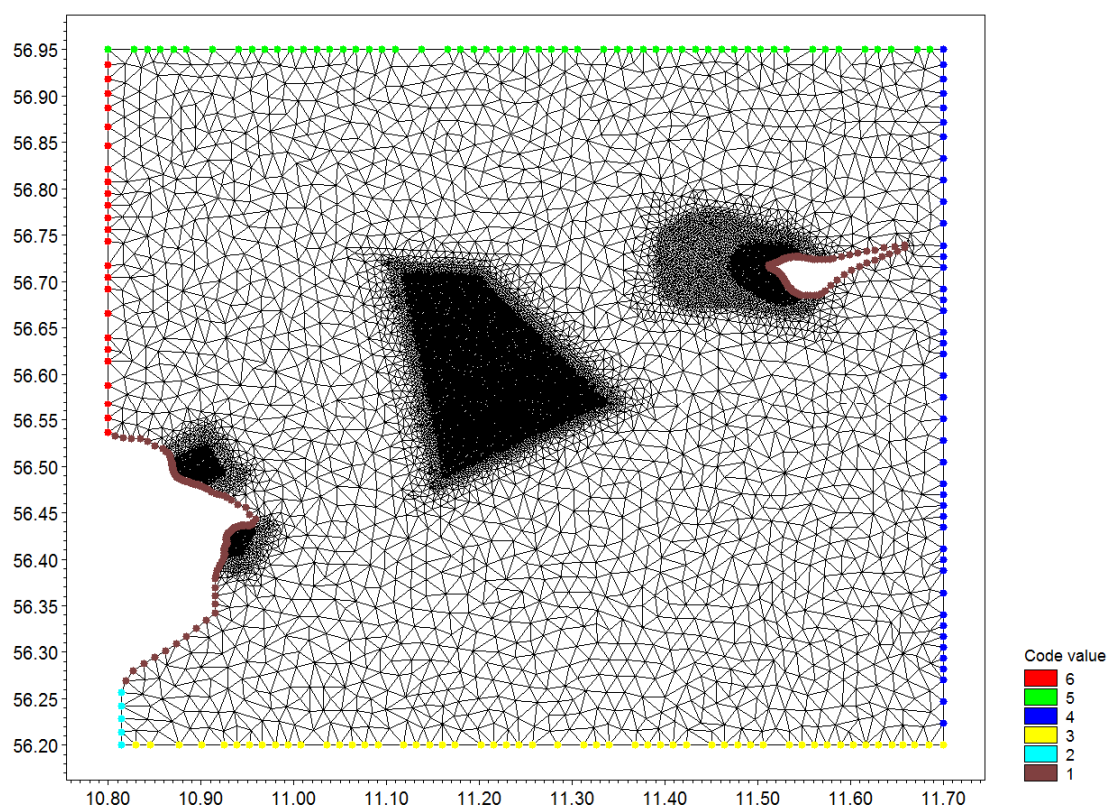
Figure 3.4   Mesh and definition of the open boundaries (referred by code 2 to code 6) of the local wave model. The model is defined in geographical horizontal coordinates.

4.   Choice of modelling year

The selection of the modelling period for calculation of the annual wave climate is carried out based on analysis of the wind climate in the years 1998-2008 at location 2 indicated in Figure 4.3. Wind roses for each year are shown in Figure 4.2 and Figure 4.3 as well as the mean wind climate for the entire period. The results presented are extracted from the 2D wind fields from Vejr2 used as input in the regional wave model (see Section 5.3.2 of the main report). The data have been validated against measured wind data at Anholt in /1/. The wind field is seen to have some variation with regard to wind speeds as well as distribution on wind directions from year-to-year. The years 1998, 2001, 2003, 2004, 2005 and 2007 are seen to have a wind climate with regard to wind speeds and directions similar to the mean wind climate. Year 2005 was selected among these.

Note that the selection of 2005 for the modelling of the annual wave climates is consistent with the calculations of annual current conditions which have been carried out for the same year.
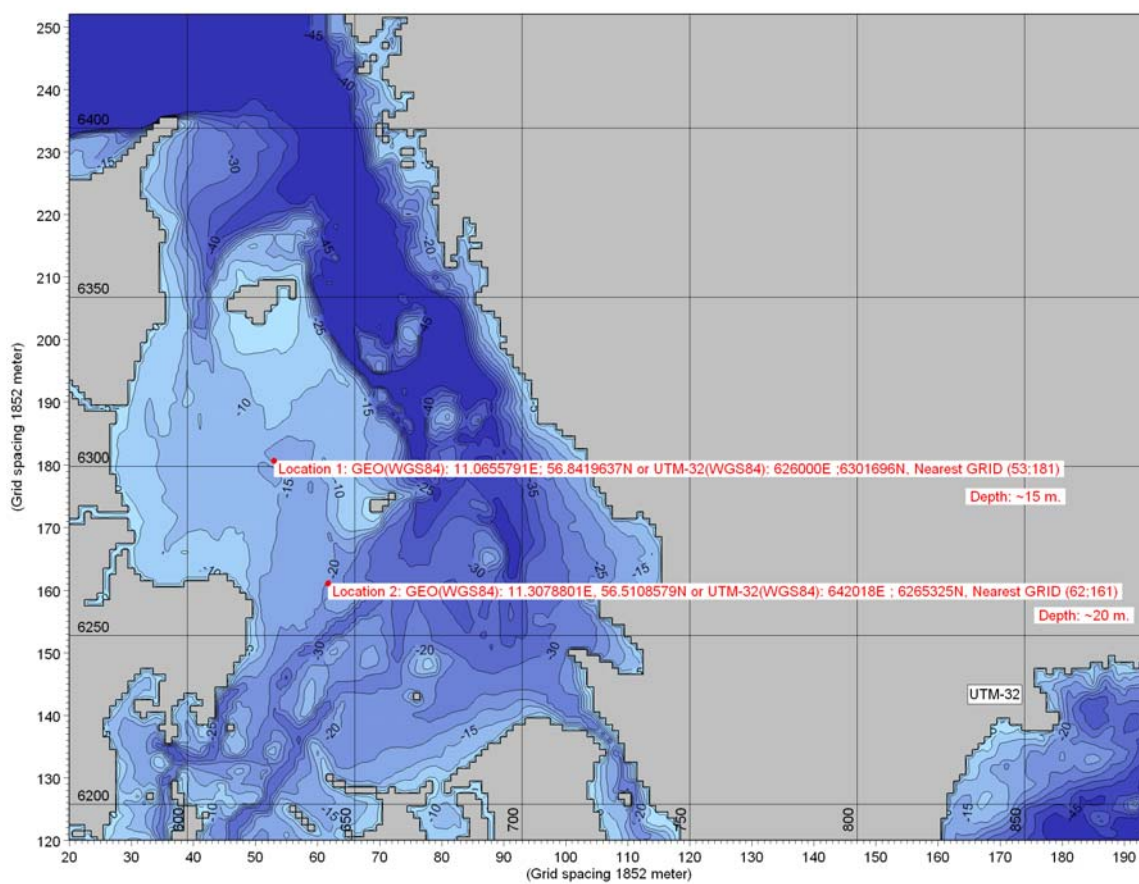
Figure 4.1   Location where the wave climates from 1998 to 2008 have been extracted. The choice of the annual modelling period of the wave climate is based on wind climates at location 2.
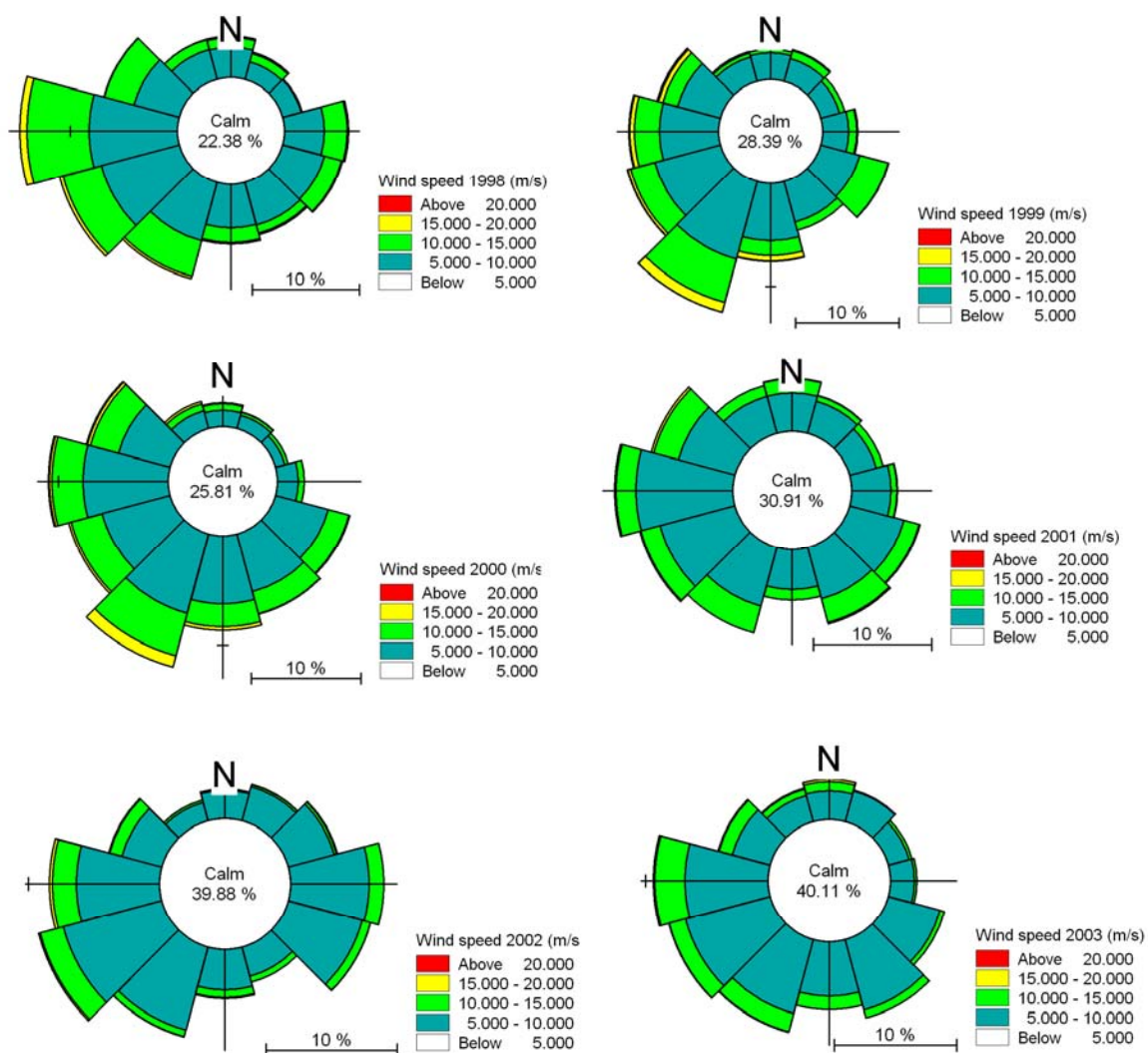
Figure 4.2   Wind roses from Vejr2 extracted at location 2 (indicated on Figure 4.3) for the years 1998-2003.
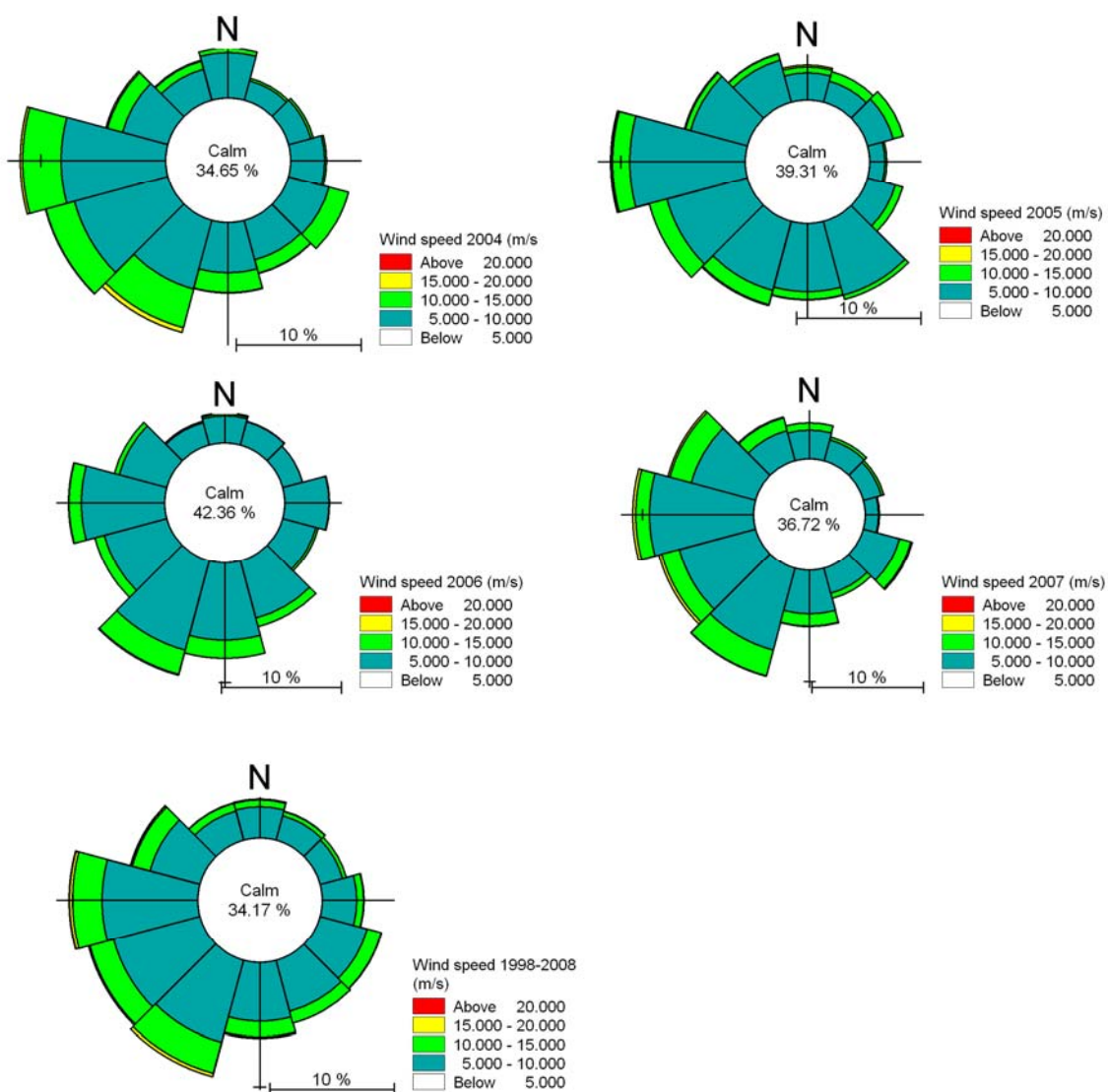
Figure 4.3   Wind roses from Vejr2 extracted at location 2 (indicated on Figure 4.3) for the
              years 2004-2008 and for the 10-year period 1998-2008.

5.   Calibration and validation

Calibration and validation of the local wave model defined above are presented in
this section.

The calibration and validation of the local wave model were carried out by comparing
results with results from the existing regional model (see Section 5.3.2 of the main
report) in terms of annual wave characteristics (significant height and mean wave
direction) variations at one specific location (11.2°E, 56.6°N (longitude, latitude), see

Figure 5.1) and instantaneous 2D wave fields at different time steps. Validation of
the regional model was described in Section 5.3.2 in the main report.
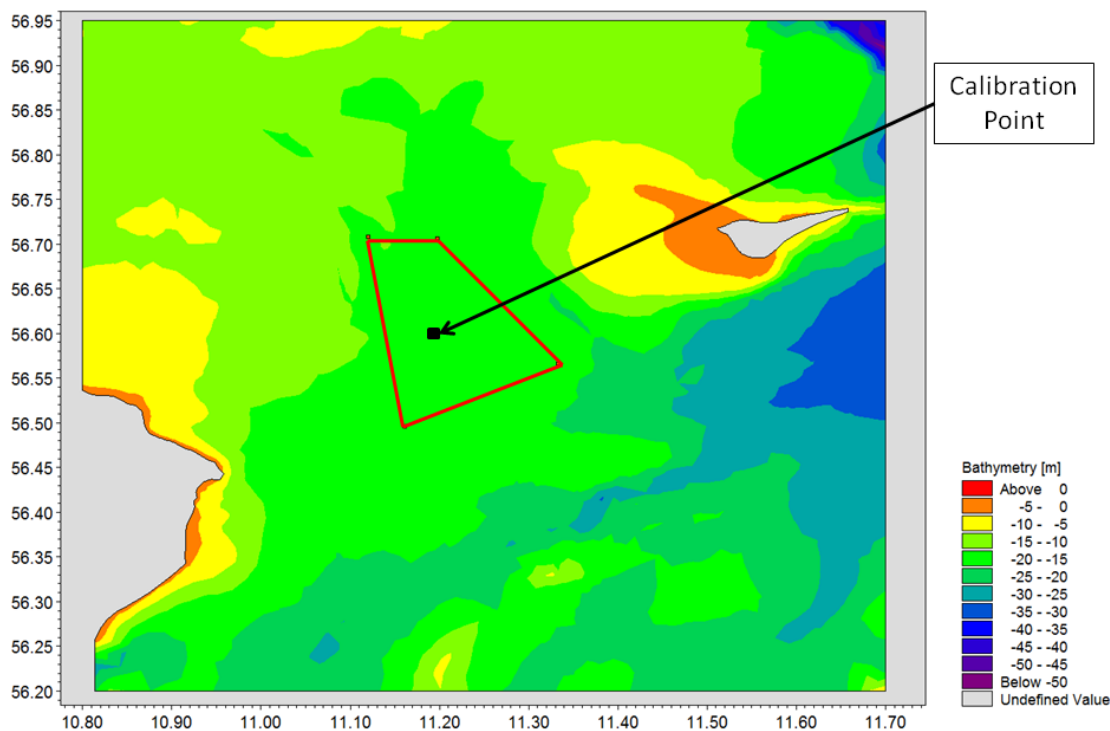

Figure 5.1   Location of the point used for the calibration of the local wave model.

The most important calibration factors used in the local decoupled quasi-stationary
formulation are listed below.

Wind forcing: The formulation of the wave generation by wind (Directional decoup-
led parametric formulation) is based on empirical relationships. It is assumed that

- the directional spreading of the energy from the wind follows a $\cos^2 q$-
  distribution

- the average frequency is independent of the direction

The Spectral Wave module includes 5 wind formulations. The SPM84 formulation has
been chosen in this case. SPM84 formulation is based on expressions derived from
the Shore Protection Manual (1984) formulation for the wave growth for fetch-
limited sea states in deep water using a power fit for the growth equations. Com-
bined to the other calibration parameters, the SPM84 wind formulation permits to
get the most relevant wave fields.

Bottom friction: the bottom friction is described through a Nikuradse roughness, k_N. A quite small value of 1.10^{-5}m is used in the whole domain.

Wave breaking (depth induced): the Gamma parameter which controls the limiting water depth condition is set up to 0.8. The two other parameters available with the decoupled parametric formulation, the alpha parameter and the wave steepness have been set to 2 and 4 respectively in order to reduce the wave dissipation which tends to be slightly too strong in the local model especially under severe wind conditions.

Figure 5.2 and Figure 5.3 display the significant wave heights and mean wave directions predicted by the regional (blue curve) and local (green curve) models during 2005 at the calibration point indicated on Figure 5.1.
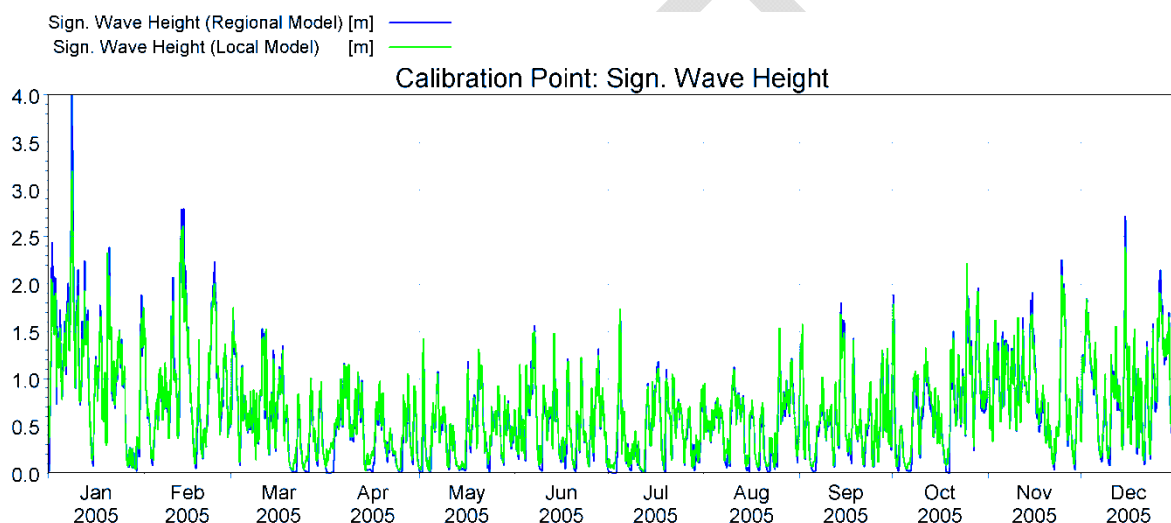

Figure 5.2   Comparison of the significant wave height predicted by the regional (blue curve) and local (green curve) models at the calibration point indicated on Figure 5.1.
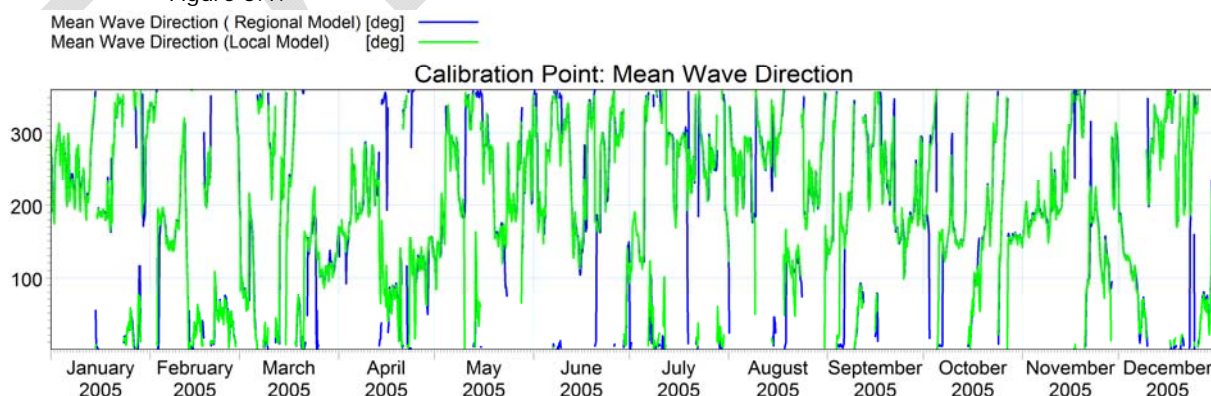

Figure 5.3   Comparison of the mean wave direction predicted by the regional and local models at the calibration point indicated on Figure 5.1.

The local model agrees well with the regional model. The time variation of the wave height is well captured by the local model at the calibration point. It can be seen that the highest peaks of wave height tend to be slightly underestimated for wave height exceeding 2 m. The wave height at the extraction point during the storm that occurred mid January 2005 is 20% smaller than the wave height predicted by the regional model; apart from this storm, the difference in the wave height is below 10% error. These events are furthermore really sporadic. Over all in term of wave height and phase at the calibration point, the local model is very similar to the regional model. Moreover, the wave study is dedicated to be a comparative study in order to see the impact of the wind mills on the wave climate; comparison of wave fields with and without wind mill effects should not be affected by these small differences in wave height. Design and operational wave heights are covered in a separate study, see Section 5.5.3 in the main report.

Concerning the mean wave direction the two models predict almost identical results. The only differences are mainly due to the character quasi-stationary of the local model. The changes in direction are not instantaneous in that case; they are smoothed compared to the results of the regional model run with an instationary formulation.

Figure 5.4 to Figure 5.7 represent instantaneous wave fields predicted by the local wave model (upper plot on each figure) and the regional wave model (lower plot on each figure) for wind conditions coming from different sectors. It can be seen that the local wave model predicts results which are in good agreement with the existing regional model. Wave fields from both wave models present similar patterns. Under storm weather conditions, the local wave model tends to underestimate wave height in the project especially for waves directed towards the north-east (Figure 5.4) and towards south-east (Figure 5.7).

To conclude the calibration work done for the local model gives satisfactory results. The comparative study of the impact of the wind farm on the annual waves (covering 2005) will be carried out using the calibrated local wave model.
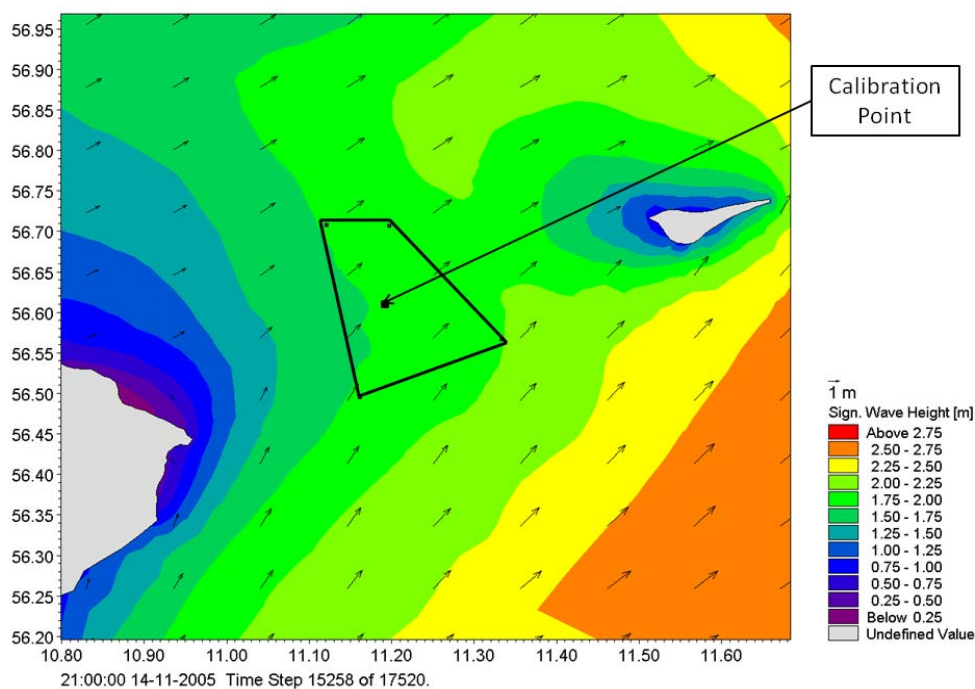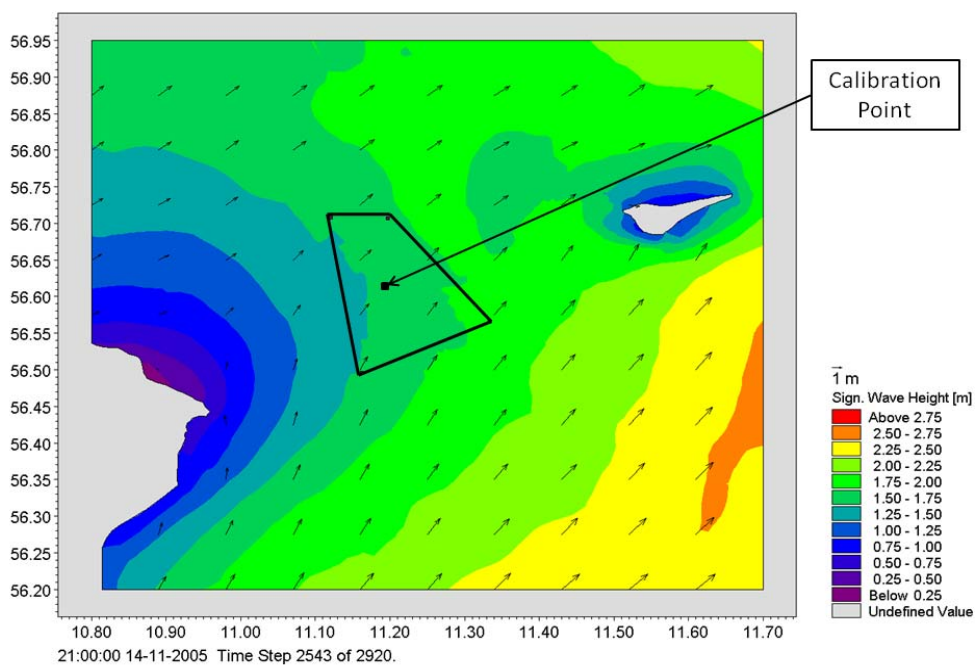
Figure 5.4   Instantaneous wave field characteristics (significant wave height and mean wave direction) from the local model (up) and the existing regional model (down) extracted on 14-11-2005 at 21:00 pm.
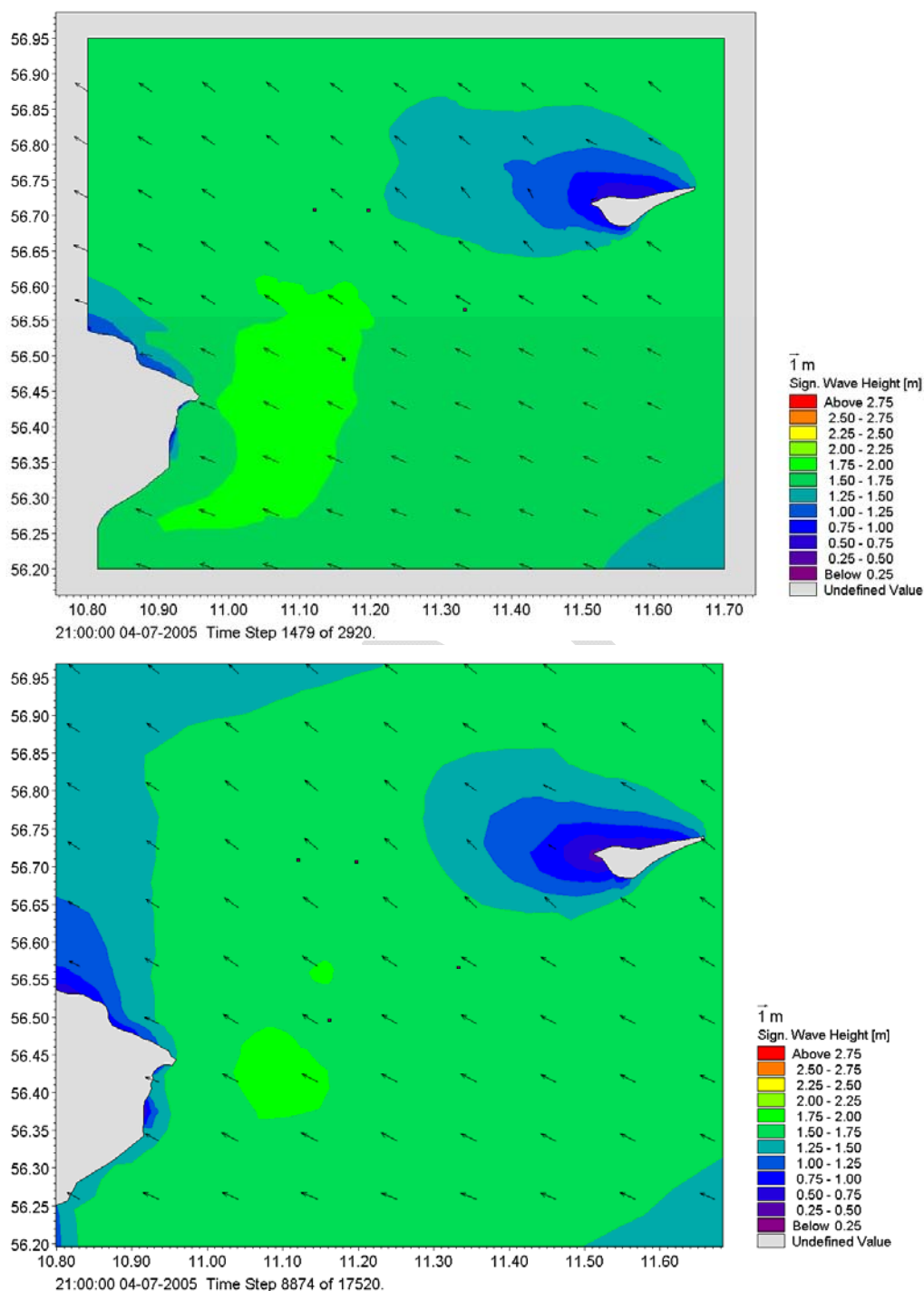
Figure 5.5   Instantaneous wave field characteristics (significant wave height and mean
              wave direction) from the local model (up) and the existing regional model
              (down) extracted on 04-07-2005 at 9:00 pm.

Figure 5.6   Instantaneous wave field characteristics (significant wave height and mean wave direction) from the local model (up) and the existing regional model (down) extracted on 01-10-2005 at 9:00 am.
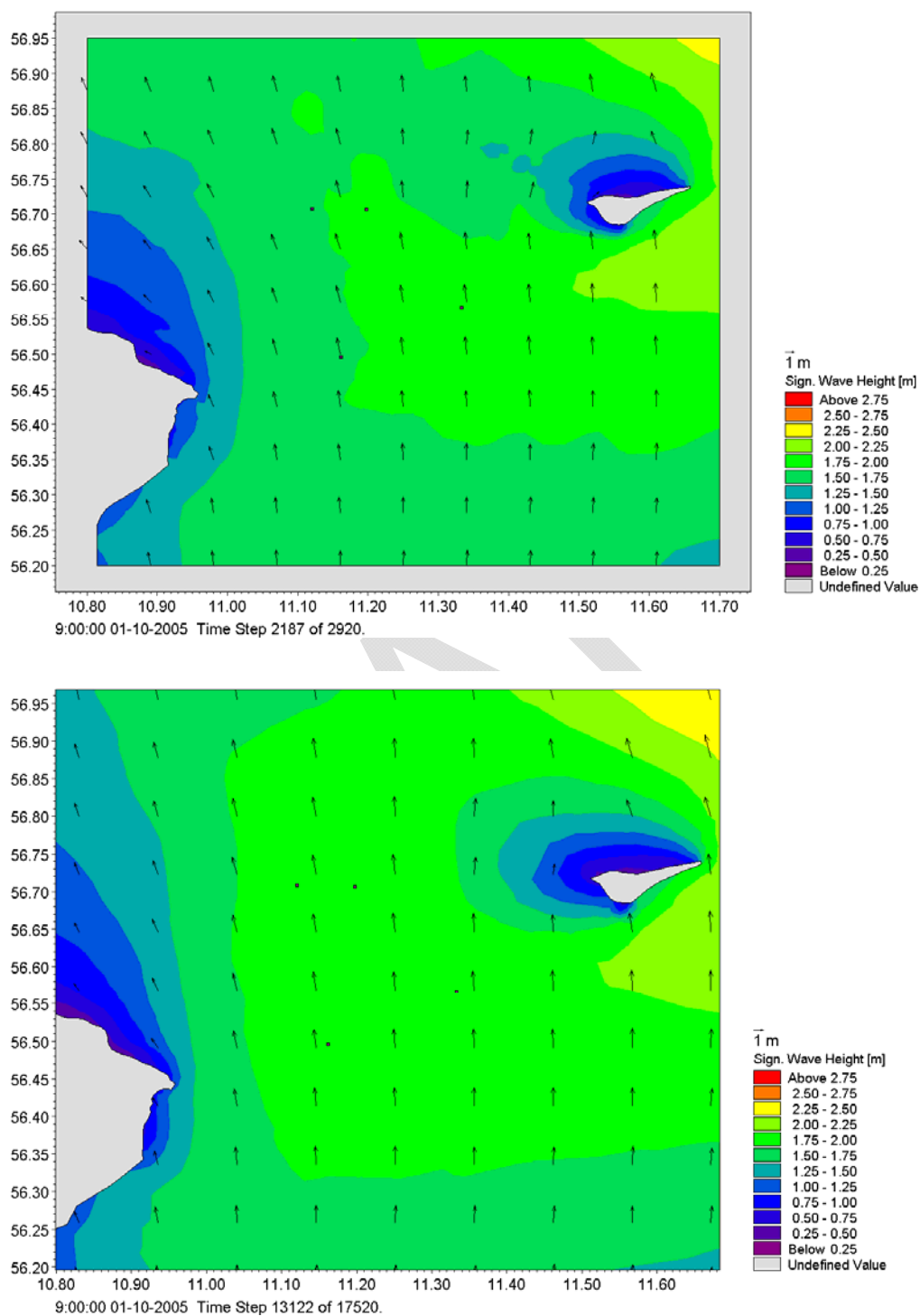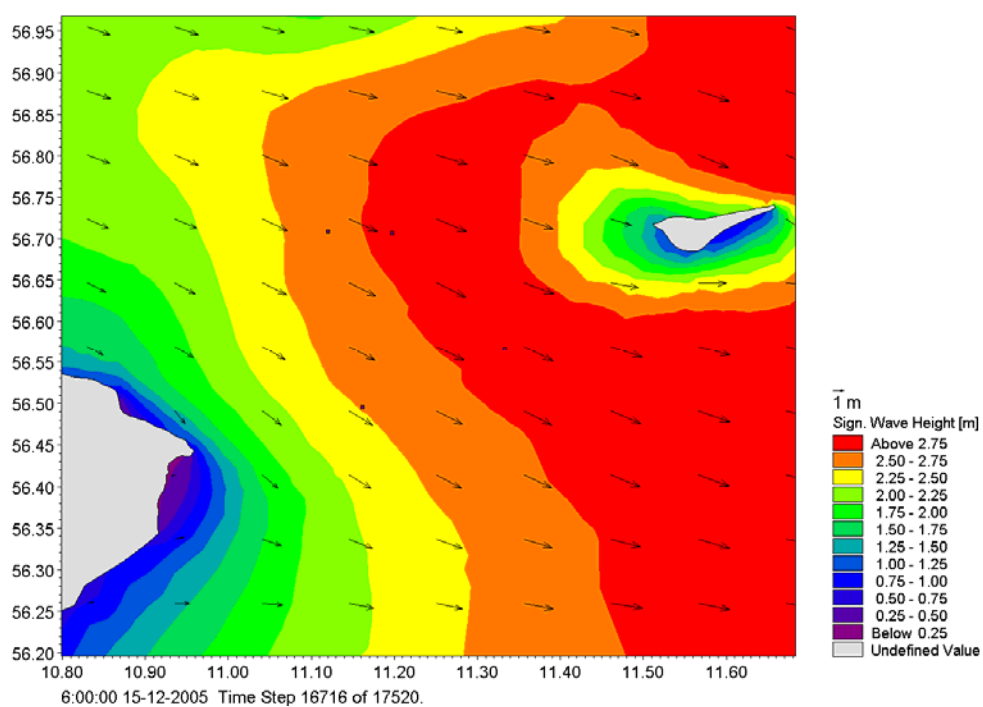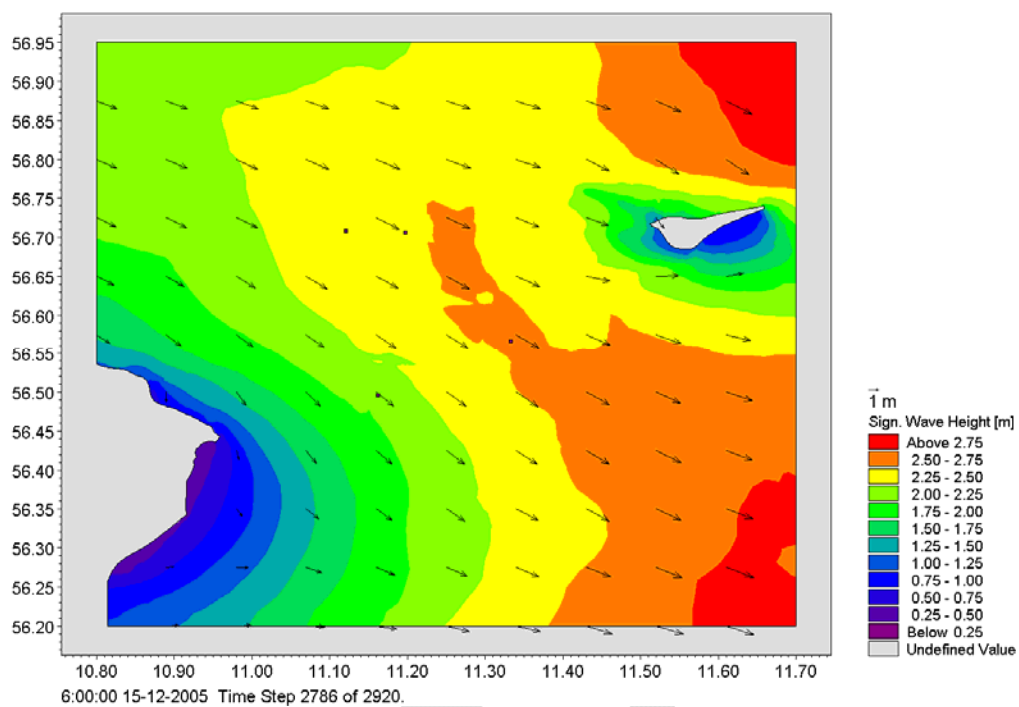
Figure 5.7 Instantaneous wave field characteristics (significant wave height and mean wave direction) from the local model (up) and the existing regional model (down) extracted on 5-12-2005 at 6:00 am.

6. Interaction between incoming waves and wind mill foundations - assessment of the impacts of reflection/diffraction effects on the wave field.

When waves hit a wind turbine foundation a part of the energy will be reflected. This will change the wave climate in the power plant and in the leeward area of the plant. The change of wave heights depend on

1. Water depth
2. Incoming wave period
3. The layout of the foundation
4. The number and spacing between the wind turbines

In order to quantify the wave height changes a 3-step procedure has been used:

1. Detailed calculations of the wave climate around a single wind turbine

2. The results are parameterised

3. The change in wave climate over the entire power plant area is calculated with SW, which is a spectral wind model.

The effect of the single wind turbine will be discussed in the following section.

6.1 Energy flux

In the calculation of the wave reflection around each individual foundation, the bed friction and possible wave breaking is neglected. By neglecting these two properties, the wave field can be described by potential theory.

The undisturbed wave energy flux over a plane bed is found from the following general expression:

$$E_f = \tfrac{1}{T} \int_0^T \int_{-h}^{\eta} (p^+ + \tfrac{1}{2}\rho(u^2 + v^2)) \cdot u \cdot dzdt \tag{1}$$

Where p^+ is the excess pressure, u and v are the horizontal and vertical velocity components, T the wave period, h the water depth. Using 1$^{\text{st}}$ order approximation the expression can be reduced to the following:

$$E_f = \tfrac{1}{T} \int_0^T \int_{-h}^{0} p^+ u \cdot dzdt \tag{2}$$

The energy flux in incoming waves can be found to be:

$$E_f = \tfrac{1}{16}\rho g H^2 c\left(1 + \frac{2kh}{sinh(2kh)}\right)$$ (3)

Where ρ is the density, g gravitational acceleration, H the wave height, c the wave celerity, k the wave number ($k = 2\pi/L$), and h the depth.

The energy that is reflected is equal to the incoming flux minus the transmitted flux. The transmitted flux can be found by integrating from the foundation surface to infinity perpendicular to the wave direction.

$$\widehat{E}_{f,transmitted} = \int_{CL}^{\infty}\left[\tfrac{1}{T}\int_0^T \int_{-h}^0 p^+ \cdot u \cdot dz dt\right] ds$$ (4)

Where $\widehat{E}_{f,transmitted}$ is the integrated wave energy flux from the CL ($y = 0$) to infinity.

In case of a cylindrical foundation the percentage of reflected wave energy can be related to the energy flux approaching the foundation multiplied with the diameter D of the vertical cylinder. (Note that only one half plane has been used in the integration above, wherefore the result should be divided with half the diameter D):

$$Re\,f_\% = \frac{E_f \cdot Y - \widehat{E}_{f,transmitted}}{E_f \cdot \tfrac{1}{2}D}100\%, \qquad Y \to \infty$$ (5)

In the general case, as in this study, the reflected wave energy can be related to a specific blocking width. This means that all the energy over this equivalent width is reflected. The expression for this is as follows:

$$Re\,f_m = 2\frac{E_f \cdot Y - \widehat{E}_{f,transmitted}}{E_f}, \qquad Y \to \infty$$ (6)

As only one half plane has been taken into account a factor two is introduced in the equation above.

The wave field around the foundation is found using WAMIT, as no analytical solution of the wave field is available for the structure. WAMIT is a panel method that finds the diffracted wave field for an arbitrary shaped structure. The theory is based on potential theory, see /2/.

The transmitted wave energy integration to infinity is sketched in Figure 6.1. It is not possible to find the velocity and pressure accurately close to the structure due to numerical inaccuracies, cf. WAMIT manual /2/. Therefore the energy flux across a line beginning at the centreline but on the lee side of the structure, (for example at x = 10 m and y = 0) and going to infinity is used instead.

The procedure includes an asymptotic solution as the results cannot be integrated all the way to infinity based on the WAMIT results alone.
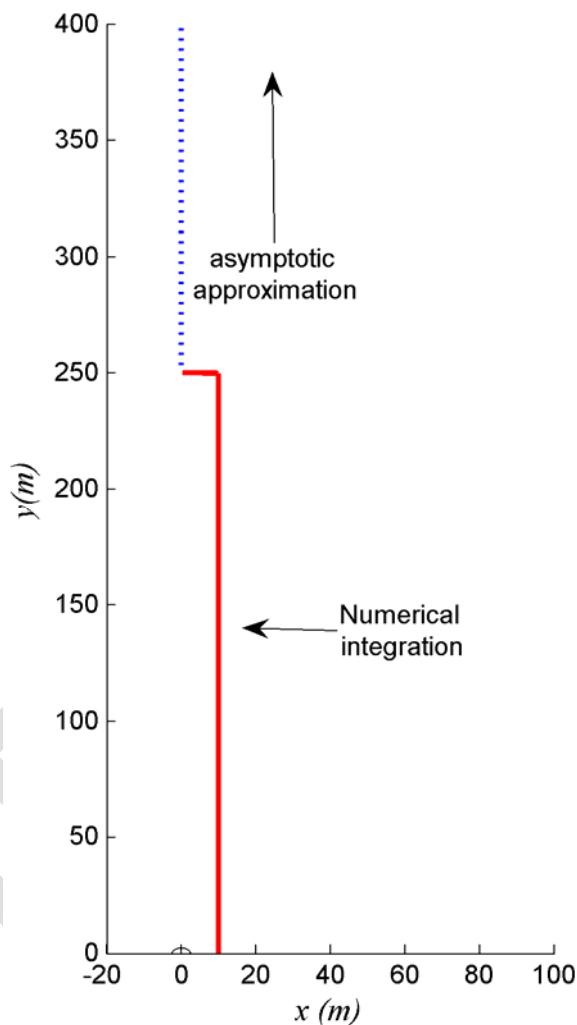

Figure 6.1   The lines of integration. The foundation has its centre in (x, y) = (0, 0). The waves approach the structure from left to right along the x-axis.

Figure 6.2 shows two examples of the panels resolving the foundation. One is located in 7.5 m water depth and another in 11.0 m. The variation of the equivalent width is given in Figure 6.3. It is clear that for increasing wave period the blocking effect decreases. For wave periods over 12 s the equivalent width is smaller than 0.5 m. Results as presented in Figure 6.3 have been tabulated and included in the SW wave modelling.
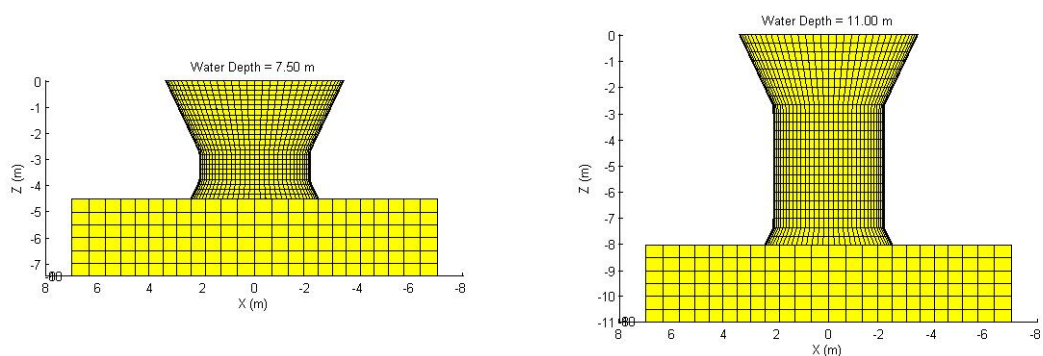
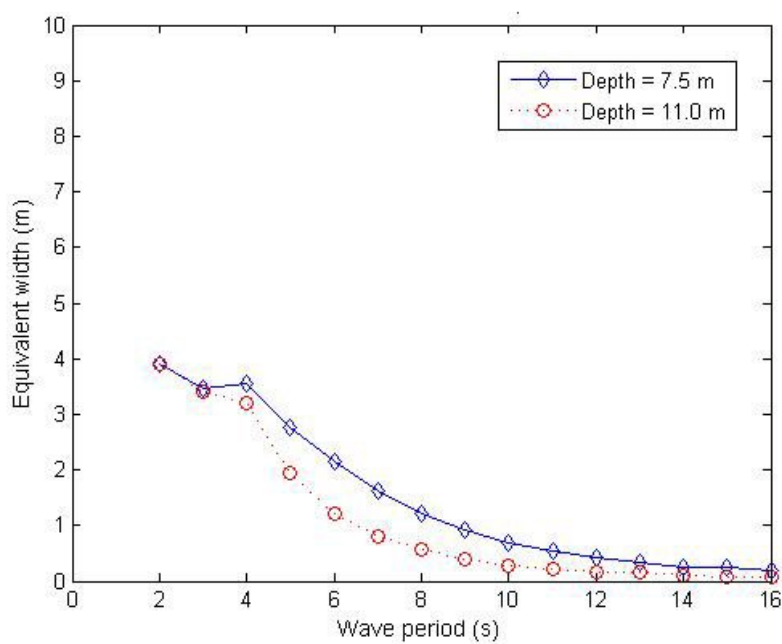Figure 6.2   Two examples of the panels used in the analyses of reflected wave energy.

Figure 6.3   Reflection on 7.5 and 11 m water depth, respectively. The equivalent width is $Re\,f_m$ as defined in eq. 6.

7. References

/1 DHI 2009, Anholt Offshore Wind Farm. Metocean Data for Design and Operational Conditions.

/2 J. N. Newman, C. H. Lee and F. T. Korsmeyer, *WAMIT version 5.3. A radiation diffraction panel program for wave-body interactions*, (Dept. of Ocean Eng., M.I.T., Cambridge, MA, 1995).

/3 J. N. Newman, Marine Hydrodynamics, (The MIT Press, Cambridge, MA, 1977)

DRAFT

Appendix C

Details of numerical Ecosystem modelling

Details of numerical Ecosystem modelling

1. General

The models applied for this project belong to the DHI models entailed in the MIKE Software suite. The driving hydrodynamic model is the MIKE 3 FM (described in detail in Annex A) whereas the ecological model is developed in the ECOLab model system. The basic ECOLab model describes algal growth and the cycling of nutrients (named the eutrophication module or EU model). This model is enlarged to include sedimentation and re-suspension of fine sediments or mud (named the mud-transport module or MT model).

2. Ecosystem model description

2.1 Standard Eutrophication model

The Standard Eutrophication models include one state variable for dissolved inorganic nitrogen (DIN) which includes total ammonium (NH_4), nitrate (NO_3) and nitrite (NO_2). Further it does not include dissolved organic matter (C, N and P). In certain marine areas the primary production is N-limited during summer. The pool of DON may have a potential for being utilized by phytoplankton. In coastal areas dominated by run-off from land a significant fraction of DON is in the form of inert DON or CDON coming from land and having a low degradation rate. The main process of incorporation CDON into food web is mediated through photo oxidation of the associated CDOC into smaller molecules, which are assimilated and degraded by bacteria. Implementation of structures like piers, foundations to wind mills or artificial reefs introduces a new hard substrate and thereby also introduces a new habitat with species adapted attaching and living on and around these structures. Massive settling of the blue mussel *Mytilus edulis* on hard surface is well known. The mussels filter the water for plankton and particulate organic matter.

In aerated systems most inorganic nitrogen will be in the form of NO_3-N, with only a minor fraction of the inorganic N as total ammonium and an even smaller fraction as NO_2-N. However, in e.g. stratified systems the supply of oxygen to lower layers is limited because of low vertical mixing and low primary production. In such systems there will be a build up of reduced substances like H_2S and total ammonium in the lower layers. These substances represent an oxygen demand which can be released when oxygen becomes available e.g. by vertical mixing of the water column.

The oxidation of NH_4 is a two step reaction mediated by bacteria with nitrite as intermediate product:

$$2NH_4^- + 3O_2 \rightarrow 4H^+ + 2NO_2^- + 2H_2O \quad \text{and}$$
$$2NO_2^- + 2O_2 \rightarrow 2NO_3^-$$
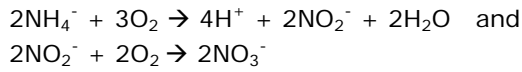
To be able to describe this oxygen demand it is necessary to include total ammonium and nitrate as separate state variables in the model.

In systems with the oxygen concentration below 1 g/m^3, pocket or micro niches with total anaerobic condition may occur and SO_4^{--} may be used as electron acceptor under production of H_2S.

$$H_2SO_4 + 2CH_2O \rightarrow 2CO_2 + 2H_2O + H_2S$$
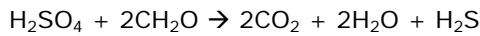
In marine or brackish waters high SO_4^{--} concentrations will ensure the SO_4^{--} respiration not being SO_4^{--} limited.

H_2S is oxidised chemically or mediated by sulphur oxidizing bacteria in a two step process:

$$2H_2S + O_2 \rightarrow 2S + 2H_2O \quad \text{and}$$
$$2S + 3O_2 + 2H_2O \rightarrow 2H_2SO_4$$
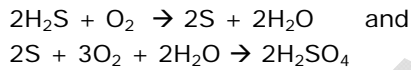
The standard EU model is presented in Figure 2.1 represented by the carbon cycle. For a more detailed description of the C, and P cycle, see the reference manual for the standard EU model, /1/, /2/.

1. Production, phytoplankton
2. Sedimentaion, phytoplankton
3. Grasing
4. Extinction
5. Excretion, phytoplankton
6. Extinction, zooplankton
7. Respiration, zooplankton
8. Mineralisation of detritus
9. Sedimentation of detritus
10. Mineralisation of sediment
11. Accumulation in sediment
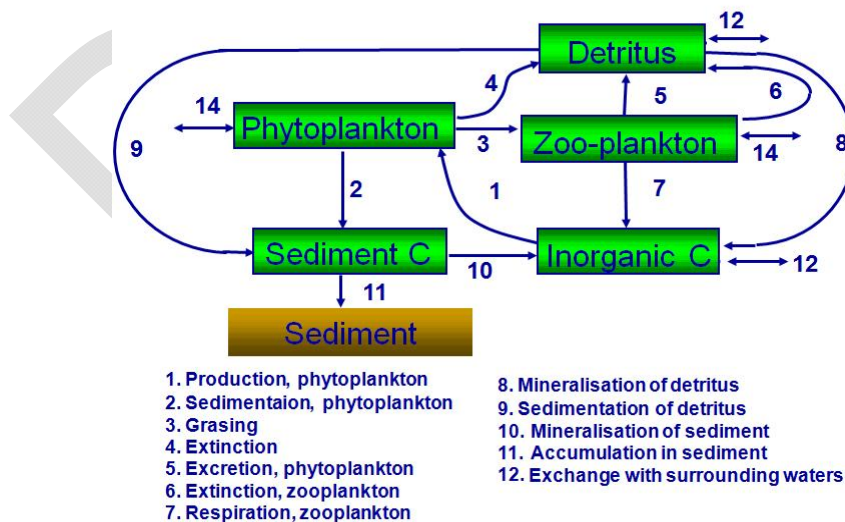12. Exchange with surrounding waters

Figure 2.1   State variables and processes for carbon in the standard Eutrophication model.

2.2   **Extended Eutrophication model for the Anholt wind farm**

The standard EU module is extended with the NH_4, NO_{3+2}, H_2S and CDON and includes a number of state variables and processes. Flow diagrams on C, N, and P of the extended Eutrophication model are presented in Figure 2.2, Figure 2.3, Figure 2.4.
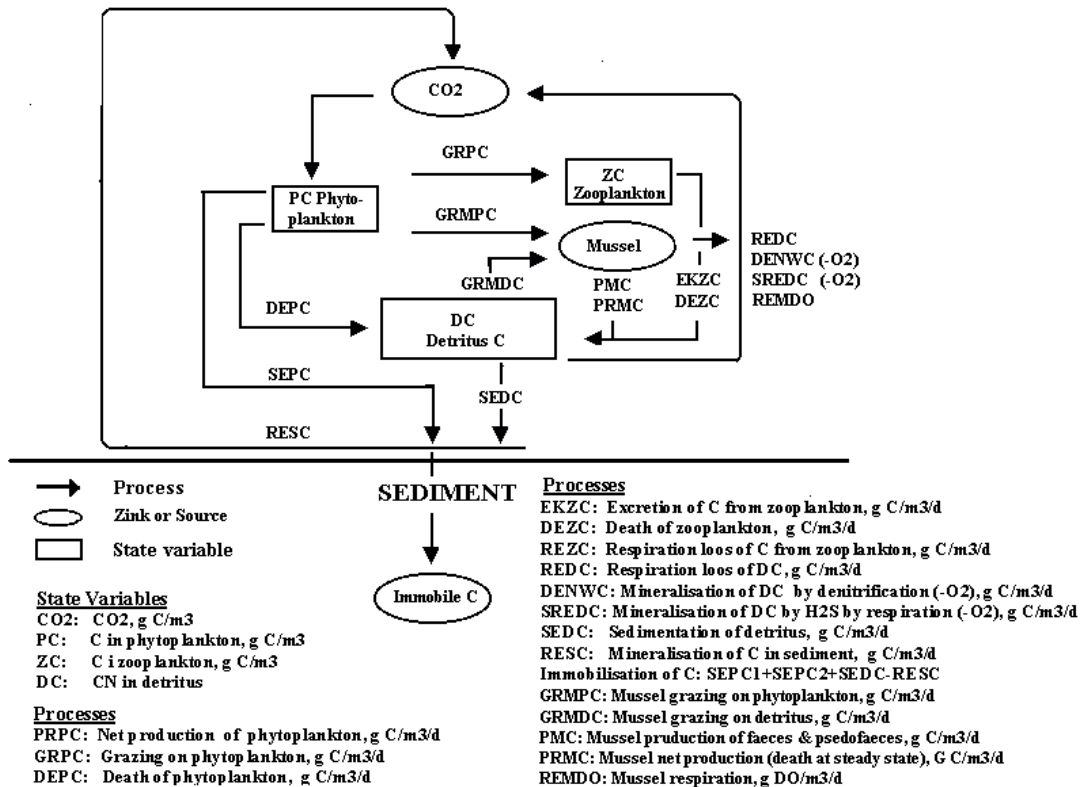

State Variables
CO2:   CO2, g C/m3
PC: C in phytoplankton, g C/m3
ZC: C i zooplankton, g C/m3
DC: CN in detritus

Processes
PRPC: Net production of phytoplankton, g C/m3/d
GRPC: Grazing on phytoplankton, g C/m3/d
DEPC: Death of phytoplankton, g C/m3/d

Processes
EKZC: Excretion of C from zooplankton, g C/m3/d
DEZC: Death of zooplankton, g C/m3/d
REZC: Respiration loos of C from zooplankton, g C/m3/d
REDC: Respiration loos of DC, g C/m3/d
DENWC: Mineralisation of DC by denitrification (-O2), g C/m3/d
SREDC: Mineralisation of DC by H2S by respiration (-O2), g C/m3/d
SEDC: Sedimentation of detritus, g C/m3/d
RESC: Mineralisation of C in sediment, g C/m3/d
Immobilisation of C: SEPC1+SEPC2+SEDC-RESC
GRMPC: Mussel grazing on phytoplankton, g C/m3/d
GRMDC: Mussel grazing on detritus, g C/m3/d
PMC: Mussel pruduction of faeces & psedofaeces, g C/m3/d
PRMC: Mussel net production (death at steady state), G C/m3/d
REMDO: Mussel respiration, g DO/m3/d

Figure 2.2   Carbon flow of the extended EU model.
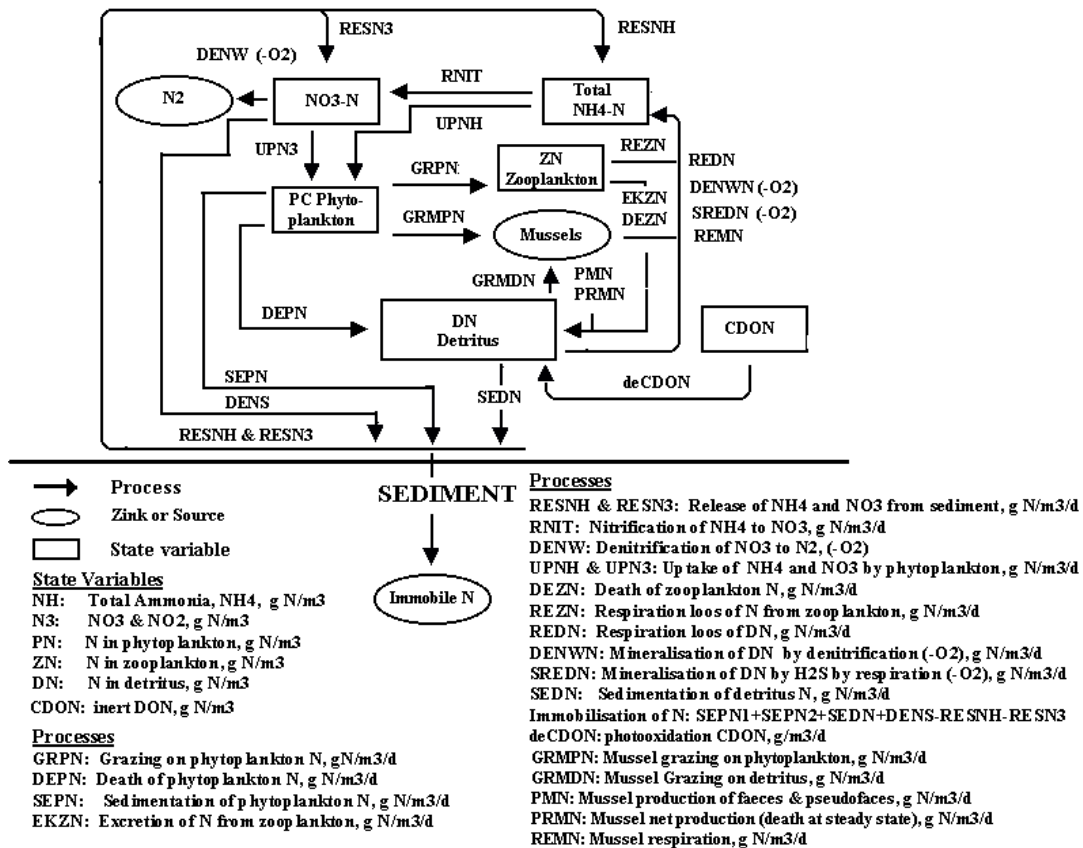
Figure 2.3   The nitrogen flow of the extended EU model.

RESP

PO4-P

UPPP

GRPP → ZP Zooplankton

PP Phyto-plankton

GRMPP → Mussels

REDP
DENWP (-O2)
SREDP (-O2)
REMP

GRMDP   PMP   EKZP
         PRMP   DEZP

DEPP → DP Detritus

SEPP

SEDP

RESP

SEDIMENT

Immobile P

→ Process
⬭ Zink or Source
☐ State variable

State Variables
IP: Inorganic P, (PO4), g P/m3
PP: P in phytoplankton, g P/m3
ZP: P i zooplankton, g P/m3
DP: P in detritus

Processes
UPPP: Uptake of PO4-P by phytoplankton, g P/m3/d
GRPP: Grazing on phytoplankton P, g P/m3/d
DEPP: Death of phytoplankton P, g P/m3/d
SEPP: Sedimentation of phytoplankton P, g P/m3/d

Processes
EKZP: Excretion of P from zooplankton, g P/m3/d
DEZP: Death of zooplankton P, g P/m3/d
REDZ: Respiration loos of P from zooplankton, g P/m3/d
REDP: respiration loos of DP, g P/m3/d
DENWP: Mineralisation of DP by denitrification (-O2), g P/m3/d
SREDP: Mineralisation of DP by H2S by respiration (-O2), g P/m3/d
SEDP: Sedimentation of detritus P, g P/m3/d
RESP: Release of IP from sediment, g P/m3/d
Immobilisation of P: SEPP+SEPP+SEDP-RESP
GRMPP: Mussel grazing phytoplankton , g P/m3/d
GRMDP: Mussel grazing detritus, g P/m3/d
PMP: Mussel production faces & pseudofaces, g P/m3/d
PRMP: Mussel net production (death at steady state), g P/m3/d
REMP: Mussel respiration, g P/m3/d

Figure 2.4   The phosphorus flow of the extended EU model.

Below is given an overview of the extended template, a detailed description of state variables and processes is presented in **/3/**.

2.2.1   State variables and Processes

The number of pelagic (AD) state variables and processes in the extended EU model increases to 14 and 52 respectively, reflecting the increased complexity of the model.

Besides the pelagic state variables additional 14 (non AD) state variables are defined to sum up primary production, net sedimentation of C, N & P to the sediment, benthic and pelagic mineralisation of C, denitrification, net sediment flux of N and P, time with DO<4 mg/l and DO<2 mg/l.

The differential equations for the pelagic state variables connected to advection dispersion scheme (AD) are listed in Table 2.1.

Table 2.1 Differential equations for pelagic state variables using the AD scheme

State variable (g/m^3)	Processes (g/m^3/d)
PC, (phytoplankton C, g/m^3)	prpc-grpc-depc-sepc-grmpc
PN, (phytoplankton N, g/m^3)	upnh+upn3-grpn-depn-sepn-grmpn
PP, (phytoplankton P, g/m^3)	uppp-grpp-depp-sepp-grmpp
CH, (chlorophyll, g/m^3)	prch-dech-sech-grmch
ZC, (zooplankton C, g/m^3)	przc-dezc-grmzc
DC, (detritus C, g/m^3)	depc2dc+ekzc-redc-sedc+dezc-denwc-sredc-grmdc+pmc+prmc
DN, (detritus N, g/m^3)	depn2dn+ekzn+deCDON-redn-sedn+dezn-denwn-sredn grmdn+pmn+prmn
DP, (detritus N, g/m^3)	depp2dp+ekzp-redp-sedp+dezp-denwp-sredp -grmdp+pmp+prmp
NH, (total NH$_4$-N, g/m^3)	edn+rezn-upnh+depn2in-rnit+denwn+sredn+resnh +remn
N3, (NO$_3$ + NO$_2$, g N/m^3)	rnit-denw+depon-upn3+resn3Simple-dens
H2S, (H$_2$S, g S/m^3)	sred-soxi+ssred
IP, (PO$_4$-P, g /m^3)	redp+rezp-uppp+depp2ip+denwp+sredp+resp +remp
DO, (Oxygen g/m^3)	odpc-oddc-odzc-odsc+rear-depc2do-soxi2do-rnit2do –remdo
CDON, (inert DON, g N/m^3)	-deCDON

The mussel population is assumed in a steady state, where net production and death outbalance each other. Consequently, mussels are not included as a state variable, but for known biomass it is possible to calculate processes like the mussels grazing on phytoplankton and detritus, production of faces and pseudofaces and net production and death.

The differential equations for the state variables not connected to the advection dispersion scheme (non AD) are listed in Table 2.2. The latter state variables are mainly used for mass balance and presentation of the effects.

Table 2.2 Differential equation of state variables not connected to the AD scheme.

State variable (g/m² or g/m³ or day)	Processes (g/m²/d) or (g/m³/d)or (day/day)
sumPRPC, (sum of net plankton production g C/m²)	PRPC_A
sum_erC_P, (sum of pelagic respiration, g C/m²)	reC_P_A
sumRESC, (sum sediment respiration, g C/m²)	resc_A
sum_seC, (sum sepc +sedc to sediment, g C/m²)	seC_A
sum_seN, (sum of sepn+sedn, g N/m²)	seN_A
sumRelS_N, (sum of NH_4+NO_3 flux sediment, g N/m²)	resn_A
sum_dens, (sum denitrifikation sediment, g N/m²)	dens_A
sum_seP, (sum sepp+sedp to sediment, g P/m²)	seP_A
sumRelS_P, (sum PO_4 flux sediment, g P/m²)	resp_A
DO_avg, (sliding DO average at bottom, g/m³)	Sado
TDO_avg4, (Accumulated time with DO<4 mg/l, bottom, day)	tdo4
TDO_avg2, (Accumulated time with DO<2 mg/l, bottom, day)	tdo2
TDO_avg4_P, (periods DO<4 mg/l, day)	tdo4_p
TDO_avg2_P, (periods DO<2 mg/l, day)	tdo2_p

The processes related to pelagic (AD) state variables are listed in Table 2.3.

Table 2.3 Processes connected to pelagic (AD) state variables.

Rates	C	N	P	S	DO
Reaeration					REAR
Phytoplankton					
Net production of algae:	PRPC				ODPC
Uptake of nutrients Other algae: NH_4, NO_{3+2}, PO_4		UPNH UPN3	UPPP		
Death of algae, C, N & P	DEPC	DEPN	DEPP		ODDEPC
Sedimentation of algae, C, N & P	SEPC	SEPN	SEPP		
Grazing of algae C, N & P by zooplankton:	GRPC	GRPN	GRPP		
Grazing of algae C, N & P by mussels:	GRMPC	GRMPN	PRMPP		
Zooplankton					
Death of zooplankton:	DEZC	DEZN	DEZP		
Mussel grazing on zooplankton	GRMZC	GRMZN	GRMZP		
Respiration of zooplankton:	REZC	REZN	REZP		ODZC
Excretion of org. matter from zooplankton:	EKZC	EKZN	EKZP		
Detritus					
Fraction of dead algae to detritus	DEPC2DC	DEPN2DN	DEPP2DP		
Mussel faeces & pseudo faeces & net production	PMC	PMN	PMP		
Mussel death (net production, assuming steady state)	PRMC	PRMN	PRMP		
Oxidation of DC, DN, DP by DO	REDC	REDN	REDP		ODDC
Oxidation of DC, DN, DP by NO_3 in water ($-O_2$)	DENWC	DENWN	DENWP		
Oxidation of DC, DN, DP by SO_4 in water ($-O_2$)	SREDC	SREDN	SREDP		
Sedimentation of detritus:	SEDC	SEDN	SEDP		
Grazing of detritus C, N & P by mussels:	GRMDC	GRMDN	GRMDP		
CDON, inert DON					
Photo oxidation of CDON		deCDON			
Inorganic N, P, S and O_2 in water					

Rates	C	N	P	S	DO
Fraction of dead algae to NH_4, NO_{3+2} & DO		DEPN2IN	DEPP2IP		DEPC2DO
Mussel respiration		REMN	REMP		REMDO
Nitrification, $NH_4 \rightarrow NO_{3+2}$		RNIT			RNIT2DO
Denitrifikation in water, $NO_{3+2} \rightarrow N_2$		DENW			
SO4 respiration, $SO_4 \rightarrow H_2S$ in water				SRED	
SO4 respiration, $SO_4 \rightarrow H_2S$ in sediment				SSRED	
H2S oxidation, $H_2S \rightarrow SO_4$				SOXI	SOXI2DO
Sediment					
Mineralization of sediment: Respiration of C, Flux of NH_4, NO_{3+2} & PO_4 from sediment. into water	RESC	RESNH RESN3	RESP		ODSC
Denitrifikation, flux of NO_3 into sediment		DENS			

In the description below only the changes relative to the Standard EU module are described in detail.

2.2.1 Inert DON, CDON

Total N consists of dissolved inorganic N (DIN) in the form of NH_4, NO_3 and NO_2, particulate organic N (PON) and dissolved organic N (DON). The latter consists of range organic compounds with a range of mineralisation rates. Some smaller compounds are easily mineralized whereas some of the larger organic compounds have a slow mineralisation rate.

A major fraction of the TN load from some catchments consists of slow degradable or inert DON with a slow mineralisation rate. This inert DON is incorporated in inert dissolved organic C (DOC) with an optical property of absorbing blue and ultraviolet light. These organic compounds, also called yellow substances or coloured DOC (CDOC), can be photo oxidised into smaller molecules which then can be picked up by bacteria thereby passing the associated C, N and P into the food web.

The user has the option of including inert DON or CDON in the model. CDON is first photo oxidised into detritus DN by light and then mineralized as DN.

The light penetration into the water is influenced by CDOC and is in the model described as a light extinction by the concentration of CDON.

2.2.2 Mussel filtration

In some ecological systems filtration by mussels can be an important factor for the flow of C, N and P. Mussels are able to filter particle from the water and deposit faces and pseudo-faces-rich in C, N and P on the bottom below the mussel beds. Further mussels are increasing the recycling of nutrient through respiration of ingested organic C, N and P.

The net growth of the mussels is based on a Monod-like function with the concentration of phytoplankton and detritus as independent variables. The growth is further regulated by temperature and DO concentration.

2.2.3 Uptake of DIN and DIP, nitrification and denitrification.

The uptake of inorganic N by phytoplankton has been changed and extended to include both NH_4-N and NO_{3+2}-N (UPNH &UPN3). Nitrification (RNIT) of NH_4-N and denitrification (DENW) of NO_{3+2}-N in the water during anoxic condition has been included as well. Denitrification in the water results in mineralisation of detritus carbon (DENWC) resulting in release of organic bound N and P as NH_4-N and PO_4-P to the water (DENWN, DENWP).

Denitrification in the sediment of NO_{3+2}-N in the water (DENS) has been described by a function using potential denitrification in the sediment, diffusion of NO_{3+2}-N in the sediment and penetration depth of DO into the sediment as independent variables. The function is an analytical solution of coupled differential equations with known border conditions using Ficks 1. law to describe an NO_3-N profile in the sediment under steady state conditions.

Besides the denitrification of NO_{3+2}-N in the water, a part of the N settling on the sediment surface is immobilized through burial and denitrification.

The process sequence in the sediment:

Ammonifikation of organic N → nitrification of NH_4 in pore water of oxic zone of sediment→ denitrification of NO_{3+2}-N to N_2 in anoxic zone of the sediment.

2.2.4 H_2S and SO_4

During anoxic conditions in the water SO_4 respiration (SRED) may take place under production of H_2S and mineralisation of organic material and associated N and P (SREDC, SREDN & SREDP). H_2S is oxidized to SO_4 by DO either chemical or mediated by bacteria using the energy in reduced S (SOXI & SOXI2DO).

3.   Model setup

3.1   Model setup for 3D model

The local model is a sub-model of the larger Bansai model. The local model area and the parameter settings for the HD model are described in Annex A.

The system has three boundaries to the adjacent marine areas - the Øresund, the southern Kattegat, and north of Læsø. All boundaries (marine areas, water courses) are forced with data extracted from the Bansai model. They include in addition to salinity and temperature (from HD model) nutrient concentrations in freshwater sources, point sources, atmospheric precipitation, all model state variables at the three boundaries. The Bansai model does not model dissolved organic nitrogen ex-plicitly, hence the values at boundaries were calculated from salinities:

CDON= 0.1696-salinity*0.00374
and assuming that CDON = 0.17 mg/l at 0 psu and 0.04 mg/l at 35 psu.

Isoplet plots of selected state variables at the northern and southern (Great Belt) boundary are shown in Figure 3.2 to Figure 3.11 and positions of data extraction are shown in Figure 3.1.
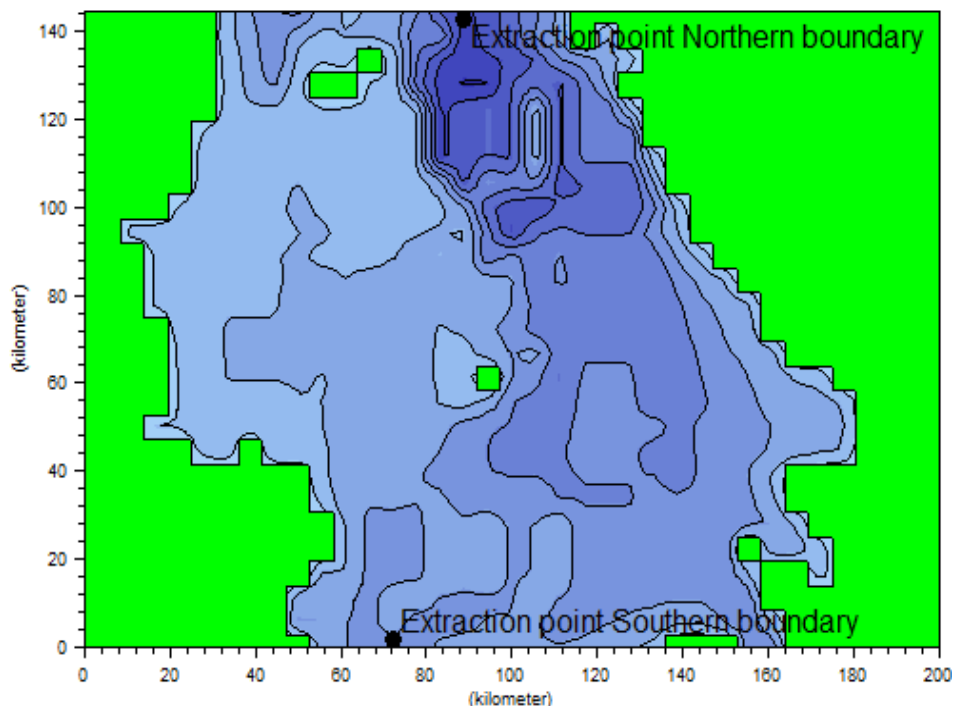
Figure 3.1   Position where boundary data were extracted from the Bansai model.
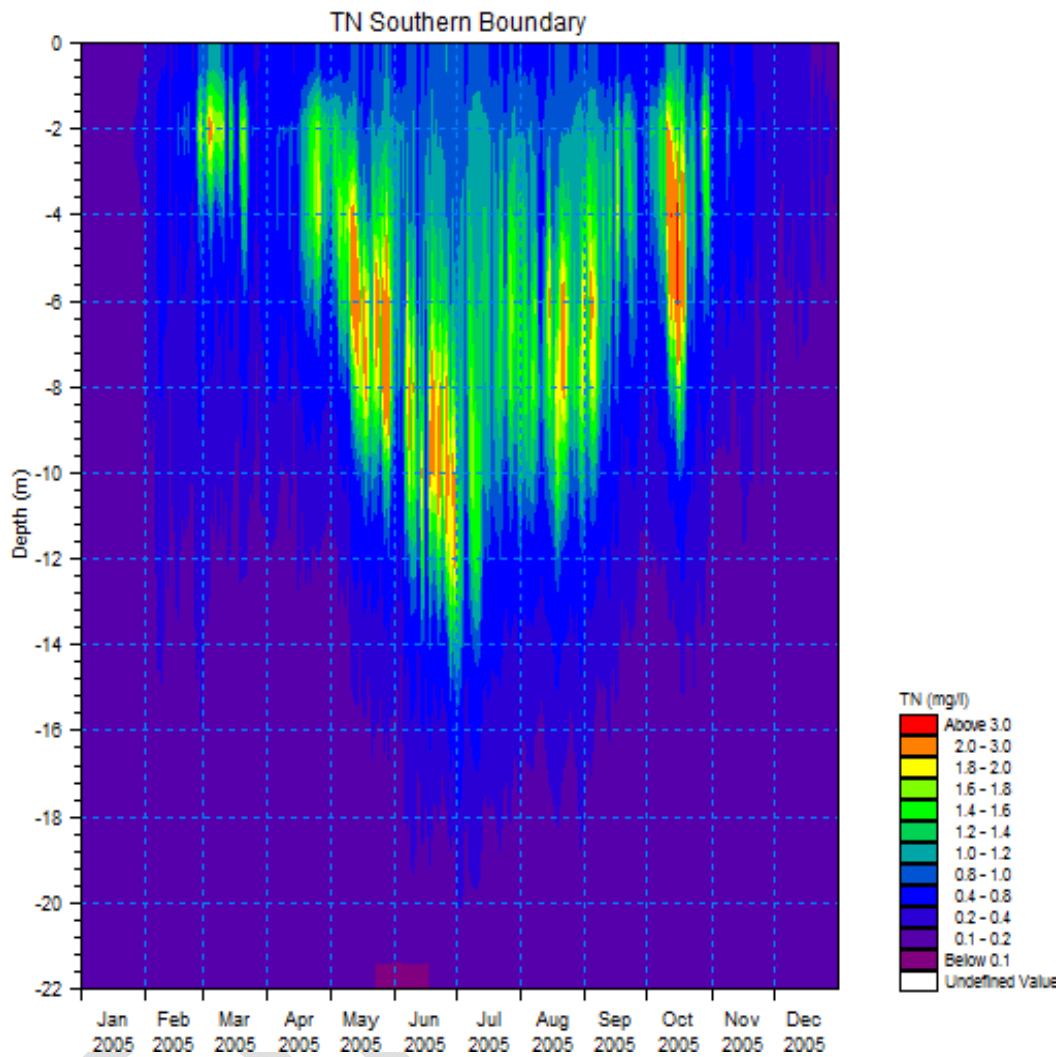
Figure 3.2   Isoplet diagram for total N at the southern boundary in Great Belt.
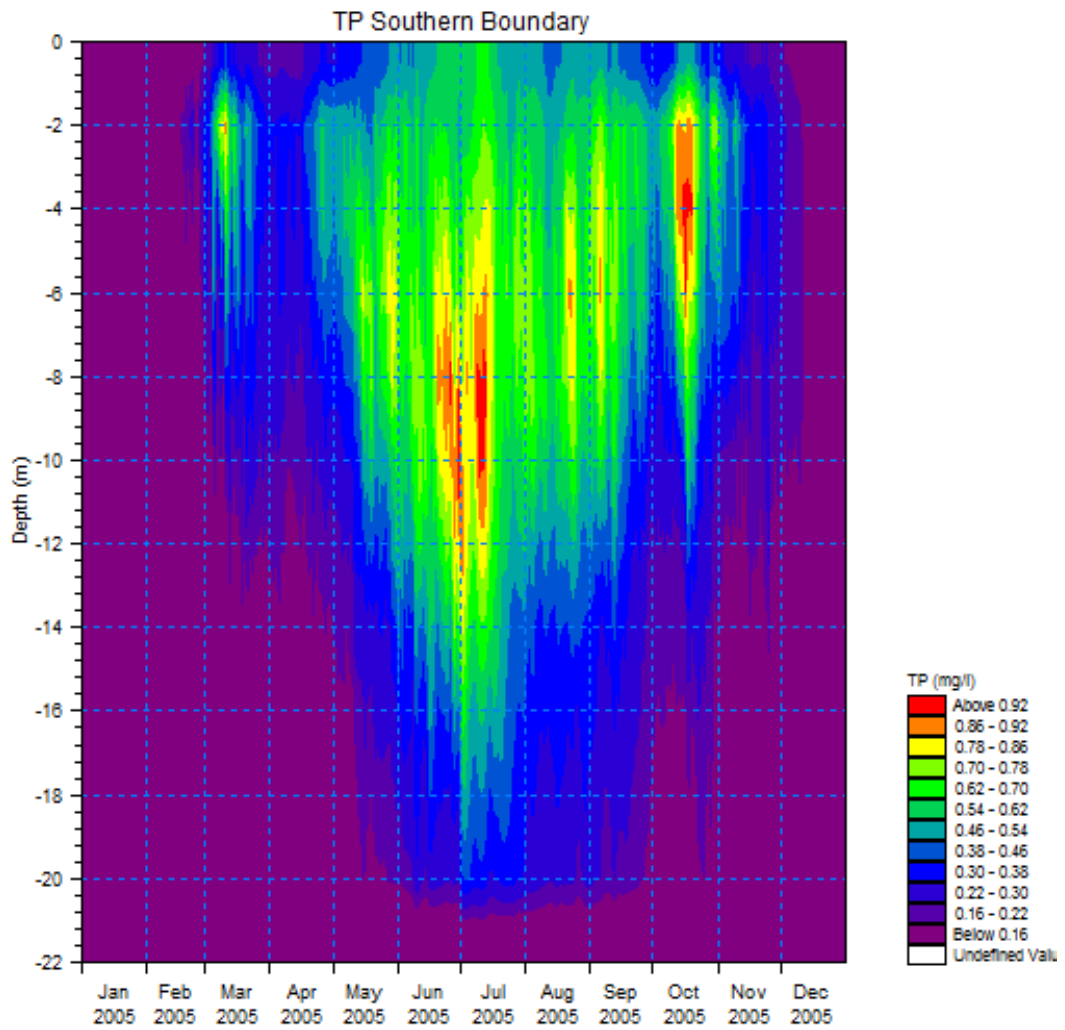
Figure 3.3   Isoplet diagram for total P at the southern boundary in Great Belt.
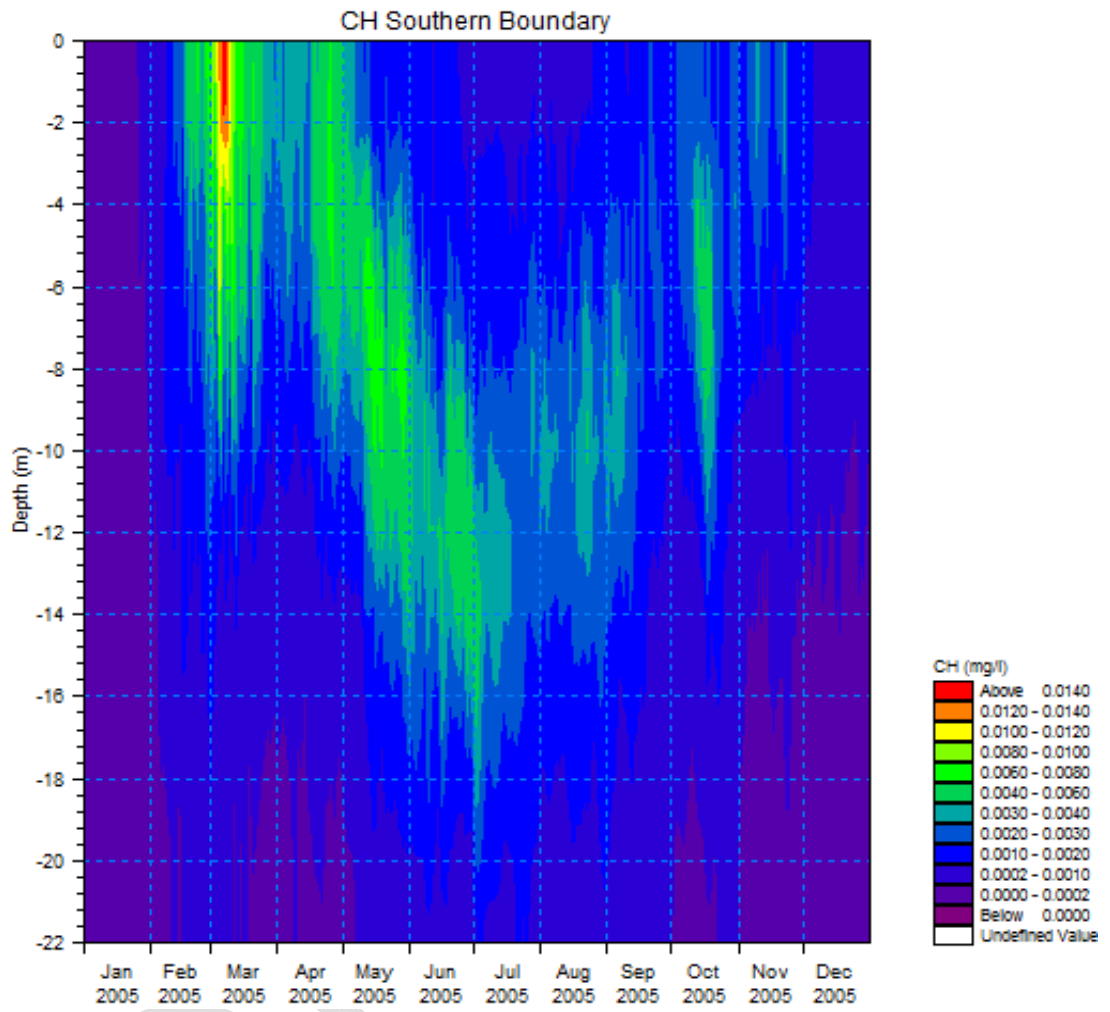
Figure 3.4   Isoplet diagram for Chl-a at the southern boundary in Great Belt
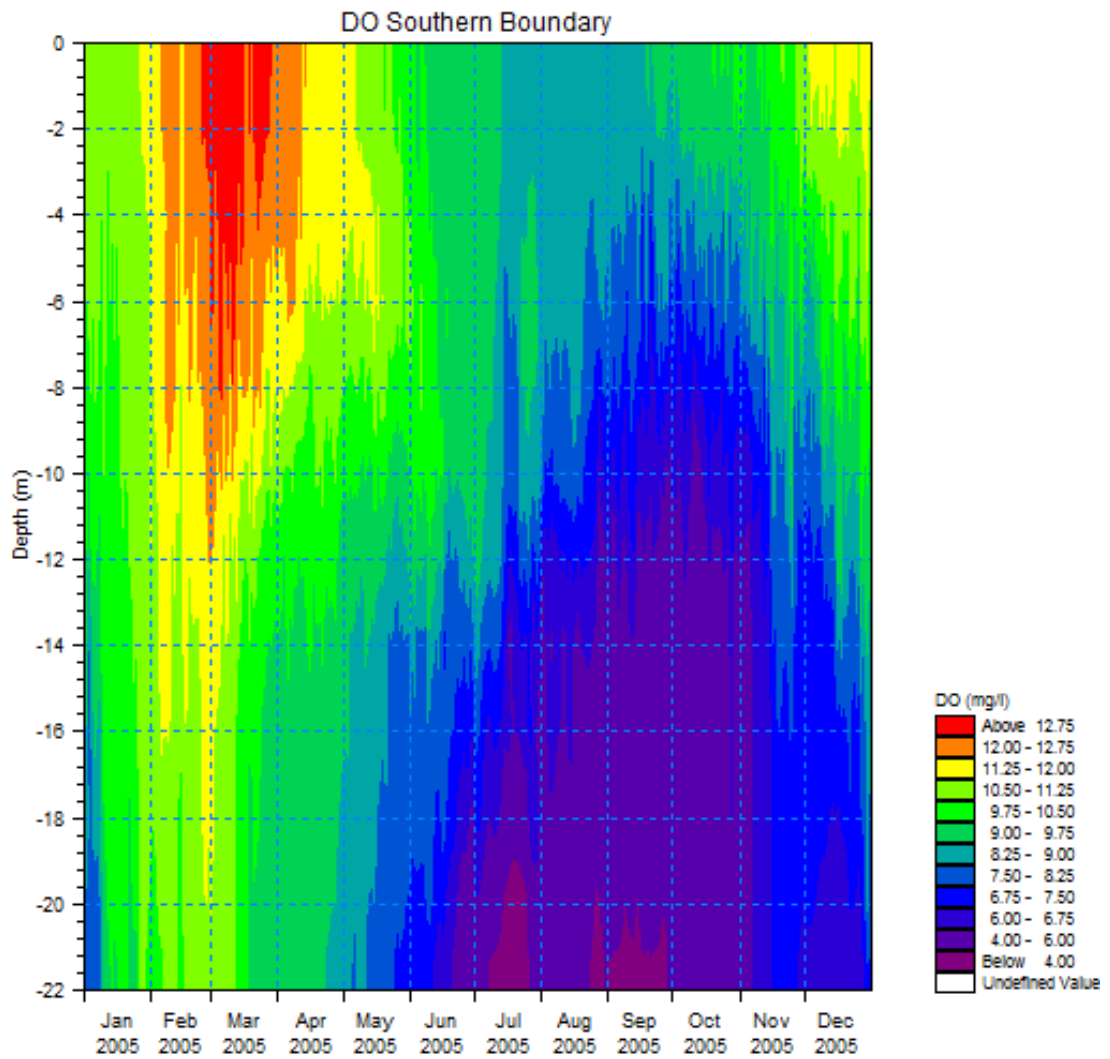
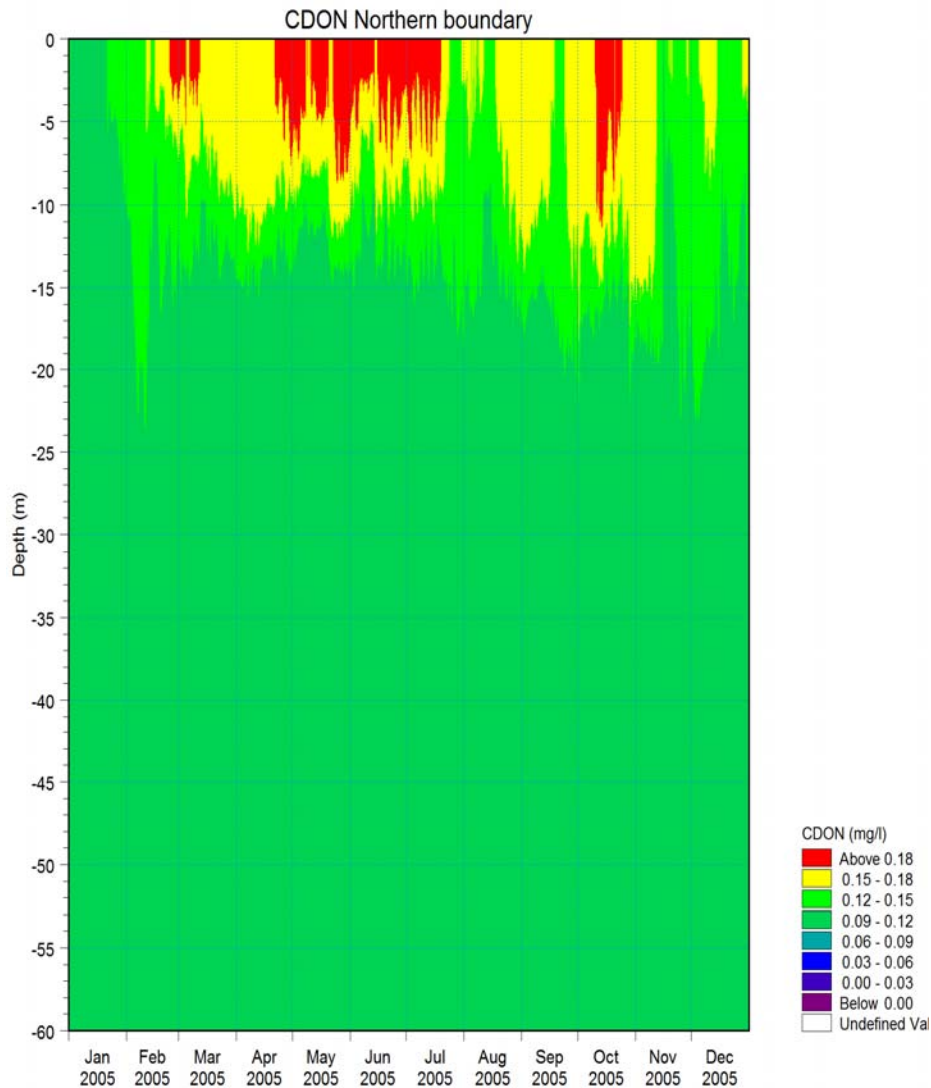Figure 3.5   Isoplet diagram for dissolved oxygen at the southern boundary in Great Belt.
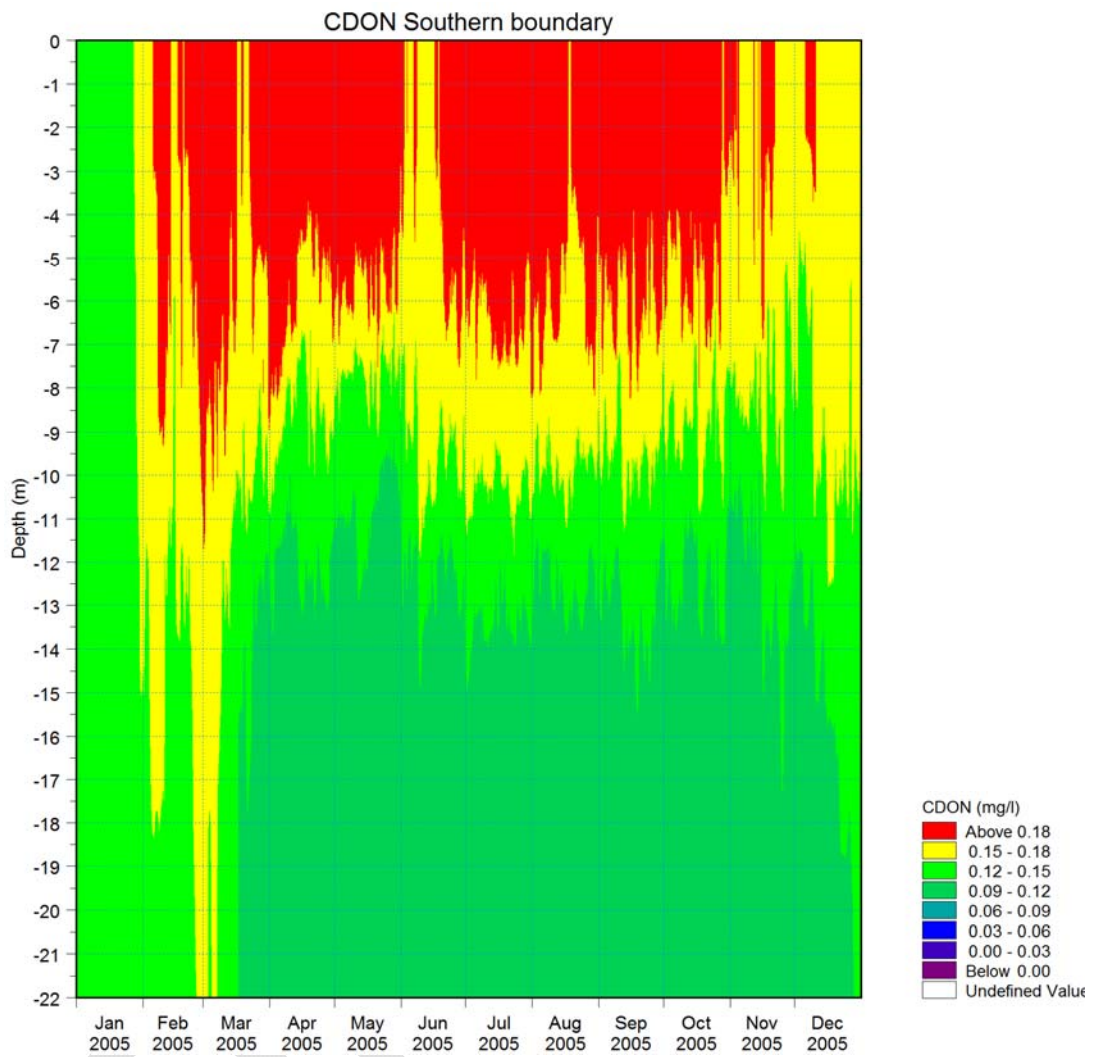
Figure 3.6 Isoplet diagram for dissolved organic nitrogen at the southern boundary in Great Belt

TN Northern Boundary
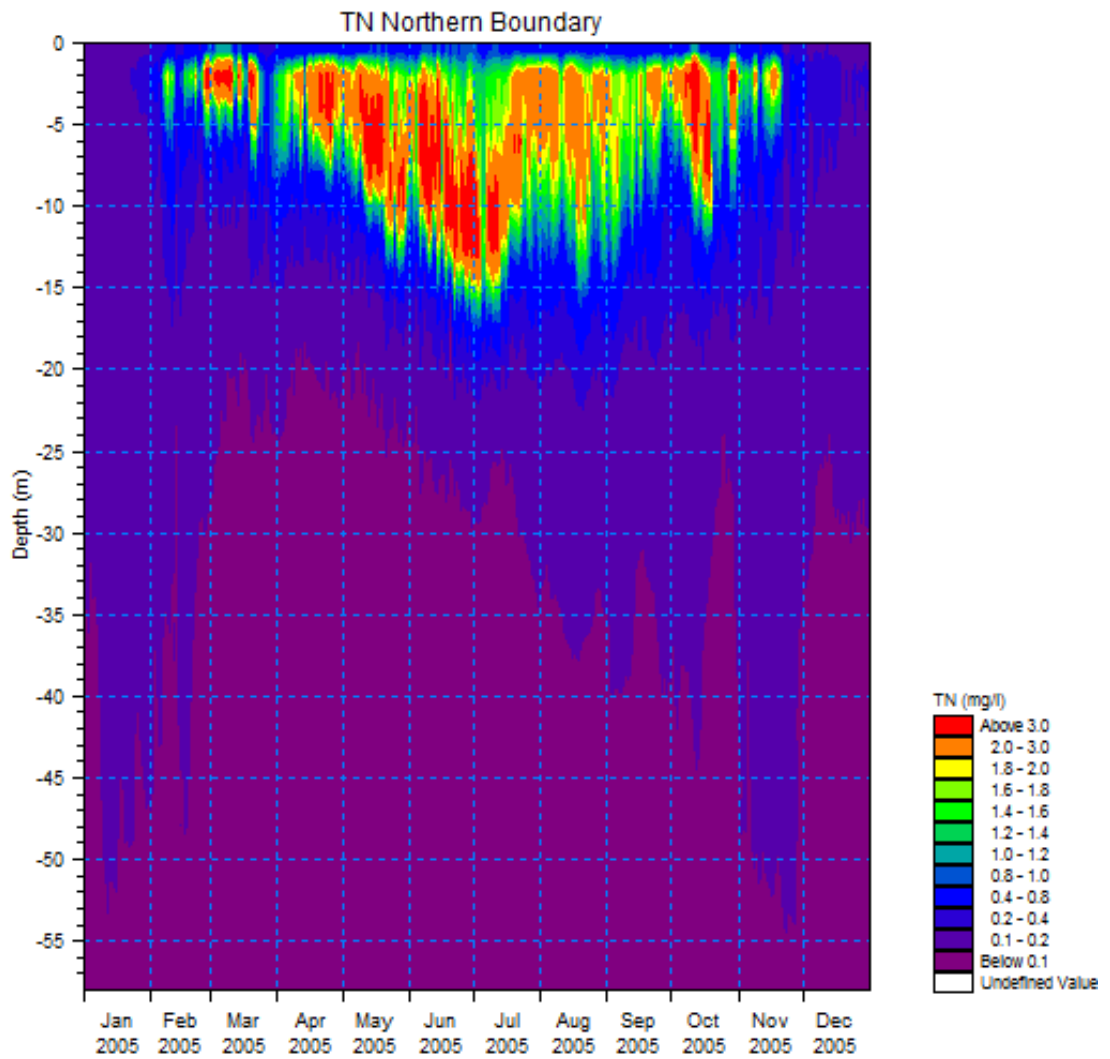
Figure 3.7   Isoplet diagram for total N at the northern boundary.

TP Northern Boundary
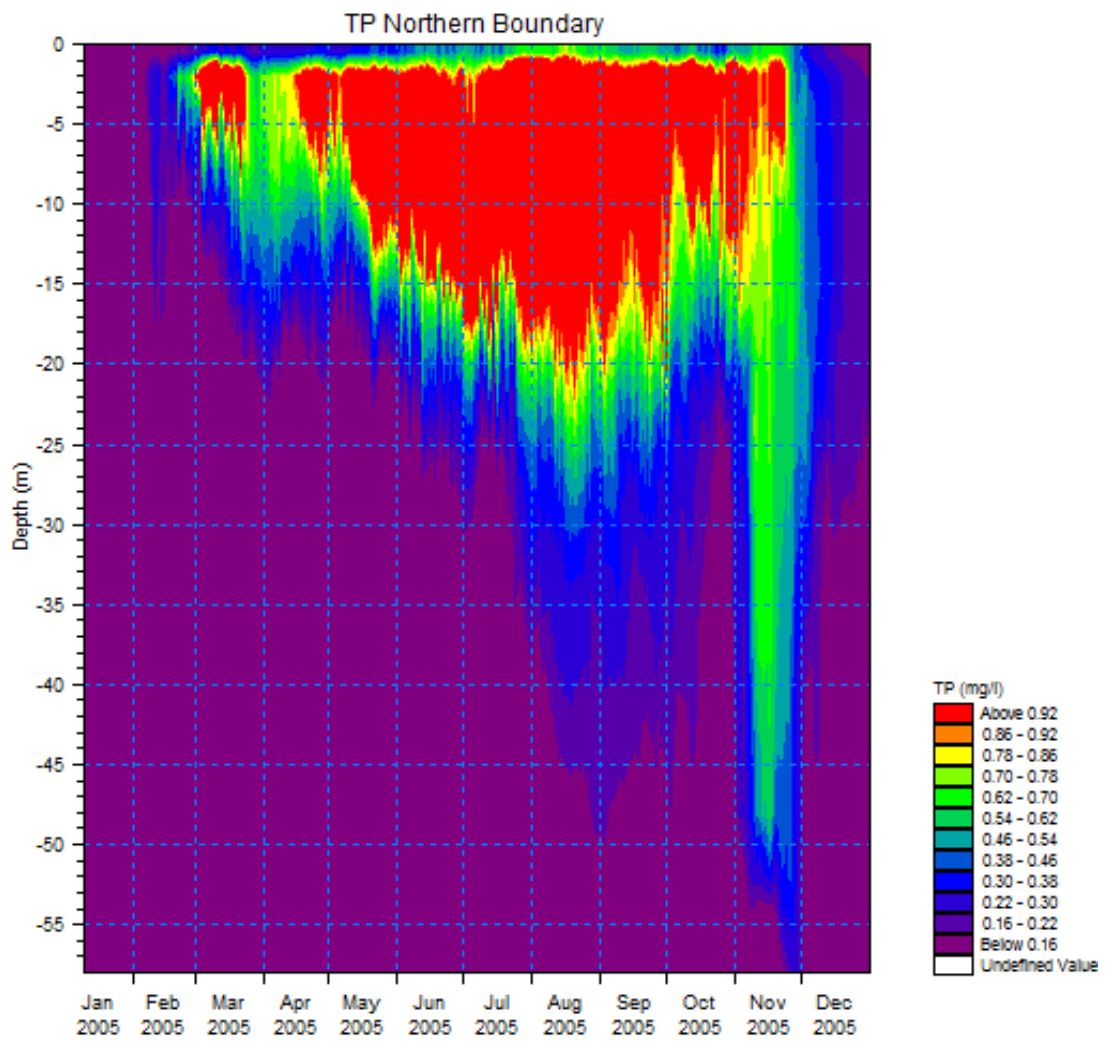
Figure 3.8   Isoplet diagram for total P at the northern boundary.
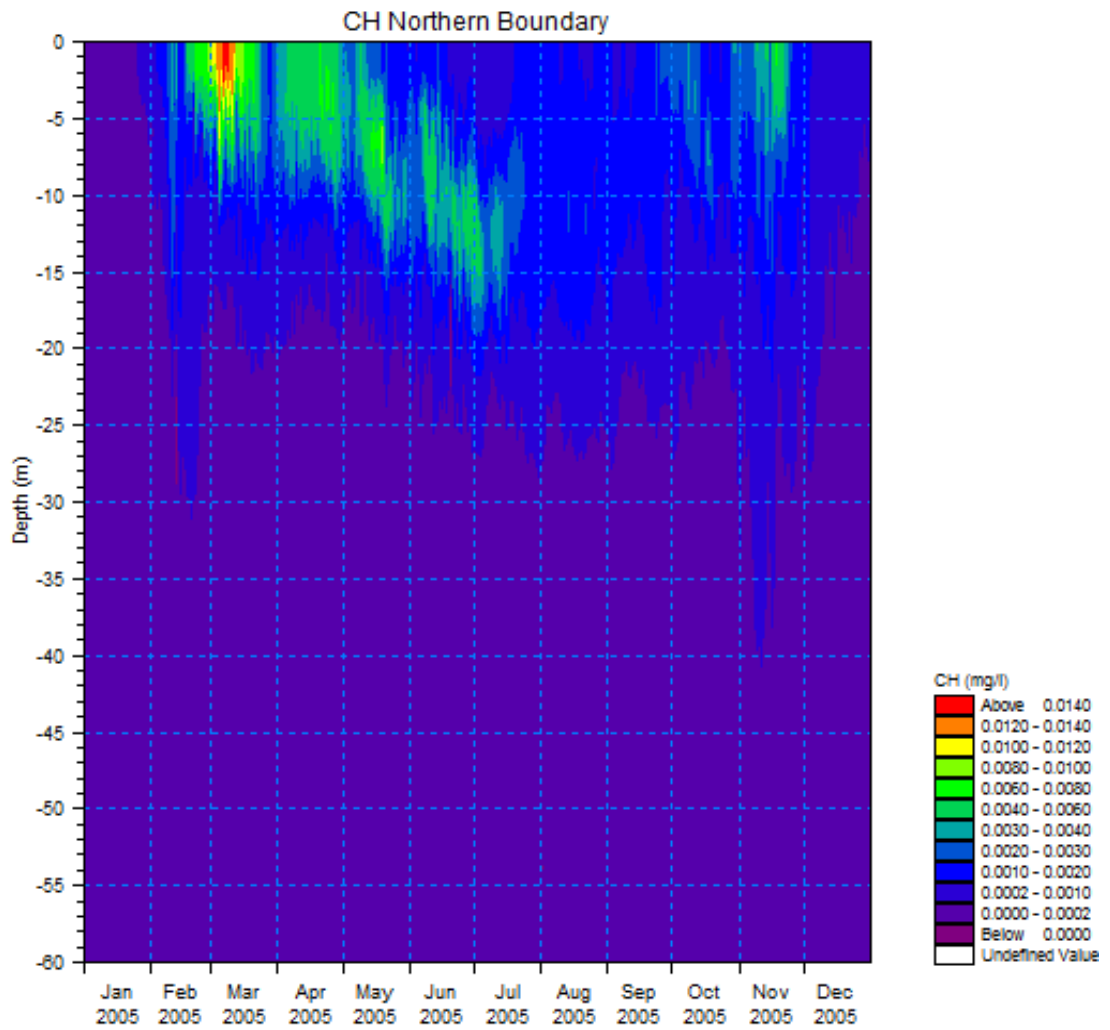
Figure 3.9   Isoplet diagram for Chl-a at the northern boundary.
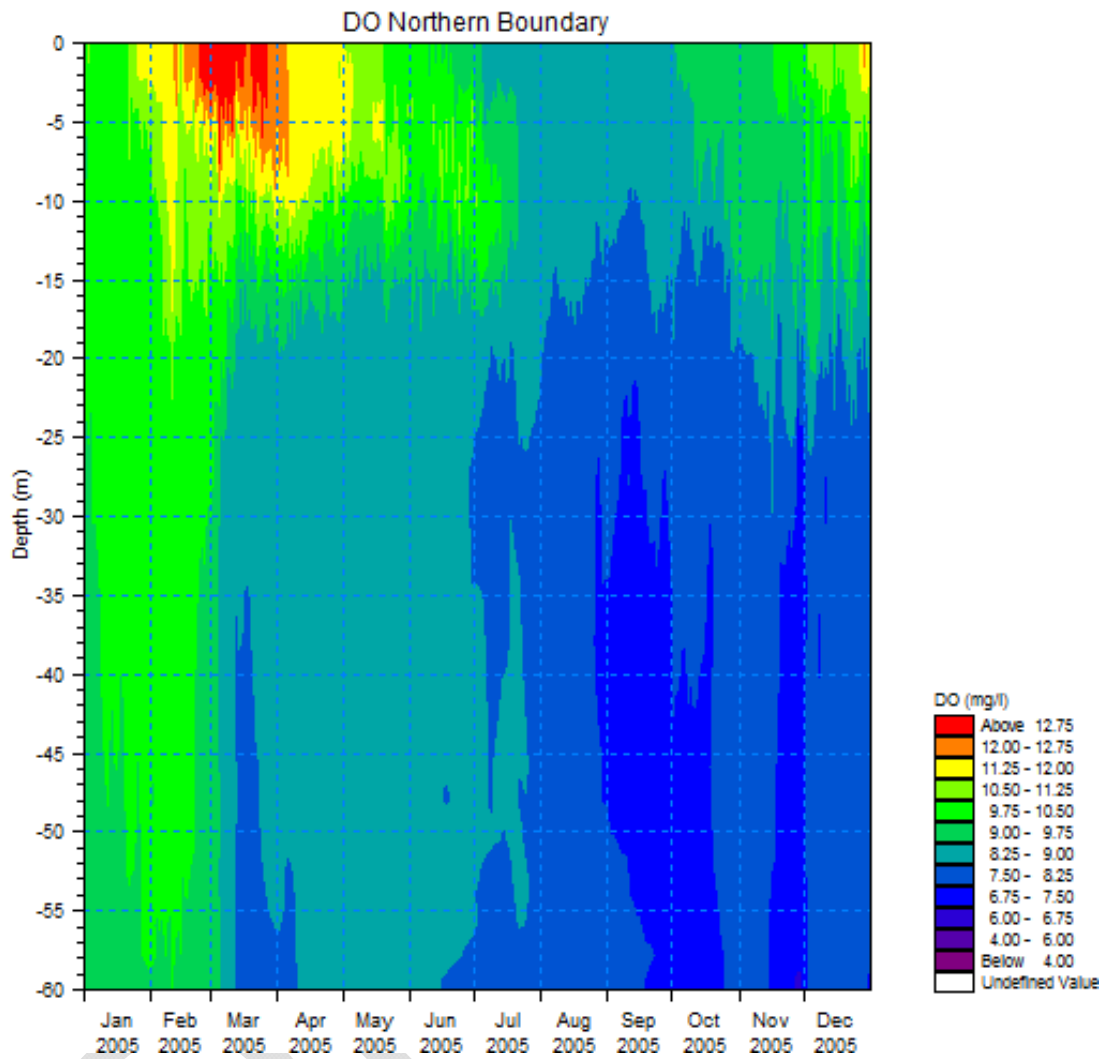
Figure 3.10   Isoplet diagram for dissolved oxygen at the northern boundary.

Figure 3.11   Isoplet diagram for dissolved organic nitrogen at the northern boundary.

3.2   **Calibration and validation of extended Ecolab model**

The Bansai model has been calibrated and validated continuously since 2000 and model results can be considered as high quality and reliable input to the local model developed in the present study. Because the model template applied in the study deviated somewhat from the Bansai model by including additional state variables the model was calibrated against monitoring data collected at 7 stations. Section 5.3 in the main report shows calibration data from Ålborg Bight station and below is shown data from additional 6 stations (Figure 3.12-Figure 3.29).
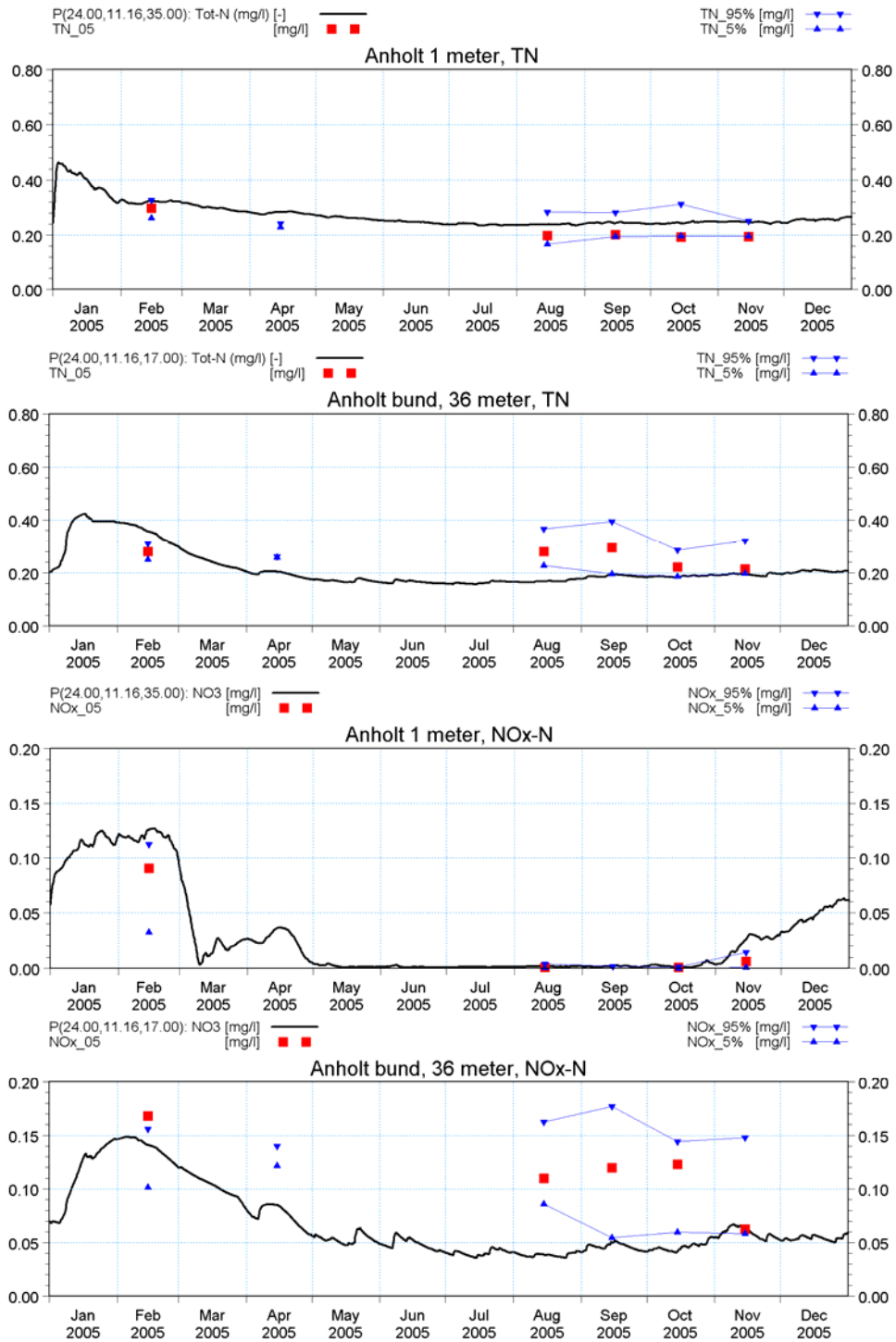
Figure 3.12   Concentration of total nitrogen (TN) and NOx-N at Anholt E station at surface and at bottom (36 m). Modelled (black line), measured in 2005 (■) and 5 and 95% percentiles covering 2000-2007.
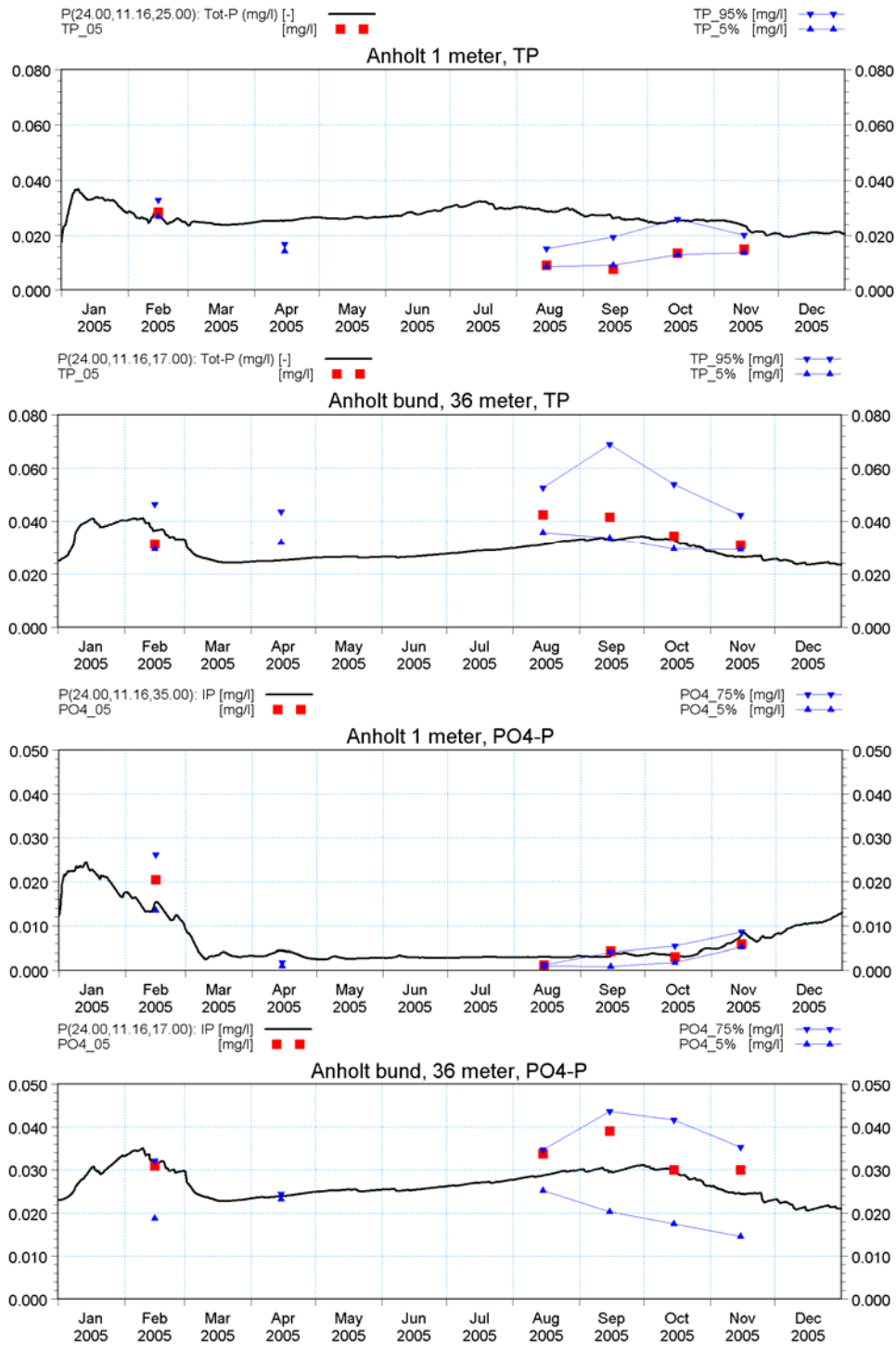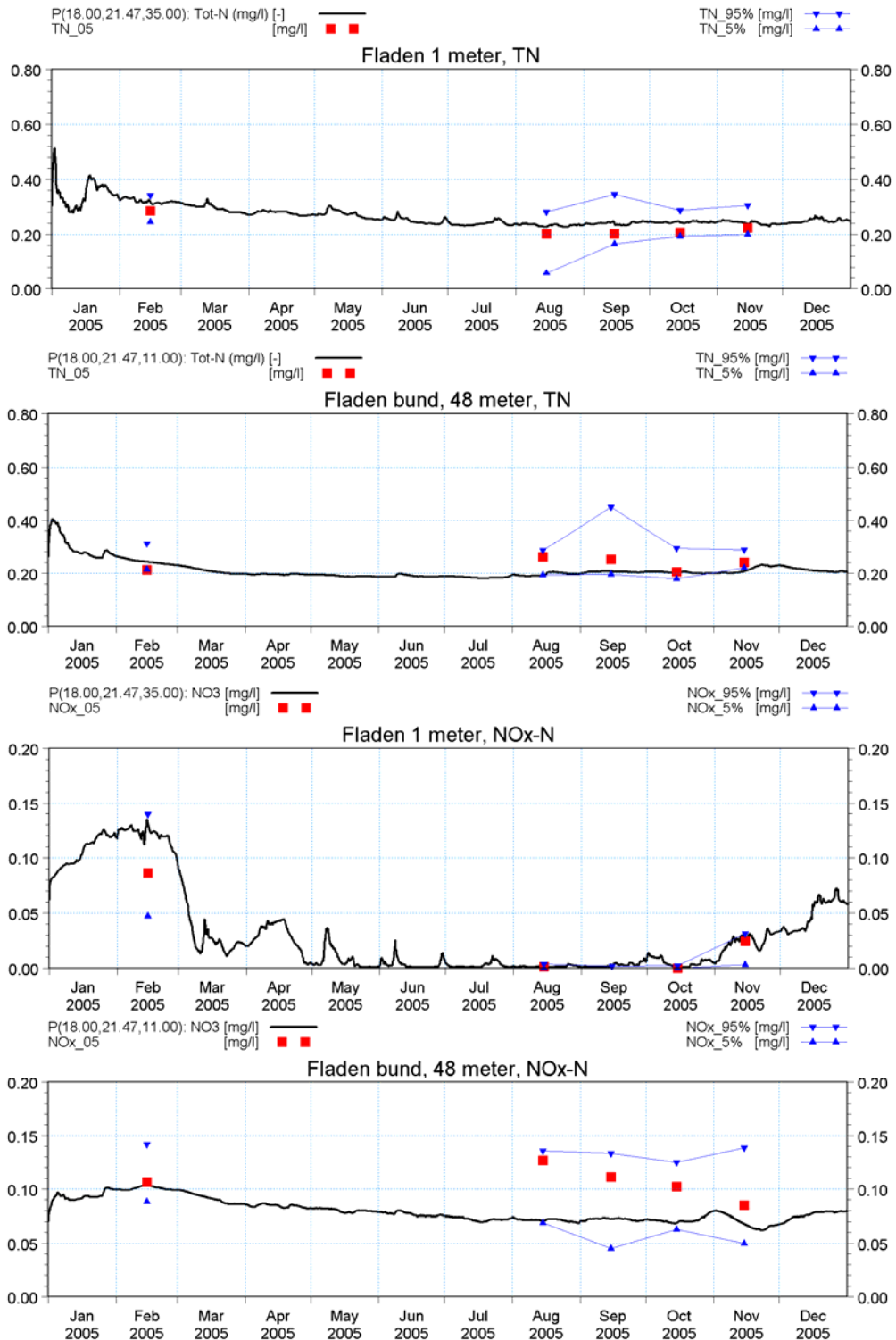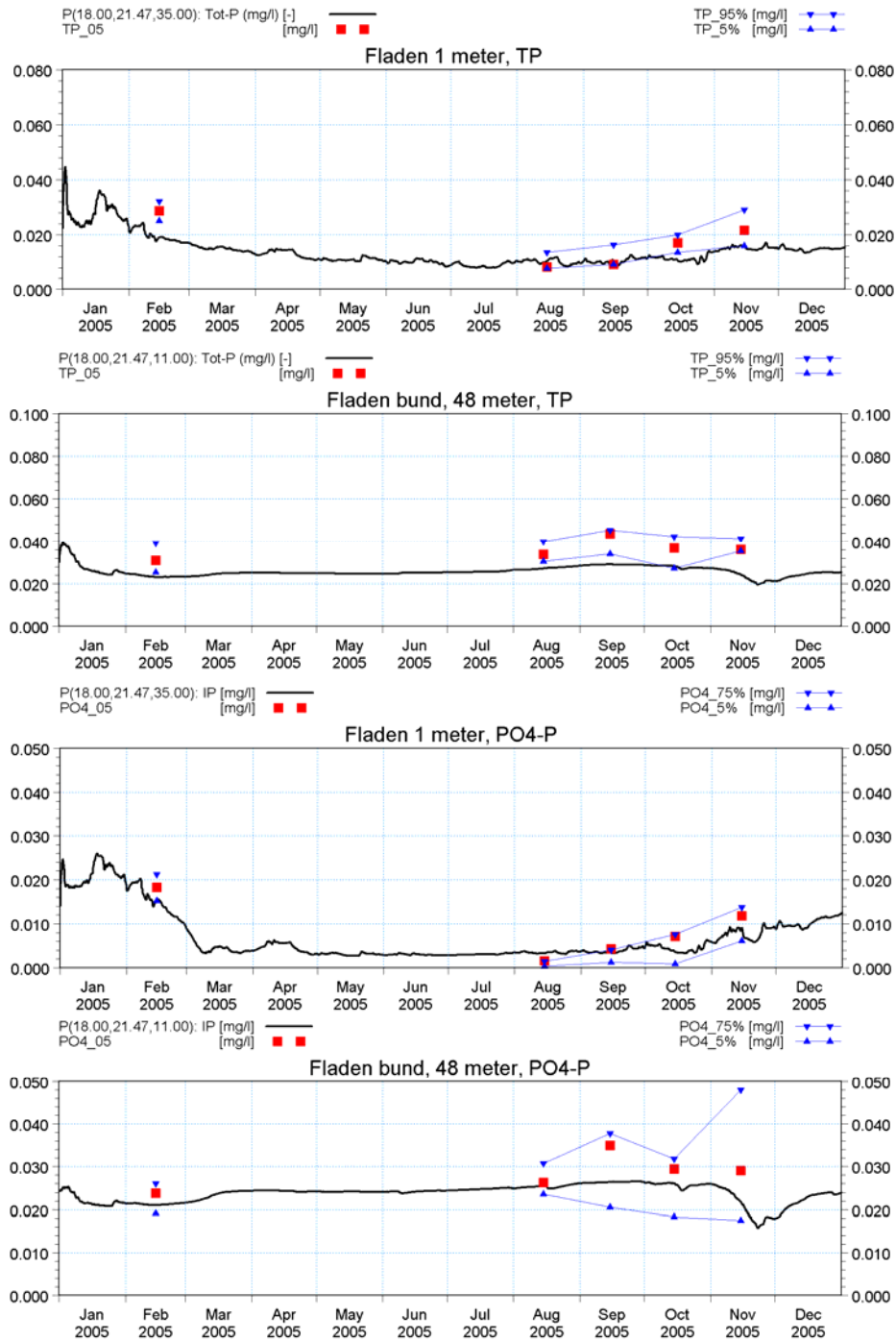
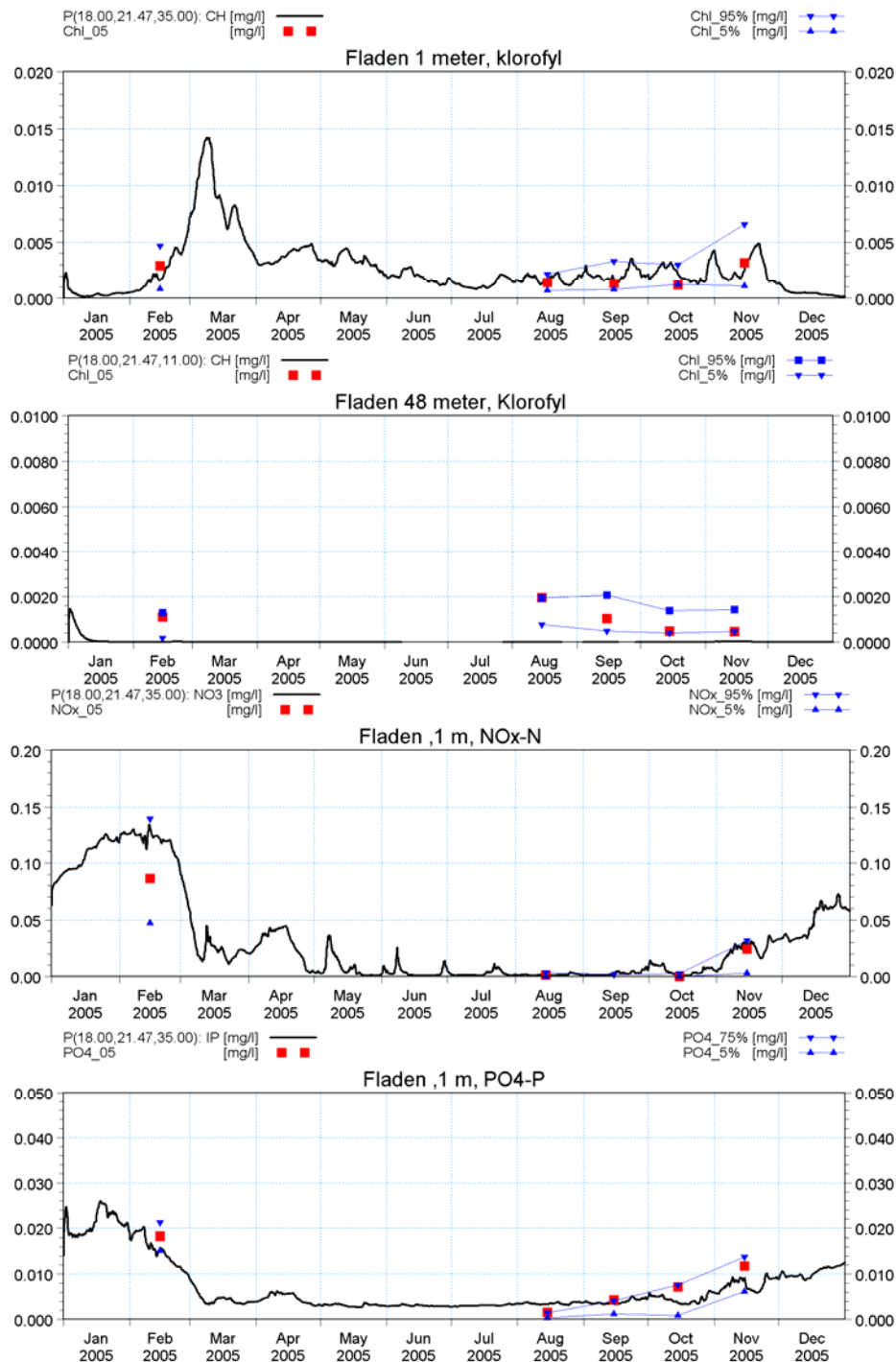Figure 3.13   Concentration of total phosphorus (TP) and PO$_4$-P at Anholt E station at surface and at bottom (36 m). Modelled (black line), measured in 2005 (■) and 5 and 95% percentiles covering 2000-2007.
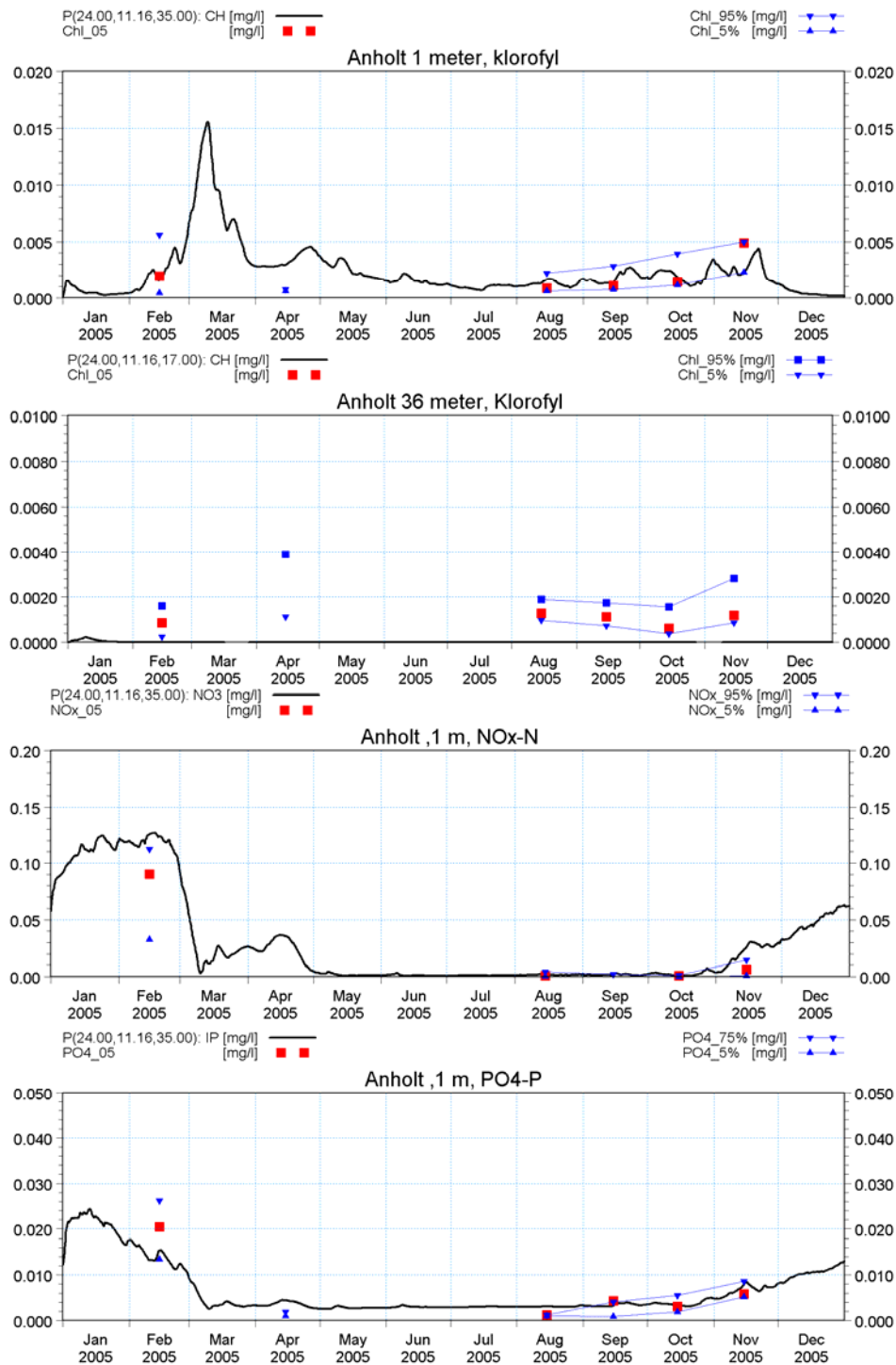
Figure 3.14   Concentration of Chla, NOx-N and PO$_4$-P at Anholt E station at surface and at bottom (36 m; Chla only). Modelled (black line), measured in 2005 (■) and 5 and 95% percentiles covering 2000-2007.

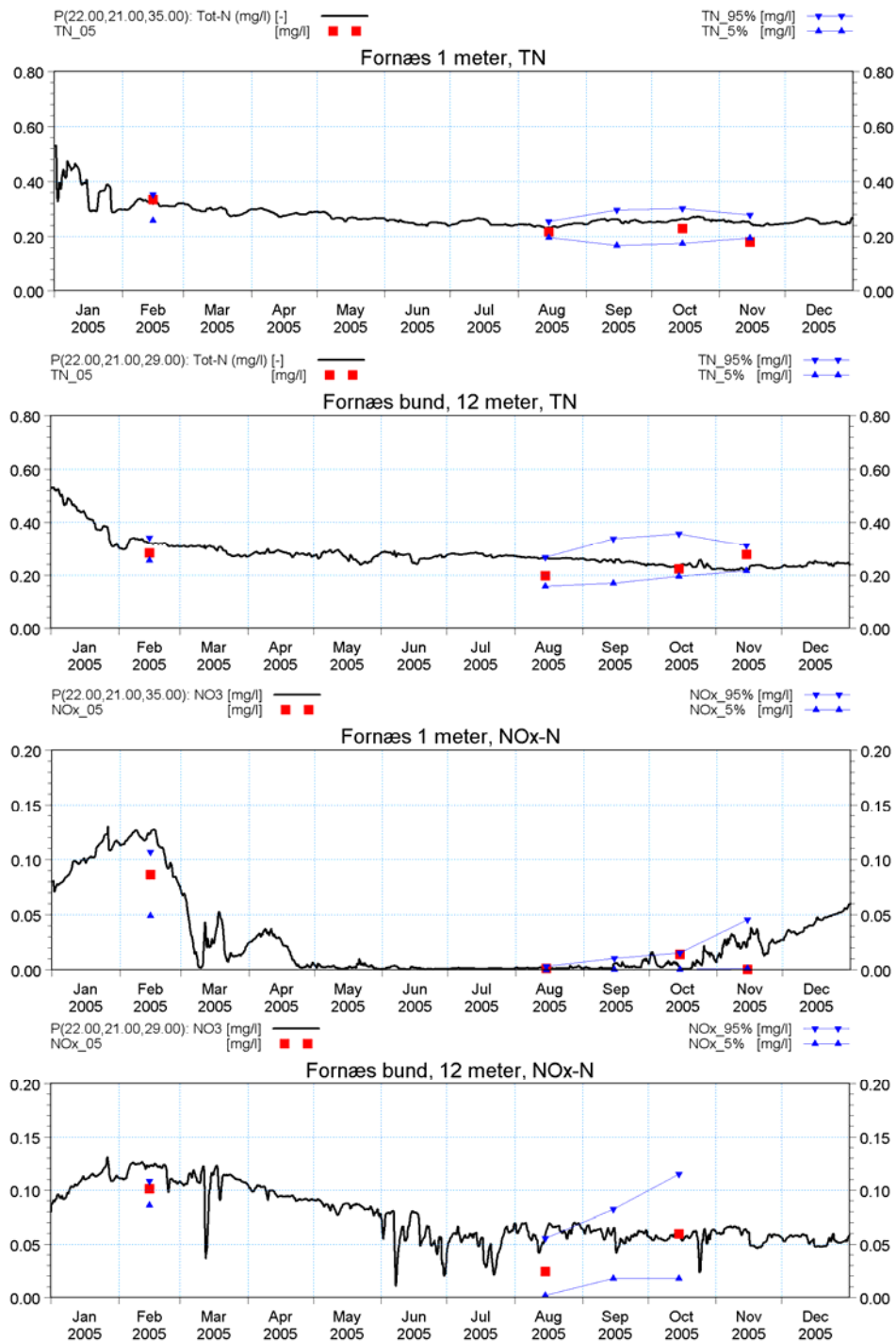Figure 3.15   Concentration of total nitrogen (TN) and NOx-N at Fladen station at surface and at bottom (48 m). Modelled (black line), measured in 2005 (■) and 5 and 95% percentiles covering 2000-2007.
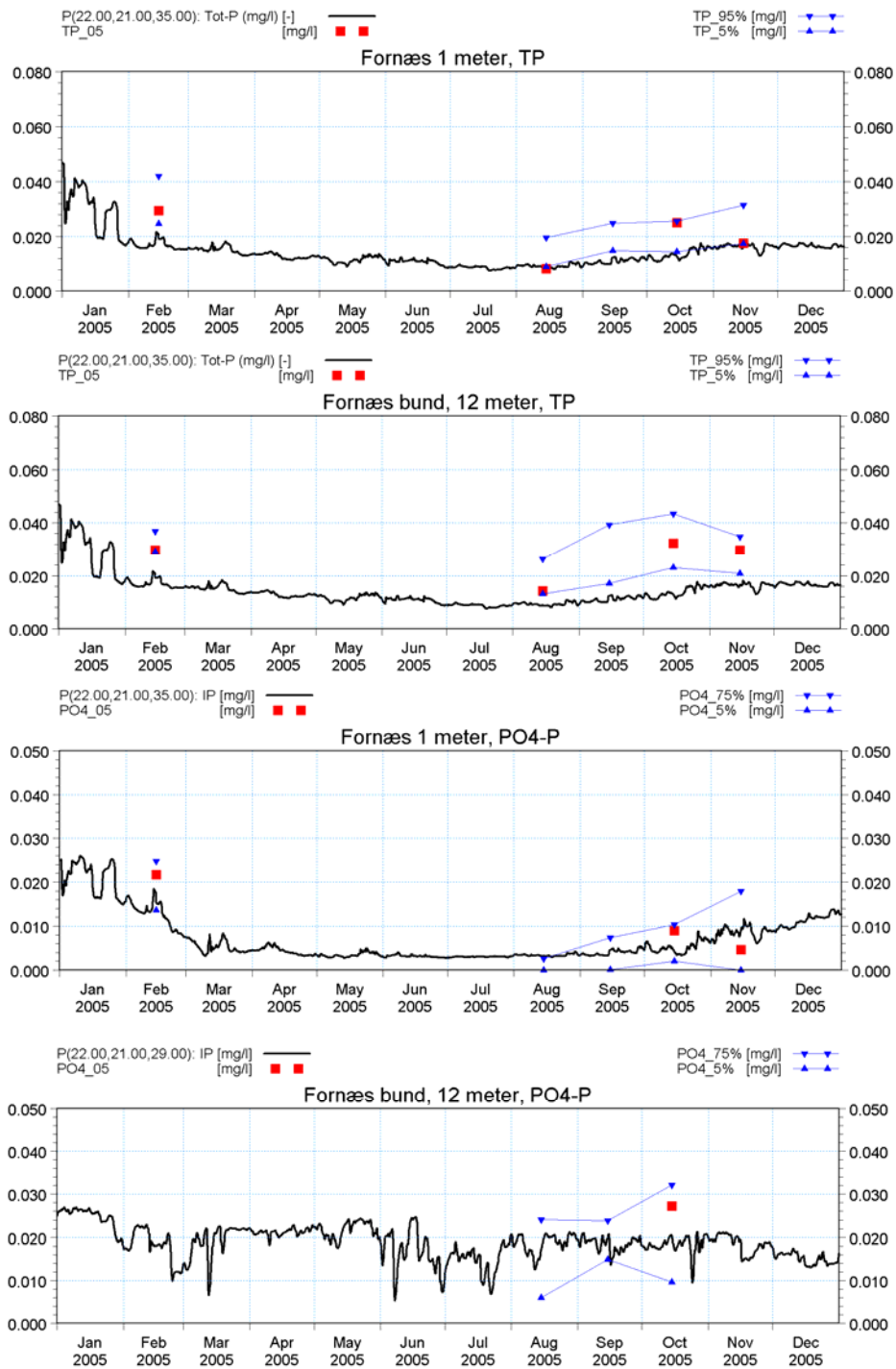
Figure 3.16   Concentration of total phosphorus (TP) and PO_4-P at Fladen at surface and at bottom (48 m). Modelled (black line), measured in 2005 (■) and 5 and 95% percentiles covering 2000-2007.

Figure 3.17   Concentration of Chla, NOx-N and PO$_4$-P at Fladen at surface and at bottom (48 m; Chla only). Modelled (black line), measured in 2005 (■) and 5 and 95% percentiles covering 2000-2007.

Figure 3.18   Concentration of total nitrogen (TN) and NOx-N at Fornæs at surface and at bottom (12 m). Modelled (black line), measured in 2005 (■) and 5 and 95% percentiles covering 2000-2007.
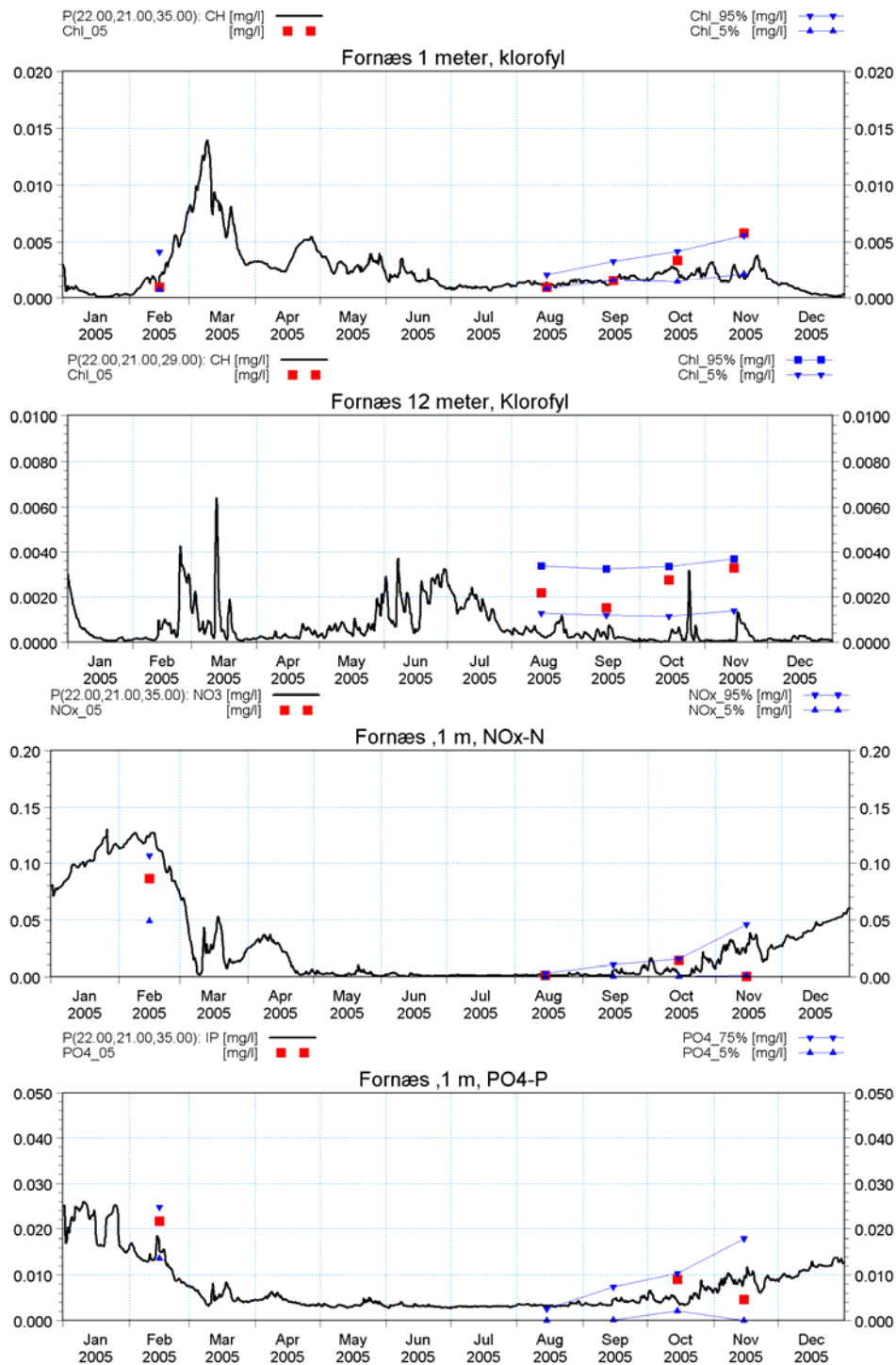
Figure 3.19   Concentration of total phosphorus (TP) and PO$_4$-P at Fornæs at surface and at bottom (312 m). Modelled (black line), measured in 2005 (■) and 5 and 95% percentiles covering 2000-2007.

Figure 3.20   Concentration of Chla, NOx-N and PO$_4$-P at Fornæs at surface and at bottom (12 m; Chla only). Modelled (black line), measured in 2005 (■) and 5 and 95% percentiles covering 2000-2007.
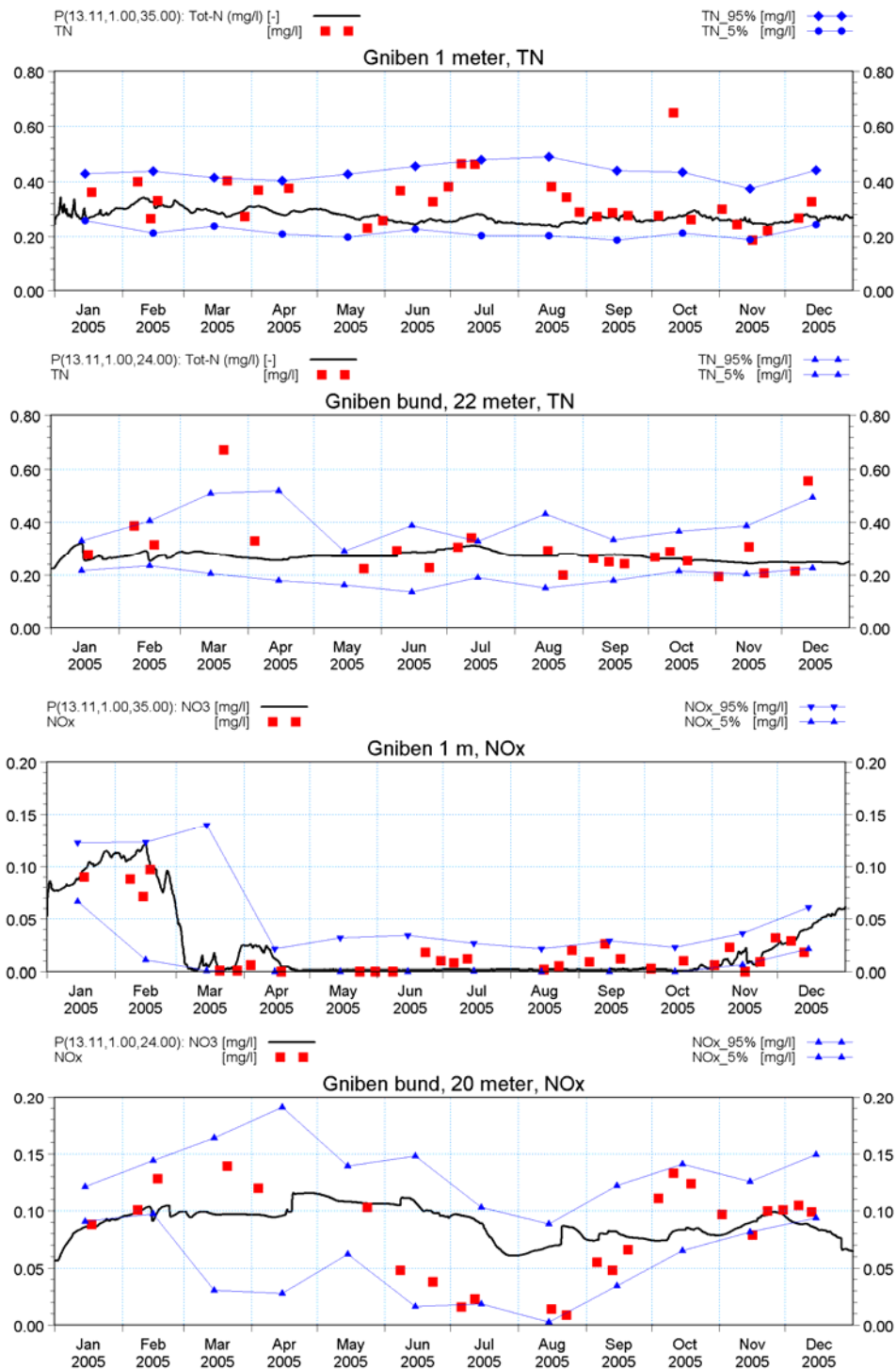
Figure 3.21   Concentration of total nitrogen (TN) and NOx-N at Gniben at surface and at bottom (20 m). Modelled (black line), measured in 2005 (■) and 5 and 95% percentiles covering 2000-2007.
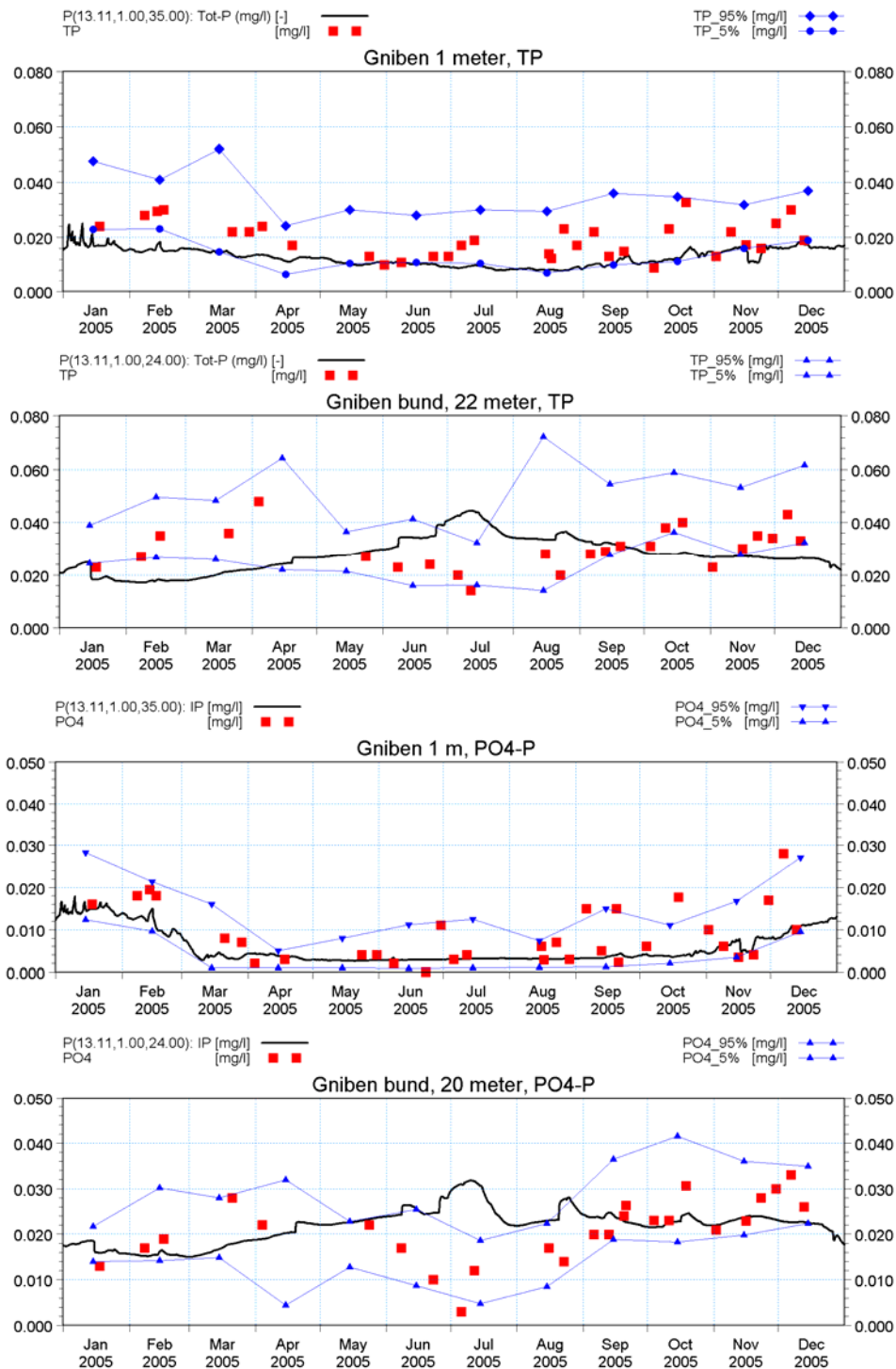
Figure 3.22   Concentration of total phosphorus (TP) and PO$_4$-P at Gniben at surface and at bottom (20 m). Modelled (black line), measured in 2005 (■) and 5 and 95% percentiles covering 2000-2007.
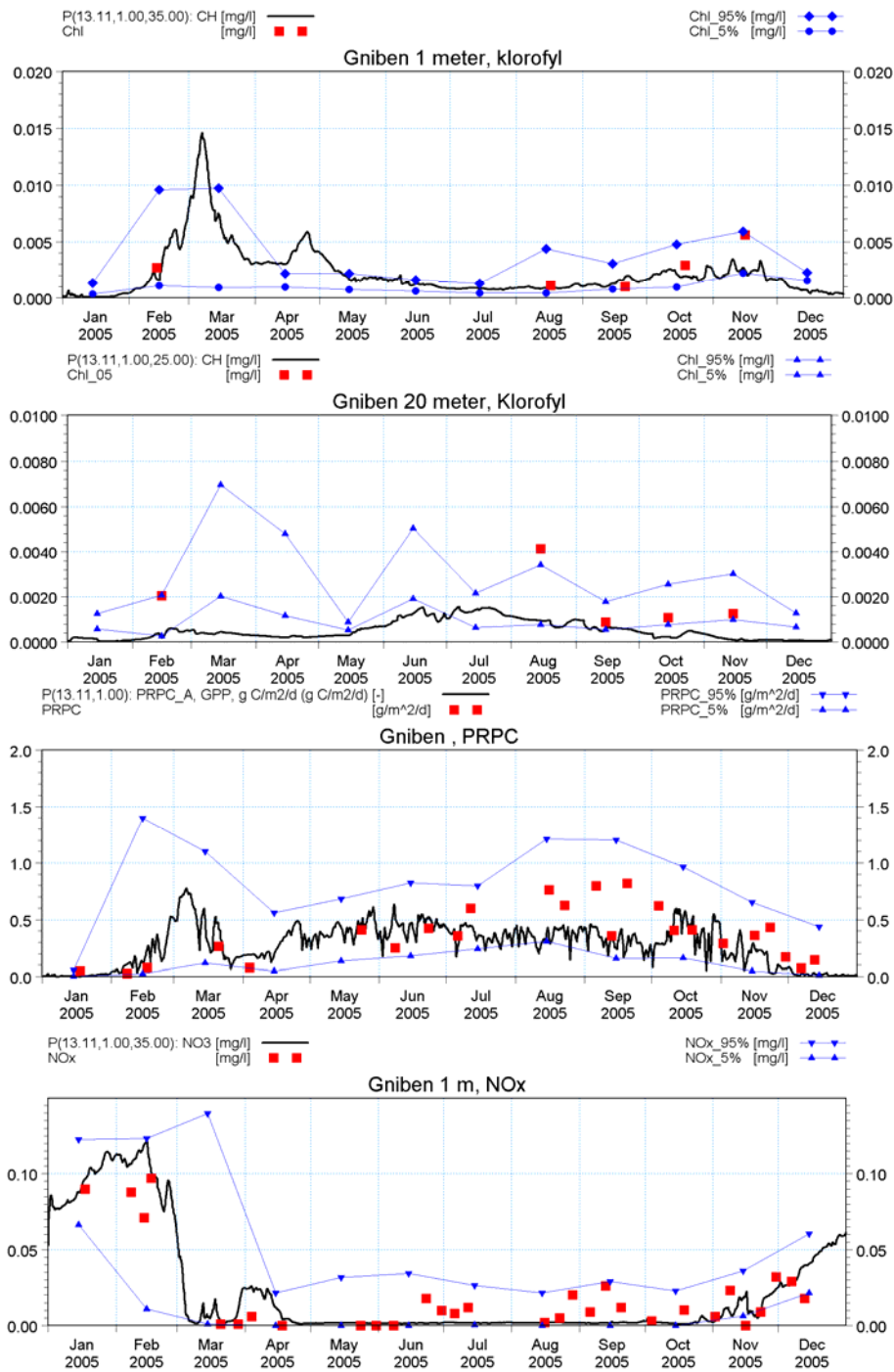
Figure 3.23   Concentration of Chla, NOx-N at Gniben at surface and at bottom (20 m; Chla only) and depth integrated primary production (PRC). Modelled (black line), measured in 2005 (■) and 5 and 95% percentiles covering 2000-2007.
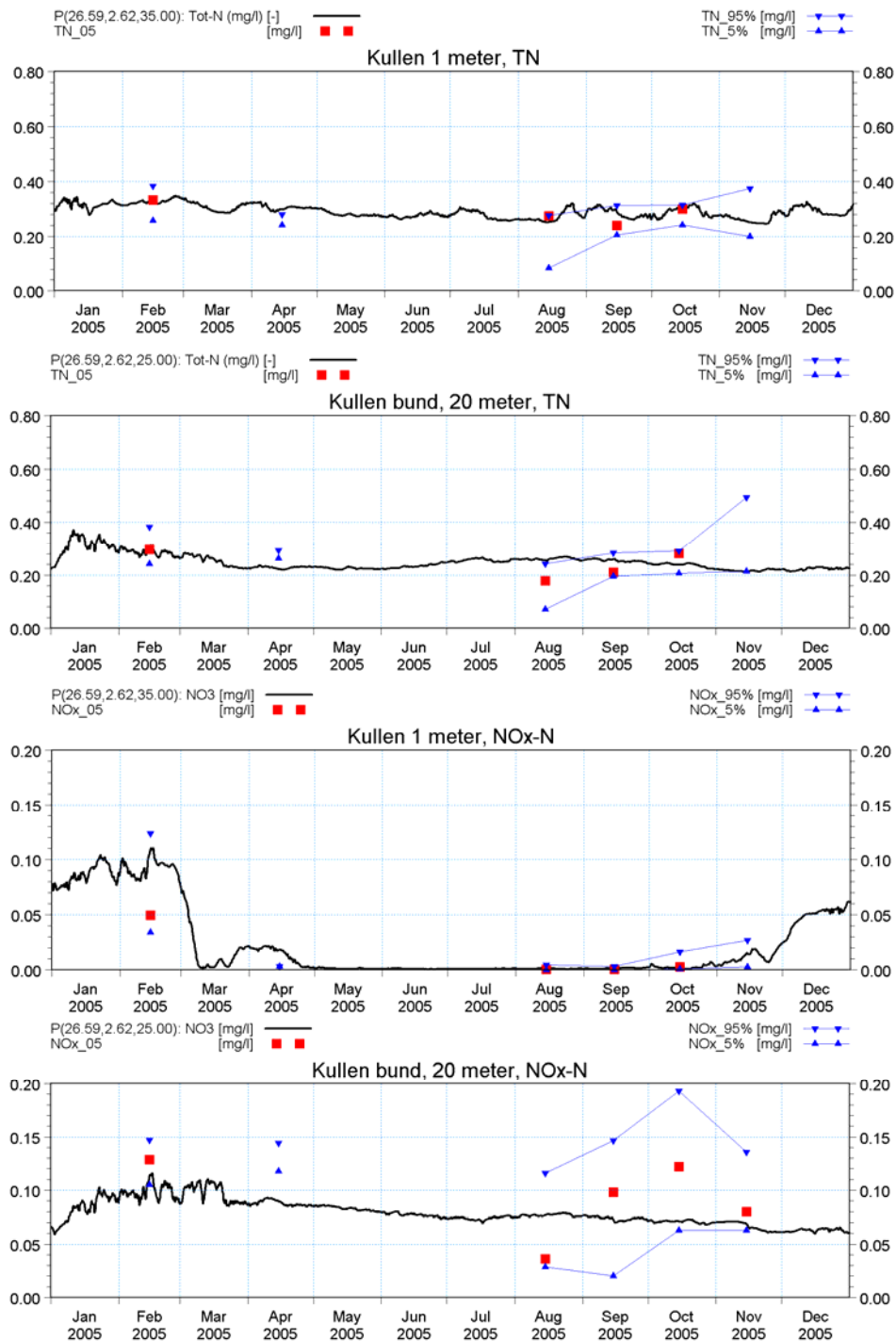
Figure 3.24   Concentration of total nitrogen (TN) and NOx-N at Kullen at surface and at bottom (20 m). Modelled (black line), measured in 2005 (■) and 5 and 95% percentiles covering 2000-2007.
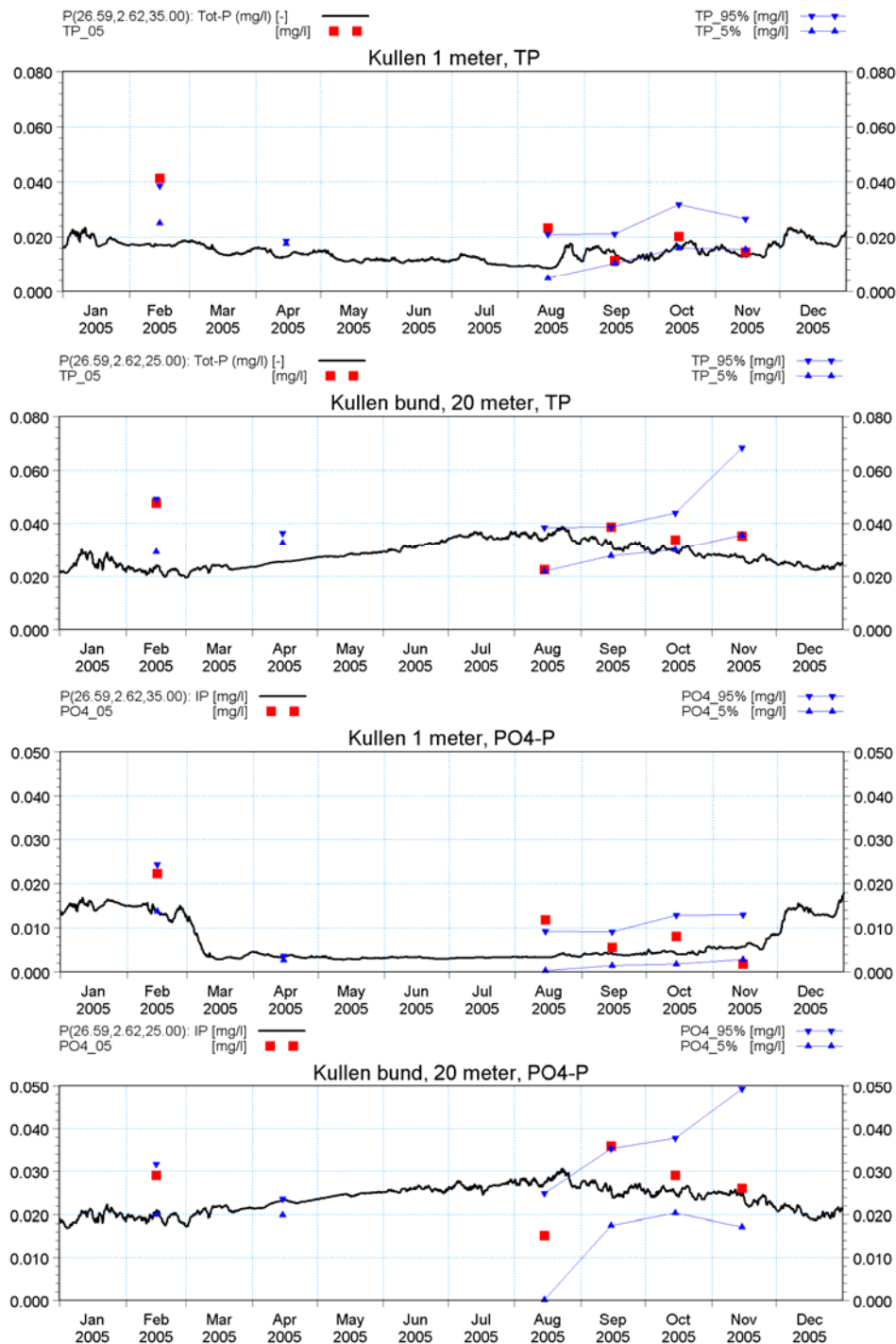
Figure 3.25   Concentration of total phosphorus (TP) and PO$_4$-P at Kullen at surface and at bottom (20 m). Modelled (black line), measured in 2005 (■) and 5 and 95% percentiles covering 2000-2007.
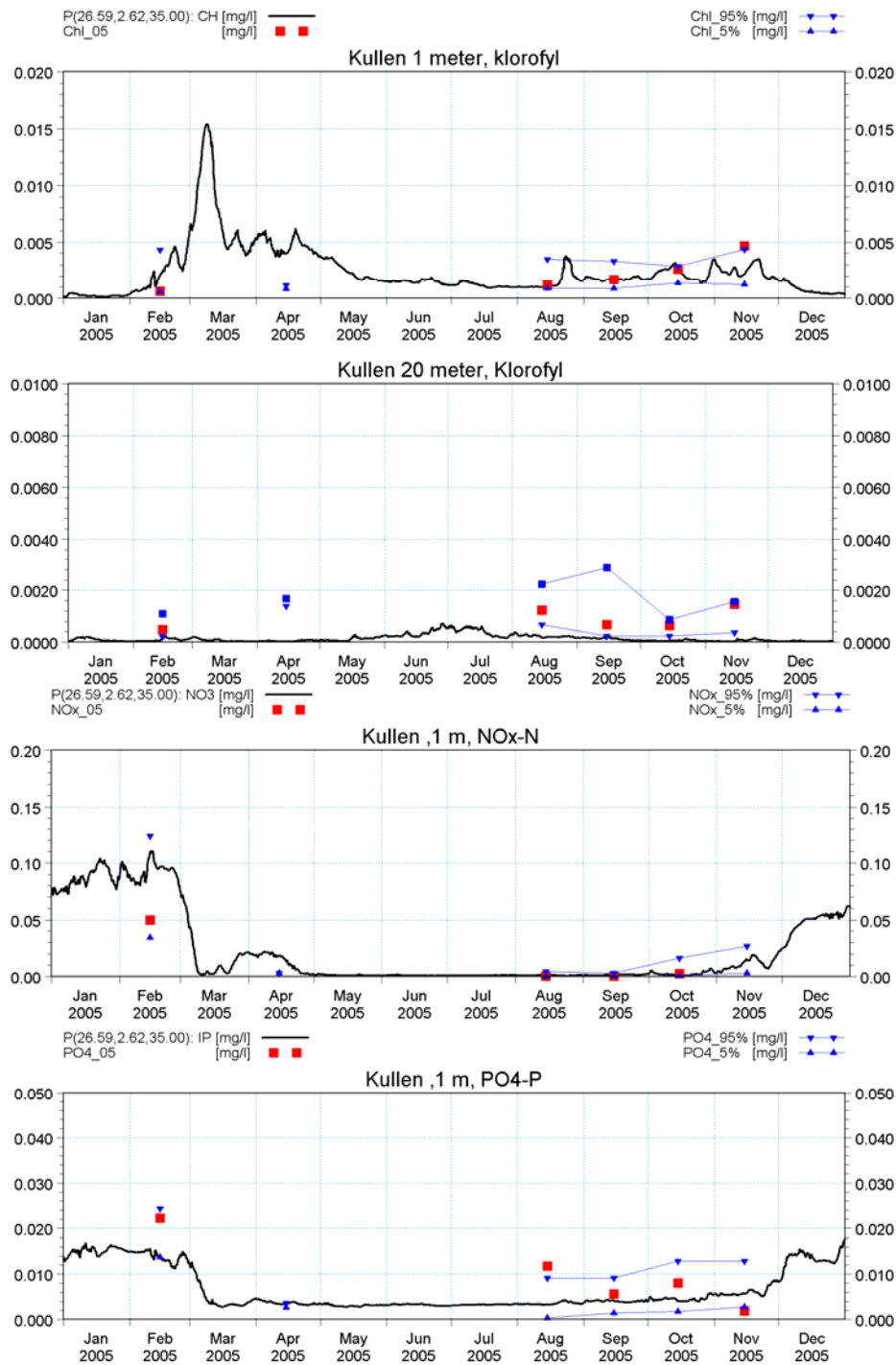
Figure 3.26   Concentration of Chla, NOx-N and PO$_4$-P at Kullen at surface and at bottom (20 m; Chla only). Modelled (black line), measured in 2005 (■) and 5 and 95% percentiles covering 2000-2007.
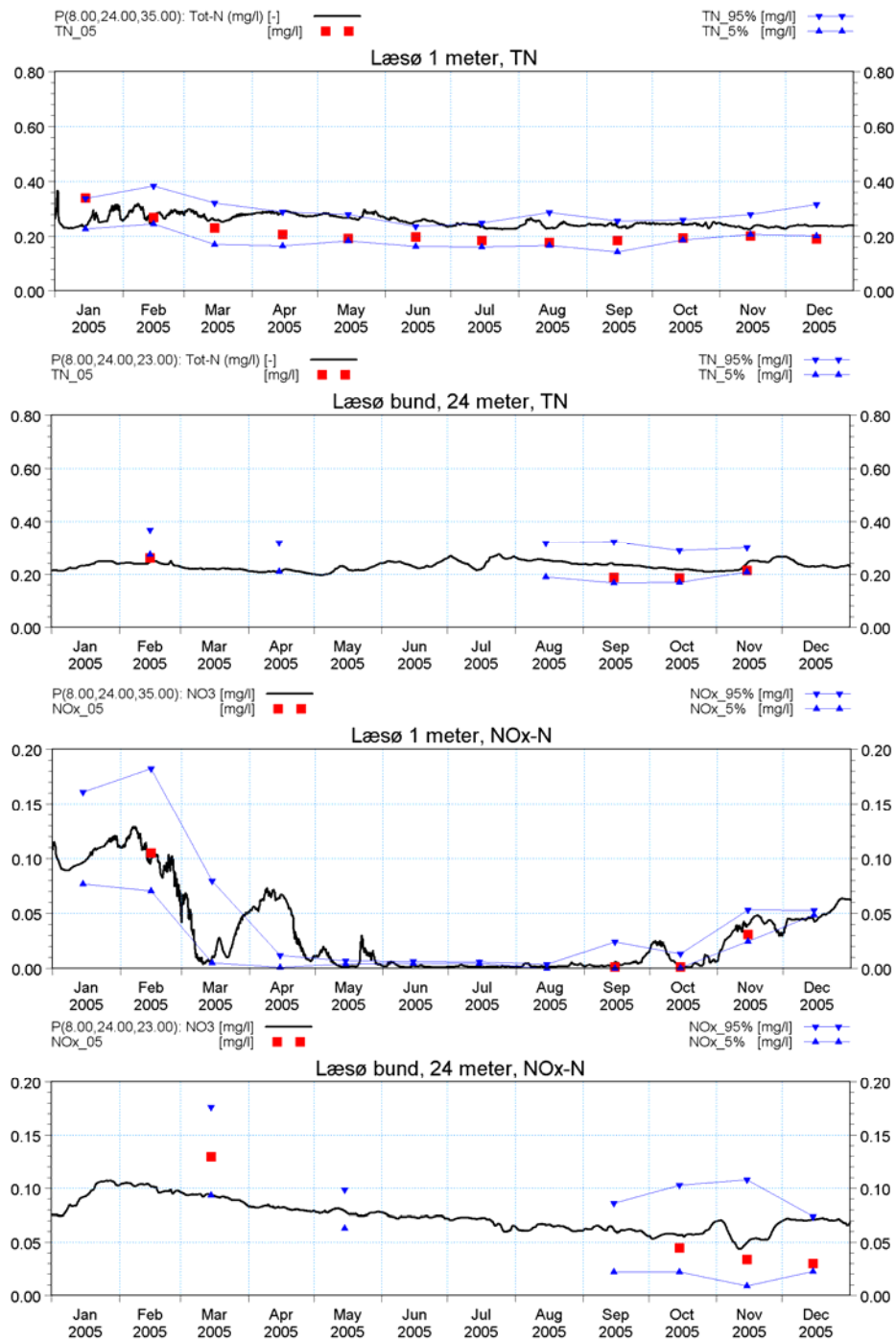
Figure 3.27   Concentration of total nitrogen (TN) and NOx-N at Læsø at surface and at bottom (24 m). Modelled (black line), measured in 2005 (■) and 5 and 95% percentiles covering 2000-2007.

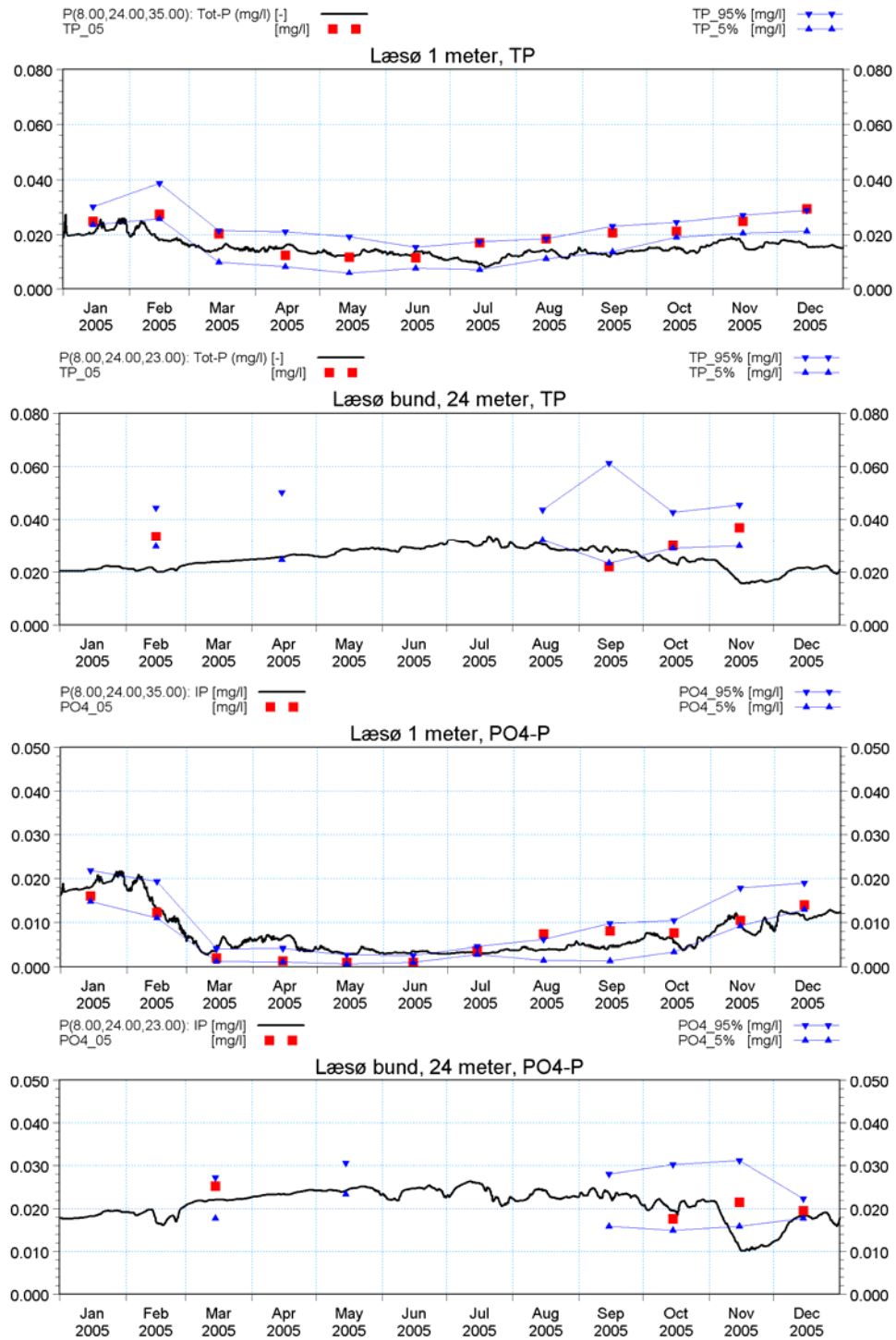Figure 3.28   Concentration of total phosphorus (TP) and PO$_4$-P at Læsø at surface and at bottom (24 m). Modelled (black line), measured in 2005 (■) and 5 and 95% percentiles covering 2000-2007.
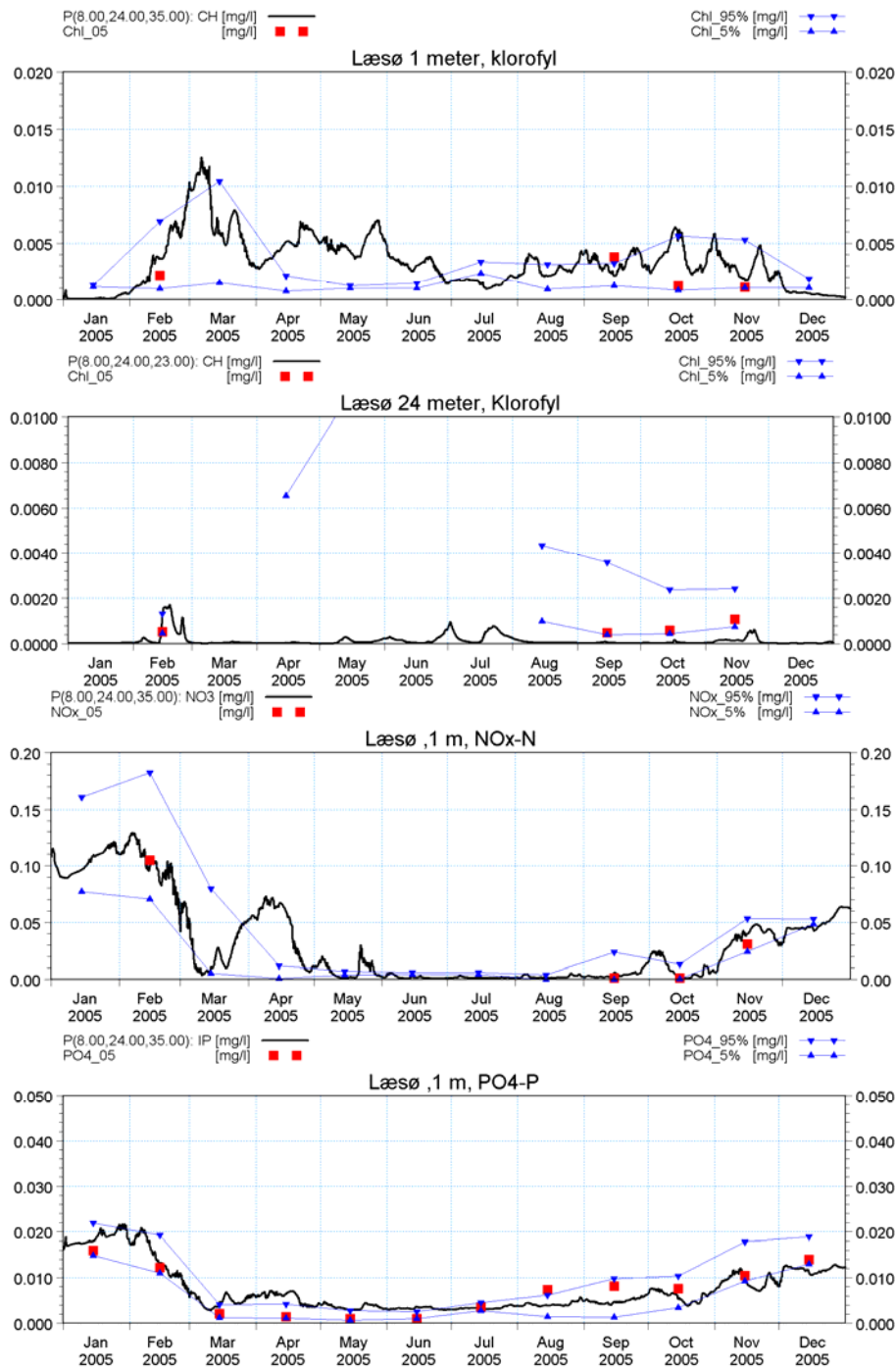
Figure 3.29   Concentration of Chla, NOx-N and PO$_4$-P at Læsø at surface and at bottom (24 m; Chla only). Modelled (black line), measured in 2005 (■) and 5 and 95% percentiles covering 2000-2007.

4.   References

/1/ DHI 2007a, ECOlab Short Scientific Description. DHI Water Environment Health, Hørsholm.

/2/ DHI 2007b, Eutrophication model 1 Ecolab template - scientific description. DHI Water Environment Health, Hørsholm.

/3/ DHI 2009, Description of model 2½ Ecolab template, DHI Hørsholm.

DRAFT

Appendix D

Estimating the local impact on stratification and mixing conditions

Estimating the local impact on stratification and mixing conditions

1.   Impact assessment

The very local effects will mainly be felt inside a distance of 1-2 diameters from the wind mills /1/; however, some mixing effects may be felt further downstream. Physically what happens locally when a cylinder is placed in steady currents is that dense water from the lower layer is lifted up into the lighter upper layer where it is mixed with the surrounding waters. A similar process occurs the other way at the same time. Laboratory tests show that the entrained water is mixed over the entire upper or lower layer and thus the interface between the layers remains at the same level /3/. The mixing process requires an input of energy. This input comes from production of turbulent kinetic energy and is converted potential energy in the mixing process. In order to determine the mixing, i.e. the actual amount of water transferred from one layer to the other and vice versa due to the presence of wind mills in a stratified flow it is necessary to determine the change in potential energy in the system. If it is assumed that the amount of energy in the system is constant then the gain in potential energy in the upper layer will be equal to the production of turbulent kinetic energy times the mixing efficiency factor.

In the following the effect on vertical mixing will be calculated. Horizontal mixing is neglected. The calculation goes as follows:

1. Calculate the work from the currents on the win dmill. Assume that this is converted to turbulence.

2. Assume that 5% of the dissipated energy goes to mixing. /3/.

3. Calculate the amount of energy needed to mix the full water column.

4. Calculate the time needed to mix the entire water column based on the energy input from the work done on the wind mill by the flow.

5. Assume that all mixing occur in a square behind the mill with side lengths equal to the diameter of the mill. Calculate the time it takes for the volume inside this square to be replaced.

6. Compare the time the considered parcel is in the square to the time it takes for full mixing and you will have the percentage of mixing compared to full mixing.

7. Apply this degree of mixing and use volumetric considerations to calculate the salinity in the upper and lower layer.

1: Calculate the work from the currents on the wind mill. Assume that this is converted to turbulence.

To assess the mixing of the water column behind a turbine foundation it is necessary to estimate the amount of turbulent kinetic energy produced at the wind mill. The energy production is proportional to the hydrodynamic force acting on the wind mill. The force F can be written as:

$$F = 0.5 * \rho * C_D * U * |U| * A \quad \text{(Newton)}$$

In which ρ is the water density, A is the cross sectional area of the wind mill, U is the upstream velocity and C_D is a drag coefficient (usually close to 1). The work done by the hydrodynamics on the wind mill (W) can be written as:

$$W = U * F \quad \text{(Joule/s)}$$

Based on this one can compute the dissipated energy due to the presence of the wind mill.

2: Assume that 5% of the dissipated energy goes to mixing.

From laboratory tests performed at DHI it is known that approximately 5% of this energy is transferred into mixing across the interface. In the following this is called the mixing efficiency factor (f). The extra energy E_{mixing} used for mixing can thus be written:

$$E_{mixing} = 0.5 * \rho * C_D * U * |U| * U * f * A \quad \text{(Joule/s)}$$

3: Calculate the amount of energy needed to mix the full water column

The gain in potential energy if the entire water column is mixed can be written as /2/:

$$E_{potgain} = 0.5 * \Delta * \rho_{lower} * g * T_{upper} * T_{lower} \quad \text{(Joule/m}^2\text{)}$$

In which T is the thicknesses of the upper and lower layers, g is the gravity accelera-tion and Δ is the density difference between upper and lower layer. This is defined as:

$$\Delta = \frac{\left(\rho_{lower} - \rho_{upper}\right)}{\rho_{lower}}$$

4: Calculate the time needed to mix the entire water column based on the energy input from the work done on the wind mill by the flow.

Though some mixing will happen downstream due to vortex shedding it is expected that the transfer of energy from the turbulent energy to mixing will mainly happen very near the wind mill. If it is assumed that the mixing of turbulent kinetic energy occurs in a narrow band along the sides of the wind mill and in an area in the wake behind the wind mill then the stratification properties can be calculated. The mixing area is the influence area of the processes illustrated in Figure 6.5 in the main re-port. In order to calculate the actual mixing it is assumed that all mixing occur in a box with side lengths equal to the wind mill diameter placed in the wake of the wind mill. The time it would take to mix the entire water column in this area using the available turbulent kinetic energy from the wind mill, under the assumption that the water is stagnant, can be calculated as:

$$dt = \frac{E_{potgain} * D^2}{E_{mixing}}$$

In which D is the diameter of the wind mill and dt is the time.

In this case dt will be larger than the time it takes for a given water body to travel out of the mixing area.

5: Assume that all mixing occur in a square behind the mill with side lengths equal the diameter of the mill. Calculate the time it takes for the volume inside this square to be replaced.

It is necessary to calculate how much energy a given water body will receive during the time it is in the mixing area. In the following an arbitrarily small water body, with side length dx, is considered. If the water body in the mixing area is not stagnant but moving downstream at the current velocity and the mixing is assumed to be constant over the mixing area then the time during which mixing is active on the water body can be written as:

$$t_{mixing} = \frac{D}{U}$$

Because the water body is small (dx<<<D) the energy input can be considered constant during the mixing period and the transition period when the parcel leaves the mixing zone can be neglected.

6: Compare the time the considered parcel is in the square to the time it takes for full mixing and you will have the percentage of mixing compared to full mixing.

If a mixing efficiency is calculated the actual mixing and thus the salinities can be calculated. The mixing efficiency is:

$$M_{mixing} = \frac{t_{mixing}}{dt} * 100 \quad (\%)$$

7: Use volumetric considerations to calculate the salinity in the upper and lower layer.

This value is the portion in percent of the energy necessary to mix the entire water column that is actually transferred to the water body. Since the energy necessary to mix the entire water column is known one can calculate the change in salinity and temperature by simple volumetric considerations. Tests indicate that mixing occur both in the top and bottom layer and that the entrained water is mixed fully with the layer it is entrained in. It can therefore be assumed that equal amounts of water are transferred from the bottom layer and up and vice versa and that the interface remains at the same level.

For a fully mixed water column, the salinity will be:

$$S = \frac{S_{upper} * T_{upper} + S_{lower} * T_{lower}}{T_{lower} + T_{upper}} \quad (PSU)$$

Following this the resulting salinity in the upper and lower layers can be calculated as follows:

$$S_{upper,new} = (S - S_{upper}) * M_{mixing} + S_{upper}$$

$$S_{lower,new} = S_{lower} - (S_{lower} - S) * M_{mixing}$$

In Figure 1.1 and Figure 1.2 this calculation is done for different currents speeds at stratification properties. Four cases are presented:

- Case 1: Salinity upper layer 15PSU. Salinity lower layer 25 PSU. Thickness upper layer 12 m. Thickness lower layer 5 m.

- Case 2: Salinity upper layer 17PSU. Salinity lower layer 20 PSU. Thickness upper layer 12 m. Thickness lower layer 5 m.

- Case 3: Salinity upper layer 15PSU. Salinity lower layer 25 PSU. Thickness upper layer 5 m. Thickness lower layer 12 m.

- Case 4: Salinity upper layer 17PSU. Salinity lower layer 20 PSU. Thickness upper layer 5 m. Thickness lower layer 12 m.

Results show that for current velocities less than 0.4 m/s – 0.5 m/s no significant mixing effect is seen and for all practical purposes mixing can be neglected in this regime. For higher current velocities mixing becomes more significant.

Results also show that mixing of the full water column is a function of how strong the stratification is but even for relatively weak stratifications (2.5 PSU) the full mixing is not achieved for naturally occurring velocities.

If this is compared to the general trend for velocities in the area then it is seen that significant mixing only occurs in 2-5% of the time. Typical velocity distributions from 2005 at the surface near the wind mill park are given in Table 1.1. Note that if the depth averaged velocity was considered the number would be even smaller.

Table 1.1 Current conditions at the surface near the wind mill park. (From modelling).

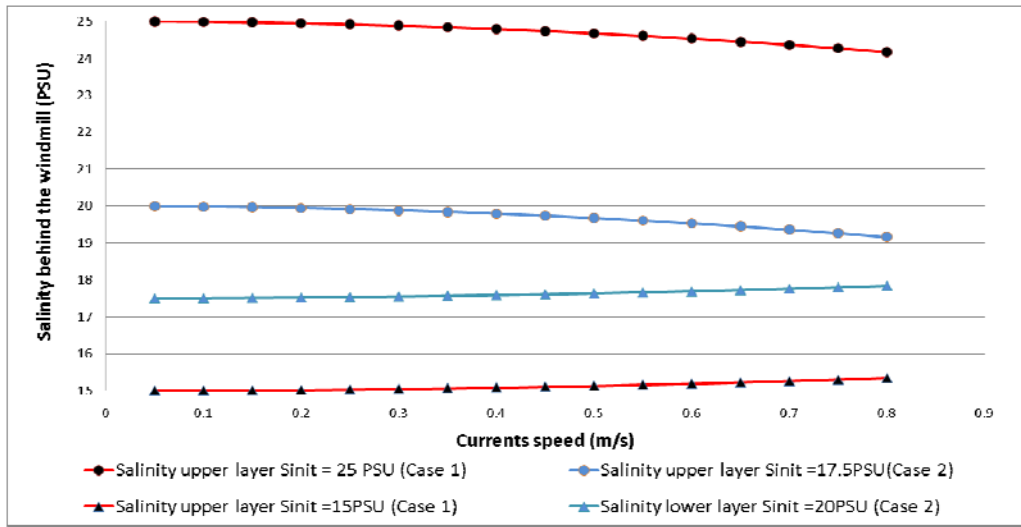| Current speed	0	0.05	0.1	0.15	0.2	0.25	0.3	0.4	0.5	0.6	0.7	0.8
% < Current speed	0.00	9.05	30.30	51.15	68.90	80.41	86.92	94.65	97.82	99.40	99.99	100.00

Figure 1.1   Salinity at distance D after the wind mill at different current speeds. S_{init} is the salinity upstream of the wind mill. The thickness of the lower layer is 5 m and the upper layer is 12 m. The diameter considered is 15 m.
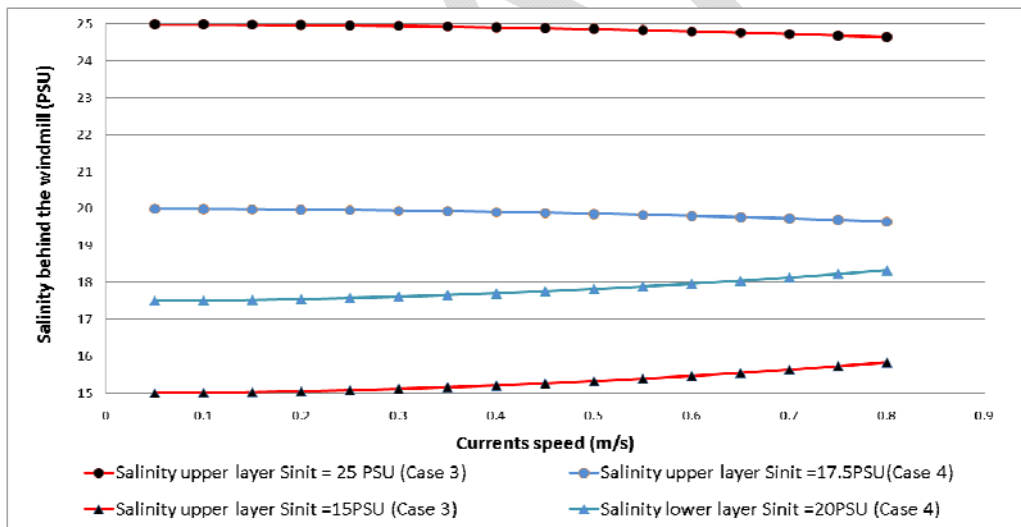

Figure 1.2   Salinity at distance D after the wind mill at different current speeds. S_{init} is the salinity upstream of the wind mill. The thickness of the lower layer is 12 m and the upper layer is 5 m. The diameter considered is 15 m.

2. References

/1/ B.M. Sumer, K. Bundgaard and J. Fredsøe: "Global and local scour at pile groups". International Journal of Offshore and Polar Engineering, vol. 15, No. 3, pp. 204-209, 2005.

/2/ Bo Pedersen, Flemming. Stratified Flows. DTU 1984.

/3/ Internal research in progress. Not published yet.